



DISSERTATION

Quantum Corrections to
Thermodynamic Properties in the
Large N_f Limit of the
Quark Gluon Plasma

ausgeführt zum Zwecke der Erlangung des akademischen Grades eines
Doktors der technischen Wissenschaften

unter der Anleitung von

Ao. Univ.-Prof. Dr. Anton Rebhan
Institutsnr: E 136
Institut für Theoretische Physik

eingereicht an der Technischen Universität Wien
Fakultät für technische Naturwissenschaften und Informatik

von

Dipl.-Ing. Andreas Ipp

Matr. Nr: 9271057
Krottenbachgasse 27
A-2345 Brunn am Gebirge
Austria, Europe

Wien, 4. November 2003

A handwritten signature in black ink, which appears to read 'Andreas Ipp', is written over a horizontal line.

Deutsche Kurzfassung

Das theoretische Studium des Quark-Gluon Plasmas gewinnt immer mehr an Bedeutung seit Teilchenbeschleuniger wie das SPS, der RHIC, oder der sich im Bau befindliche LHC die erforderlichen hohen Energiedichten in Schwerionenkollisionen erreichen, die es erlauben, diesen neuen Materiezustand experimentell zu untersuchen. Einfache Anwendungen der Quantenfeldtheorie im Rahmen einer störungstheoretischen Entwicklung nach der Kopplungskonstante versagen bei hohen Temperaturen, und trotz eifriger Bemühungen, die Situation in den Griff zu bekommen, haben wir quantitative theoretische Aussagen über den Phasenübergang nur von Gittersimulationen. Diese wiederum versagen für ein Quark-Gluon Plasma bei hohem chemischem Potential und niedrigen Temperaturen, wie man es im Kern von dichten Sternen vermutet. Large- N_f -QCD - das ist Quantenchromodynamik (QCD) mit einer großen Zahl von Quark-Sorten (number of quark flavors - N_f) - erlaubt es, Wechselwirkungseffekte von thermodynamischen Größen wie dem thermischen Druck oder der Entropie exakt in der effektiven Kopplung $g_{\text{eff}}^2 \propto g^2 N_f$ für alle Temperaturen T und chemische Potentiale μ_q zu berechnen. Dies macht Large N_f QCD zu einem idealen Testwerkzeug für verschiedene Näherungsmethoden.

In der vorliegenden Arbeit präsentieren wir das exakte Large- N_f Resultat für den thermischen Wechselwirkungsdruck in der kompletten T - μ_q -Ebene in einem Bereich, in dem der Einfluss durch den Landau-Pol numerisch vernachlässigt werden kann. Für kleine Werte der Kopplung vergleichen wir unser Resultat mit existierenden störungstheoretischen Ergebnissen in der Literatur, einschließlich der aktuellen Berechnung des Drucks durch Vuorinen für endliche Temperatur und chemisches Potential sowie einer älteren Rechnung von Freeman und McLerran für verschwindende Temperatur und hohes chemisches Potential. Unsere numerische Genauigkeit erlaubt uns, existierende störungstheoretische Koeffizienten zu verifizieren und zum Teil sogar zu verbessern, und auch störungstheoretische Koeffizienten zur sechsten Ordnung in der Kopplung numerisch zu bestimmen, die analytisch bislang noch nicht berechnet wurden. Für verschwindendes chemisches Potential berechnen wir lineare und nicht-lineare Quarkzahl-Suszeptibilitäten. Wir zeigen, dass das moderate Skalierungsverhalten, das durch die Quarkzahl-Suszeptibilitäten nahegelegt wird, ziemlich abrupt bei $\mu_q \gtrsim \pi T$ zusammenbricht, aber dass dieser nicht-perturbative Effekt in μ_q immer noch in guter Näherung durch die Ergebnisse von Vuorinen bei kleinen Kopplungen und endlichem T beschrieben wird. Nur für $T \ll \mu_q$ versagt auch dieser Zugang, und wir kommen in den Bereich der sogenannten Non-Fermi-Flüssigkeit, die im Gegensatz zur klassischen Fermi-Flüssigkeit von langreichweitigen, quasistatischen transversalen Eichbosonen dominiert wird. In diesem Limes können wir nicht nur den bereits bekannten führenden $T \ln T^{-1}$ Beitrag zur spezifischen Wärme vervollständigen, sondern auch über die führende Ordnung eine störungs-

theoretische Reihe mit anomalen gebrochene Potenzen $T^{(3+2n)/3}$, die durch dynamische Abschirmung verursacht werden, angeben. Wir berechnen deren Koeffizienten analytisch bis zur Ordnung $T^{7/3}$ und finden, dass diese tatsächlich das führende anomale Verhalten der vollen QED und QCD bestimmen (also bei endlichem N_f).

Abstract

The theoretical study of the quark gluon plasma gains increasing interest as particle accelerators like the SPS, RHIC, or the currently built LHC will reach sufficiently high energy densities in heavy ion collisions that allow us to probe this new state of matter experimentally. Straightforward application of quantum field theory at high temperatures fails in a perturbative expansion in the coupling constant, and despite some effort during the last decades to improve the situation, so far quantitative theoretical knowledge about the phase transition merely comes from lattice simulations. Lattice simulations on the other hand fail for a deconfined quark-gluon plasma at large quark chemical potential and small temperatures which is expected to be found in the core of dense stars. Large N_f QCD - that is quantum chromodynamics with large number of quark flavors - allows one to calculate thermodynamic properties like the interaction contribution of thermal pressure or entropy exactly in the effective coupling $g_{\text{eff}}^2 \propto g^2 N_f$ for all temperatures T and chemical potentials μ_q . This makes large N_f QCD an ideal testing ground for various approximation methods.

In this work we present the exact large N_f NLO calculation of the thermal interaction pressure in the whole T - μ_q -plane where the presence of the Landau pole is negligible numerically. For small values of the coupling we compare our results to existing perturbative results in the literature, in particular the recent calculation by Vuorinen for finite temperature and chemical potential or an older calculation by Freedman and McLerran for zero temperature and high chemical potential. Our numerical accuracy allows us to verify and even improve some of the existing perturbative coefficients, and to predict new coefficients to the sixth order in the coupling numerically that have not been calculated analytically yet. For larger couplings we determine where perturbation theory ceases to be applicable. At zero chemical potential we calculate linear and non-linear quark number susceptibilities. We show that the moderate scaling behavior suggested by the quark number susceptibilities breaks down rather abruptly at $\mu_q \gtrsim \pi T$, but that this non-perturbative effect in μ_q can still be reproduced well by the calculation by Vuorinen for small couplings and finite T . Only for $T \ll \mu_q$ also this approach breaks down and we enter the range of a so-called non-Fermi liquid, which in contrast to a classical Fermi liquid is dominated by long-range quasi-static transverse gauge-boson interactions. In this limit, we complete the previously known leading $T \ln T^{-1}$ contribution to the specific heat, and also to go beyond this order to find a series involving anomalous fractional powers $T^{(3+2n)/3}$ caused by dynamical screening. We calculate their coefficients analytically up to order $T^{7/3}$ and find that these contributions indeed determine the leading anomalous contribution in full QED and QCD (i.e. at finite N_f).

心急吃不了热豆腐¹

¹xīn jí chī bù liǎo rè dòu fu: Those of impatient heart can not eat hot tofu (bean curd).
(*traditional Chinese saying*)

Contents

Prolog	1
1 Introduction	3
1.1 The experiment	3
1.2 QCD Phase Diagram	5
1.3 Outline	8
2 Large N_f	9
2.1 Introduction to Large N_f QCD	9
2.1.1 Why Large N_f ?	9
2.1.2 Comparison to strict perturbative expansion in g	11
2.1.3 Outline	13
2.2 Pressure at Large- N_f QCD	14
2.3 Leading-order gauge boson self-energy	18
2.4 Landau pole ambiguity	25
2.5 Results and discussion	27
2.5.1 Comparison to dimensional reduction	28
2.5.2 Pressure at zero chemical potential	35
2.5.3 Quark number susceptibilities	43
2.5.4 Pressure at zero temperature	47
3 Non-Fermi Liquid	51
3.1 Introduction	51
3.1.1 From ideal gas to non-Fermi liquid	51
3.1.2 Non-Fermi liquid	54
3.2 Entropy at small temperatures	56
3.3 Transverse contribution	57
3.3.1 Leading log contribution	59
3.3.2 Straightforward improvements	60
3.3.3 Approximations to order T^3	62
3.3.4 Momentum integration	64
3.3.5 Pressure, entropy and specific heat	70
3.3.6 Higher order corrections	71

3.4	Longitudinal contribution	72
3.5	Full result	73
3.5.1	Extension to full QED and QCD	74
3.6	Discussion	75
3.6.1	Specific heat	75
3.6.2	Effect near the CSC critical temperature	77
4	Summary and Outlook	81
A	Abbreviations	85
B	QCD Feynman rules	87
B.1	Motivation for a unifying approach	87
B.2	Derivation of Feynman rules	89
B.3	Comparison with literature	95
B.4	Summary of rules	99
C	Thermodynamic relations	103
C.1	Specific heat at NLO	103
C.2	Derivative relations	104
D	Gauge boson self-energy	105
D.1	Exact result at $T = 0$	105
D.2	Approximations to second order in frequency	107
E	Fractional power expansion	109
E.1	Introduction to Puiseux series	109
E.2	Workaround for <i>Mathematica</i>	111
	Bibliography	114
	Acknowledgements	127
	Curriculum Vitae	129

Prolog

LHC/CERN in Swiss, 2007²

SWOOOOSH....!!!

"Oh my god! What was that?" - "They are trying to smash us!" - "Oh mum! I wanna get out!". A bunch of hysterically screaming lead ions flying almost at the speed of light can barely fight the 8.36 Tesla magnetic fields (some 100,000 times the strength of Earth's magnetic field) that keep them on spiraling orbits in the Large Hadron Collider (LHC).

SWOOOOSH....!!!

"Aahhh!" - "That was VERY close!!! I can't believe they are doing this to us!". With only 27 km collider circumference, the ion bunches approach themselves some 11,000 times per second.

SWOOOOSH....!!!

"Ok, that's it! Let us oooooout!!!" - "They already ripped off an electron from me! What else do they wanna do?". The darkness in the collider is tantalizing, as are the 1.9 K (some -270°C) coldness from the 5,000 surrounding super-conducting magnet coils.

SWOOOOSH....!!!

"I'm cold!!!" - "Brrrr... I'm freezing!!!"! "You'll feel warmer soon", Old uncle Joe tried to soothe them. In his billions of years of life he had gone through many phases. So far he had survived everything.

SWOOOOSH....!!!

"What the..!" - "They are not... no!! Don't tell me they want to smash us into..." - "...into the Quark Gluon Plasma!!!"

SWOOO - KABOOM!!!!

Let me not go into too much detail - it's a horrible view: atoms are smashed head on head, their inner protons and neutrons are torn apart, even the formerly strictly confined up- and down-quarks end in a disgusting soup of unconfined quarks and gluons, whining and wincing only as shock fronts penetrate them. But this is science: Scientists have to take the loss of some lead atoms for the sake of knowledge about the Quark Gluon Plasma (QGP).

²Data in this prolog are taken from the LHC design performance website 2003 [1].

Chapter 1

Introduction

1.1 The experiment

The study of the quark-gluon plasma in heavy ion collision experiments is one of the focal points of contemporary high energy physics. Historically, scientists smashed elementary particles since the 1930's with Earnest Lawrence's invention of the cyclotron, which improved earlier attempts with linear accelerators tremendously. In a cyclotron, charged particles from electron or ion sources are accelerated on a circular orbit before they hit a target. Even higher energies can be reached with synchrotrons, first constructed at the General Electric Research Laboratory for the University of California, Berkeley, in 1949. Contrary to the continuous beam of a cyclotron, the synchrotron works with beam pulses which ride on electro-magnetic waves.

Modern particle accelerators like the Super Proton Synchrotron (SPS) at CERN or the Relativistic Heavy Ion Collider (RHIC) at Brookhaven National Laboratory are based on this concept of the synchrotron, relying on several steps of particle acceleration. For example, heavy ions at RHIC are produced in the Tandem Van de Graaff by static electricity. These particles are then carried to the Booster synchrotron where they are accelerated to 37% the speed of light, before they are transferred to the Alternating Gradient Synchrotron where they reach 99.7% the speed of light. From there they will be injected into the first RHIC ring in clockwise direction or into the second RHIC ring in counter-clockwise direction, where particles will be collided into one another in one of the six interaction points of the ring [2].

It is interesting to note that for proton-anti-proton collisions like in the LHC one only needs one collider ring instead of two, as positively charged protons and negatively charged anti-protons can travel clockwise and counter-clockwise in the same magnetic field. However, the LHC also has two collider rings to also allow for lead-lead collisions, proton-lead collisions, proton-oxygen collisions, or collisions of protons with other light ions [3]. A summary of accelerators that are producing or will produce the quark-gluon plasma

Name	Location	Year	Energy	Beam	Orbit
SPS	CERN	1994	160 GeV	lead ions	6.9 km
RHIC	Brookhaven	2000	200 GeV	gold ions	3.8 km
LHC	CERN	2007	7 TeV	proton, lead	26.7 km

Table 1.1: Particle accelerators that produce or will produce the quark gluon plasma (QGP). The year marks the date of starting operation for search of the QGP, center-of-mass energy is given per nucleon for SPS and RHIC. The abbreviations of the names mean Super Proton Synchrotron (SPS) [5], Relativistic Heavy Ion Collider (RHIC) [2], and Large Hadron Collider (LHC) [1].

is given in table 1.1. Besides hadron colliders (using ions or protons) which will probe the quark-gluon plasma, future collider plans also include lepton colliders as CERN's proposed electron linear accelerator CLIC (Compact Linear Collider), or muon colliders. Since leptons are fundamental particles (contrary to hadrons which consist of quarks and gluons), these colliders are especially apt for precision measurements of particle properties. [4]

The press releases about evidence for the production of the quark-gluon plasma in heavy ion collisions at the SPS were first announced in 2000 [6]. Only indirect observations are possible since the QGP formed in the initial stage is quickly turned into a system of hadrons - a process called "hadronization". Detection of single quarks is not possible due to color confinement, a property of strong interactions at low energies, according to which quarks must always combine to color-neutral hadrons before being able to travel to the detector. A number of experiments was necessary before scientists dared to announce the discovery of the QGP: The theoretical analysis of the measured hadron abundances resembles a state of "chemical equilibrium" at a temperature of about 170 MeV which marks the quark-hadron transition. In particular, there is an observed enhancement of hadrons containing strange quarks by a factor of 2 to 15 (depending on the hadron), relative to proton-induced collision, and an observed suppression of the charmonium states J/ψ and ψ' [7] which contain charm quarks with masses of about 1.2 GeV, much higher than the transition temperature of about 170 MeV. Direct observations of the QGP via electromagnetic radiation at the SPS are difficult due to high backgrounds from other sources. Higher energies at RHIC and the LHC may allow for better observation of the plasma radiation and enable detailed studies of the early thermalization processes and dynamical evolution of the quark gluon plasma. These experiments might also help to study the order of the phase transition and to locate the tricritical point within the QCD phase diagram, where the first-order transition changes into a crossover behavior.

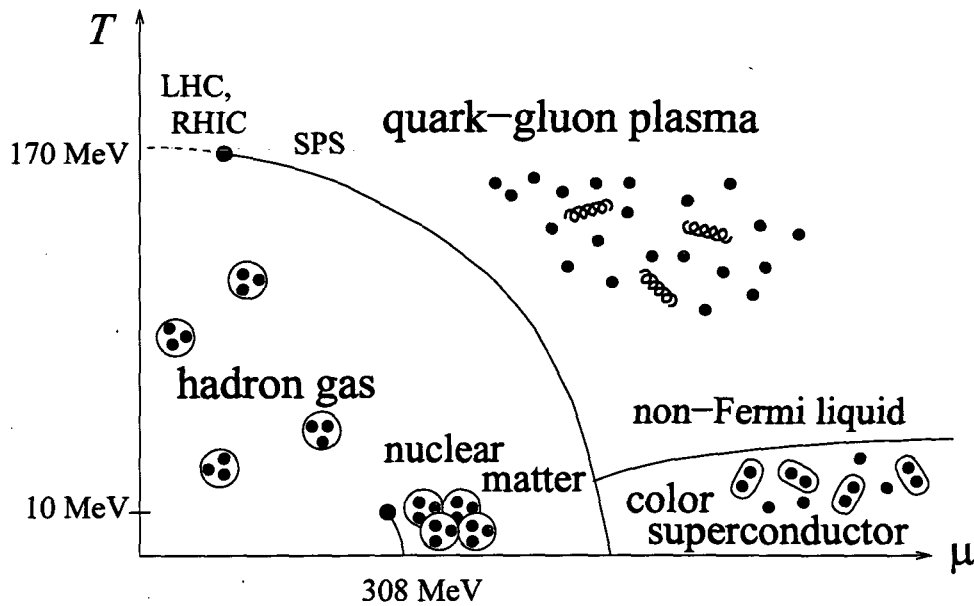


Figure 1.1: Schematic QCD phase diagram of strongly interacting matter.

1.2 QCD Phase Diagram

Depending on temperature and particle density, matter exists in various phases. Just like water can exist in the familiar phases of solid, liquid, or gaseous state with phase transitions between them, so will it enter a new phase of a plasma (ionized gas) at high enough temperature to break up chemical bonds and to ionize hydrogen and oxygen atoms. If the temperature still increases, matter undergoes another phase transition where quarks and gluons, which are the constituents of protons and neutrons, leave their nuclear confinement to form a quark gluon plasma. On the lower end of the temperature scale, matter may exist in the phase of a Bose-Einstein condensate, suprafluids, or superconductors.

The fundamental theory describing quarks and gluons is the theory of strong interactions, quantum chromodynamics (QCD). Unlike electromagnetism, which becomes stronger as the mutual distance decreases, strong interaction gets weaker. As a consequence, quarks, the fundamental particles of QCD, are confined in packages of three (called "baryons", like protons and neutrons) or two ("mesons", e.g. pions) at low temperatures. Any attempt to separate confined quarks rather produces a new quark-antiquark pair from the gluon field in-between that combines with the separated quarks so that no single quark or net color charge can be observed.

In figure 1.1 we see a schematic view of the QCD phase diagram. Strongly interacting matter can exist in three distinct phases, depending on temperature T and chemical potential μ : the hadronic phase (confined to hadrons

as a hadron gas or nuclear matter), the quark-gluon plasma, and the color-superconducting quark-matter. Our world is located on the lower line of the diagram around the phase transition of 308 to 313 MeV, in the form of hadron droplets (nuclei). Temperature T is given in units of MeV which can be converted to Kelvin using the Boltzmann constant $k_B = 1.3807 \times 10^{-23} \text{ J/K} = 8.617 \times 10^{-5} \text{ eV/K}$. For a nice day of 27°C we get $27^\circ\text{C} \approx 300 \text{ K} \approx 25.9 \text{ meV}$. The core of our sun has a temperature of about $1.6 \times 10^7 \text{ K} \approx 1.35 \text{ keV}$. To get to the quark-gluon plasma we still need to increase temperature by five orders of magnitude to at least 170 MeV.

The other axis of the diagram shows the quark chemical potential μ . The term "chemical potential" may be misleading since we deal with temperatures and densities far from ordinary chemistry, but it denotes a useful quantity that is applicable to any thermodynamic system: The chemical potential is the change in the energy of the system when an additional constituent particle is introduced, with the entropy and volume held fixed (or equivalently the change in the Helmholtz free energy with temperature and volume held fixed). For systems containing different species of particles, there is a separate chemical potential associated with each species. If the particles can be transformed into one another, particle species with higher chemical potential will transform into a species with lower chemical potential, releasing heat. Therefore in an equilibrium state of several species, the chemical potentials of all species must equal each other. At zero temperature, (infinite) nuclear matter has a ground state at a quark chemical potential of $\mu = 308 \text{ MeV}$. This is the nucleon mass $m_N \approx 939 \text{ MeV}$ minus the binding energy 16 MeV divided by three for the average energy per quark or quark chemical potential. In our everyday life we find nuclear matter density only in atomic nuclei - the droplets in which quarks are confined. Only if we increase the pressure of the system so that all droplets start touching and overlapping each other, we can build a phase of infinite nuclear matter. Up to this point, the pressure of the system at zero temperature is zero, because any compression just means decrease of the void space between the droplets. If the density is increased beyond the point where the droplets start to touch, pressure will start to increase, too. This is the so-called liquid-gas phase transition between the hadron gas and nuclear matter.

The pressure always changes continuously if we change from one phase to another, but if its first derivative with respect to T is discontinuous, we call this a phase transition of first order. If the first derivative of the pressure is continuous, but its second derivative is discontinuous, we have a second order phase transition. Finally, if the pressure is continuous to all orders, but there is a rapid change in pressure, we can talk of a crossover. Usually, points of phase transition in the diagram form a line that starts at one of the axis of the diagram and may terminate at a critical point. Also the first-order liquid-gas phase transition has a critical point for a temperature of about 10 MeV where the transition becomes second order. Above this temperature

one cannot distinguish between the gaseous and the liquid phase.

Below a temperature of 170 MeV and chemical potential of about 350 MeV, quarks stay confined in hadrons. If we further increase temperature and/or quark density, we arrive at the quark-hadron phase transition at which quarks cease to be bound in individual nuclei and become either a deconfined quark-gluon plasma or a color superconductor. For a range of medium quark chemical potential, the phase transition is of first order, but for higher temperatures and smaller chemical potentials there is a critical point below which we only have a crossover, as suggested by lattice calculations. Particle detectors like SPS, RHIC or LHC probe will probe the quark-gluon plasma in a range around this tricritical point. This is also the path that our universe took in early times, some 20-30 μ s (\approx 170 MeV) after the big-bang, starting with high temperature and a quark chemical potential of about 10^{-6} MeV passing the quark-gluon phase transition down to our universe temperature of 2.725 K [8] and an average quark chemical potential of about 313.6 MeV [9].

For small temperatures and high chemical potential we enter the phase of a color superconductor [10, 11]. This phase has been studied extensively during the last decade, and its theoretical foundations include concepts taken from the theory of ordinary superconductors: In ordinary superconductors, electrons are bound together by phonon interactions into Cooper pairs. Color superconductivity occurs because in the anti-triplet channel there is an attractive interaction between two quarks at the Fermi surface [12, 13]. These quarks then condense in the new ground state of the system by forming Cooper pairs. Depending on T , color superconductivity can again be classified in different phases: If only up and down flavors are involved, we have a 2-flavor color superconductor (2SC), for three flavors including the strange quark we have a color-flavor-locked (CFL) phase. Other phases studied involve a color-spin-locked (CSL) phase and a polar phase. Matter may further occur in the form of crystalline LOFF (named after Larkin, Ovchinnikov, Fulde and Ferrell) where Cooper pairs with nonzero total momentum are favored [14]. Color superconductivity may exist up to a temperature of 6 to 60 MeV [15], above which we enter the quark-gluon-plasma phase.

For small to medium temperature ranges, the QGP may be described as a non-Fermi liquid. It is called "Non-Fermi", because its behavior cannot entirely be described by the classical (Landau-)Fermi liquid theory of non-interacting cold fermions. This is due to transverse gauge bosons (transverse gluons) which are not screened at small temperatures due to the properties of dynamical screening. We have long-range, quasi-static interactions which give anomalous contributions to thermodynamic quantities like the specific heat. Such non-Fermi liquid behavior might have influence on astrophysical calculations, for example the cooling rate of proto-neutron stars [16]. Non-Fermi liquid behavior also appears in solid state physics experiments, for example in the specific heat of the YbRh_2Si_2 crystal [17, 18].

1.3 Outline

This thesis is organized as follows:

In chapter 2 we will introduce large N_f QCD where the number of quark flavors N_f is sent to infinity while the effective coupling $g_{\text{eff}} \propto g^2 N_f$ stays of order 1. We will see that this theory is exactly solvable in the effective coupling at next-to-leading order of the $1/N_f$ expansion. Also, the scale dependence is completely solvable to this order. Therefore this theory is particularly suitable for testing other perturbative and non-perturbative approaches against this limit. In contrast to lattice gauge theory, large N_f can be readily extended to finite μ .

In chapter 3 we will explore the non-Fermi-liquid regime of the large N_f theory. We will derive the pressure and the specific heat perturbatively and show that beyond the leading logarithm there are anomalous fractional powers and we calculate their coefficients up to order $T^{7/3}$ in the specific heat. We will see that fractional powers appear from the transverse gluon propagator whose calculation is carried out in careful detail, but both, longitudinal and transverse contributions to the pressure are needed to complete the leading logarithm of the specific heat.

The final chapter 4 gives a summary and an outlook.

Chapter 2

Large N_f

2.1 Introduction to Large N_f QCD

2.1.1 Why Large N_f ?

Large N_f QCD is quantum chromodynamics (QCD) with the number of quark flavors N_f assumed to be large ($N_f \rightarrow \infty$) and the strong coupling $\alpha_s = g^2/(4\pi) \rightarrow 0$ assumed to be small so that the effective coupling (which we will define later) $g_{\text{eff}}^2 \sim g^2 N_f \sim \alpha_s N_f \sim O(1)$ stays of order 1. Also, the number of colors N_c stays small $N_c \sim O(1)$.

Why do we want to study $N_f \rightarrow \infty$? After all, in our everyday world we only experience two quark flavors, that are the “up” and “down” quarks with masses of the order of 1-10 MeV. For the quark gluon phase transition at a temperature of about 170 MeV, only one more quark flavor, the “strange” quark with a mass of about 80-155 MeV [19], will play a considerable role in the thermal state. Even if we consider the other known quark types “charm”, “bottom” (also called “beauty”), and “top” (which is barely called “truth” anymore) with masses beyond a GeV, we end up with a total of $N_f \leq 6$ quark flavors. Clearly, the aim is not to realistically model QCD, but to study the theory in a well defined limit that turns out to be exactly solvable up to next-to-leading order in an $1/N_f$ expansion while containing essential physics of the full theory.

Ideally, we would like to solve full QCD, but so far only approximate numerical results from lattice simulations are available (at least for small μ/T), but with not completely understood systematic uncertainties. For temperatures far above the intrinsic scale of QCD, $T \gg \Lambda_{\text{QCD}}$, we expect the coupling g to get small [20]. Due to this property of strong interaction, called asymptotic freedom, we can expand the theory in terms of small g . It turns out that a strict perturbative expansion of thermodynamic parameters like the pressure in terms of the small coupling g would only work for ridiculously high temperatures and fails to work for the interesting region of tempera-

ture values slightly above the phase transition T_c or the QCD scale Λ_{QCD} : Successive orders in perturbation theory show very poor convergence. But this is not the only problem: Hot QCD has an intrinsically nonperturbative scale in the magnetostatic sector at wave numbers $k \sim g^2 T$. For the pressure this means that perturbation theory ceases to work at order $g^6 T^4$ [21, 22]. For other observables, this might even mean stricter restrictions to an expansion in g : Nonperturbative corrections are suppressed only by a power of g^2 for photon emissivity [23], a power of g for the Debye screening length [24, 25], or even not suppressed at all but appear at leading order in the case of the baryon number violation rate [26, 27]. But even in theories without the problem of a nonperturbative magnetostatic scale like in hot QED, the poor convergence of the perturbative series remains [28, 29, 30, 31, 32].

There have been attempts to improve the situation by reorganizations or partial resummations of the perturbative expansions of hot QCD. In scalar models where one already meets similar difficulties of poor convergence [33], Karsch et al. [34] proposed to keep a screening mass unexpanded at any given order of the loop expansion and to fix this mass by a stationarity principle, which technically means subtracting a mass term from the bare Lagrangian and adding it to the interaction part. This successful approach was extended to QCD by Andersen et al. [35, 36, 37, 38, 39, 40] by replacing the simple mass term by the gauge-invariant hard-thermal-loop (HTL) action [41, 42], a method which they termed HTL perturbation theory. Another approximation method is based on Φ -derivable approximations [43, 44] for 2PI skeleton diagrams advocated by Blaizot et al. [45, 46, 47, 48, 49]. Here, the starting point is an expression of the thermodynamic potential in terms of dressed propagators, where bare propagators are functionals of the full propagators that have to satisfy a stationarity condition. Truncation in this scheme does not happen in terms of the coupling g , but one resums diagrams to a given loop order of the 2PI skeleton diagrams.

All of these approaches show improved convergence properties, but it is difficult to tell to what extent these resummations can predict the correct behavior of full QCD. Apart from the necessary condition that these theories should coincide with perturbative QCD at very small couplings (corresponding to temperatures far beyond the scope of current collision experiments), only lattice calculations [50, 51] could give truly independent indications as to which resummation scheme to trust. Lattice theory on the other hand works more like a “black box” for theorists and provides only limited insight into the actual underlying physics, like screening effects or collective modes. One has therefore been looking for simpler theories that could be solved exactly, so that other resummation schemes could be tested within that simpler framework. One such theory is large- N scalar field theory with ϕ^4 interaction [52, 53] with an exactly solvable $N \rightarrow \infty$ limit. Another limit that has been studied in the past is the large N limit of a scalar field theory in 6 dimensions with cubic interactions [53] that mimics QED with N flavors. It

is richer than large N ϕ^4 -theory in that self-energies vary with momentum and wave-function renormalization is needed just like in full QCD. Yet, this theory involves instabilities which prevents one from direct comparisons to QCD. A more appealing test bed is large N_f QCD.

Besides being exactly solvable up to next-to-leading (NLO) order in $1/N_f$, large- N_f QCD contains the same complicated frequency and momentum dependent gauge field screening and damping as full QCD and its perturbative series shows similarly poor behavior as full QCD. One should keep in mind though that since large N_f QCD only resembles part of the full QCD theory, we do not expect large N_f to give any useful predictions for a small number of flavors. In fact, with a running coupling that leads to a Landau pole (like in QED) and excludes the possibility of confinement, large N_f at NLO is quite different from full QCD. Also, the leading order contributions to full QCD in an expansion in the coupling g are numerically dominated by sub-leading powers of $1/N_f$ for small N_f , as we will see in the next section. Yet, large N_f can be regarded as an important test theory, and any resummation scheme had better get close to the exact NLO result in the large N_f limit. On the other hand, even if a theory turns out to reproduce the right large N_f limit, that does not guarantee that it will correctly predict the full QCD result. After all, large N_f is a test theory, but contains a lot of the physics of full QCD, so if we can do this test, let's better do it.

2.1.2 Comparison to strict perturbative expansion in g

It is instructive to see which terms of perturbation theory survive in the large N_f limit. Strict perturbation theory has a long tradition. An overview over the known coefficients is given in figure 2.1. The leading order result to the pressure of perturbative QCD is just the Stefan-Boltzmann pressure of non-interacting quarks and gluons. The first non-trivial contributions to this result proportional to α_s were calculated independently by Shuryak and Chin in 1978 [54, 55] by calculating one- and two-loop vacuum graphs. The next order already turned out to be non-analytic in α_s and required the resummation of an infinite subset of diagrams. This was done by Kapusta to order $\alpha_s^{3/2}$ [56] and Toimela to order $\alpha_s^2 \ln \alpha_s$ [57]. Subsequent orders demanded new tools for evaluating sum-integrals by Arnold, Zhai and Kastening [28, 29, 58], or the introduction of dimensional reduction [59, 60, 61] by Braaten and Nieto [62]. The last perturbative series coefficient that has been calculated so far for full QCD is the $\alpha_s^3 \ln \alpha_s$ coefficient by Kajantie, Laine, Rummukainen, and Schröder [63, 64]. The order α_s^3 coefficient is completely non-perturbative as pointed out by Linde [21] and Gross, Pisarski, and Yaffe [22]. Recently the perturbative result has been extended to finite chemical potential by Vuorinen [65].

In this perturbative series the effect of large N_f is straightforward to be seen: Since we keep the quantity $\alpha_s N_f \sim O(1)$ of order one while we send

Perturbative calculations of QCD at high T/μ

$$\begin{aligned}
 P = \frac{8\pi^2}{45} T^4 & \left\{ 1 + \frac{21}{32} N_f \right. && \text{Planck 1900} \\
 & - \frac{15}{4} \left(1 + \frac{5}{12} N_f \right) \frac{\alpha_s}{\pi} && \text{Shuryak/Chin 1978} \\
 & + 30 \left(1 + \frac{N_f}{6} \right)^{\frac{3}{2}} \left(\frac{\alpha_s}{\pi} \right)^{\frac{3}{2}} && \text{Kapusta 1979} \\
 & + \frac{135}{2} \left(1 + \frac{N_f}{6} \right) \ln \frac{\alpha_s}{\pi} \left(1 + \frac{N_f}{6} \right) \cdot \left(\frac{\alpha_s}{\pi} \right)^2 && \text{Toimela 1983} \\
 & + \left\{ 237.2 + 15.97 N_f - 0.413 N_f^2 \right. && \text{Arnold\&Zhai 1995} \\
 & \left. - \frac{165}{8} \left(1 + \frac{5}{12} N_f \right) \left(1 - \frac{2}{33} N_f \right) \ln \frac{\bar{\mu}}{2\pi T} \right\} \left(\frac{\alpha_s}{\pi} \right)^2 \\
 & + \left(1 + \frac{N_f}{6} \right)^{\frac{1}{2}} \left\{ -799.2 - 21.96 N_f - 1.93 N_f^2 \right. && \text{Zhai\&Kastening 1995} \\
 & \left. + \frac{495}{2} \left(1 + \frac{N_f}{6} \right) \left(1 - \frac{2}{33} N_f \right) \ln \frac{\bar{\mu}}{2\pi T} \right\} \left(\frac{\alpha_s}{\pi} \right)^{\frac{5}{2}} && \text{Braaten\&Nieto 1996} \\
 & + \left\{ 1139.8 + 65.89 N_f + 7.653 N_f^2 \right. && \text{Kajantie, Laine,} \\
 & \left. - \frac{1485}{2} \left(1 + \frac{N_f}{6} \right) \left(1 - \frac{2}{33} N_f \right) \ln \frac{\bar{\mu}}{2\pi T} \right\} \ln \frac{\pi}{\alpha_s} \left(\frac{\alpha_s}{\pi} \right)^3 && \text{Rummukainen \&} \\
 & + \left\{ ?! + ? N_f + ? N_f^2 + C(\bar{\mu}) N_f^3 \right\} \left(\frac{\alpha_s}{\pi} \right)^3 + O\left(\frac{\alpha_s}{\pi} \right)^{\frac{7}{2}} && \text{Schröder 2002}
 \end{aligned}$$

* extension to $\mu_q \neq 0$: Vuorinen 2003

* $C(\bar{\mu}) = 0.040\dots$ for $\bar{\mu} = \pi T$ (A.I.&A.Rebhan 2003, see section 2.5.2)

* ?!: completely non-perturbative (Linde 1980; Gross, Pisarski & Yaffe 1980)

Figure 2.1: Known coefficients for the pressure of perturbative QCD by 2003. The coefficient marked as ?! denotes the breakdown of perturbation theory in the order α_s^3 . Only a few coefficients of this series contribute to the NLO contribution of the large- N_f limit, namely those of the form $\alpha_s^n N_f^n$. Particularly, terms containing a logarithm of the coupling $\ln \alpha_s$ do not survive the large- N_f limit. The large- N_f coefficient $C(\bar{\mu})$ of order $N_f^3 \alpha_s^3$ has been extracted numerically from the exact NLO result.

$N_f \rightarrow \infty$ and $\alpha_s \rightarrow 0$, the leading order (LO) contribution to the pressure is just given by the contribution proportional to N_f : $P = 7\pi^2 N_f T^4/60$. Actually, this contribution is infinitely large for $N_f \rightarrow \infty$, but we can always subtract this known leading order contribution to obtain a finite correction at next-to-leading order (NLO). From figure 2.1 we see that now all orders in the coupling α_s contribute to the large N_f NLO result which are of the form $\alpha_s^p N_f^p$ with $p = 0, 1, \frac{3}{2}, 2, \frac{5}{2}$. A graphical comparison of the partial sums of the series against the exact large N_f NLO calculation will be presented below in figure 2.8.

2.1.3 Outline

The pressure in large N_f QCD was first calculated by Moore for zero chemical potential [66]¹ and successively extended to finite chemical potential [68]. In the following sections we will present the exact large N_f result for the thermal pressure and some derived quantities thereof like the quark number susceptibilities or the entropy. The theory inevitably contains a Landau pole. We will study its effect on the result and show for which range of the coupling the effect of the Landau pole is negligible. At zero chemical potential we compare the exact large N_f result of the pressure and the quark number susceptibilities with known results from thermal perturbation theory [29, 58, 69] obtained at small chemical potential where dimensional reduction [59, 70, 61] is applicable. We verify the recent three-loop result of Vuorinen [71] on quark number susceptibilities numerically in the large N_f limit as well as a numerical coefficient in the pressure at zero temperature obtained long ago by Freedman and McLerran [72, 73]. For small values of the coupling g , our numerical accuracy allows us to extract a number of perturbative coefficients at order g^6 that are not yet known from analytical calculations.

It is remarkable that large N_f can be safely calculated all the way down from large temperatures and zero chemical potential to large chemical potential and zero temperature for effective couplings $g_{\text{eff}}^2 \lesssim 20$, which is a main advantage compared to lattice gauge theory. For a long time, the so-called “sign problem” prohibited calculations of fermions with finite chemical potential on the lattice. Only recently there has been important progress regarding calculation of thermodynamic quantities within lattice gauge theory [74, 75, 76, 77, 78, 79]. Using the large N_f limit, we can test the scaling behavior noticed in lattice calculations by Fodor, Katz, and Szabo [75] and find that it breaks down rather abruptly at $\mu_q \gtrsim \pi T$. We can also test the range of applicability of dimensional reduction by comparison to perturbative calculations at finite temperature and chemical potential by Vuorinen [65], where we study the effect of the choice of the renormalization scale.

¹ The first published version contained an unfortunate coding error which was revealed and corrected by an independent calculation involving the author of this thesis [67].

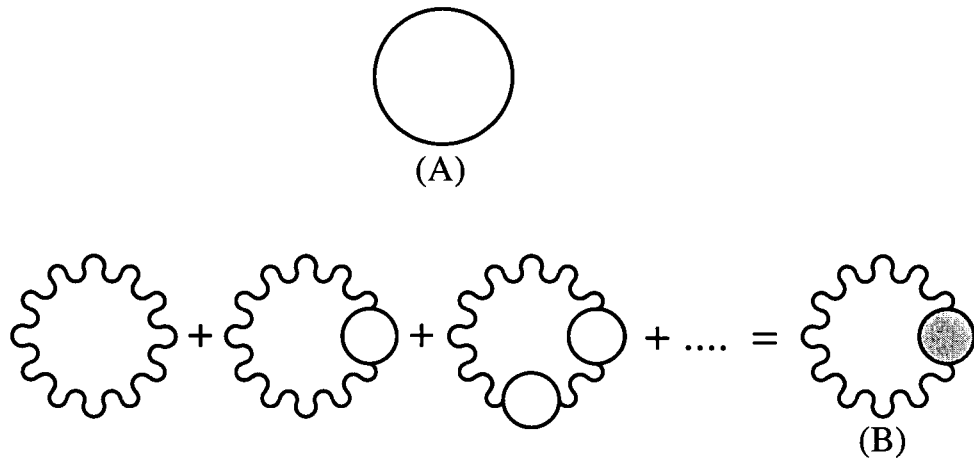


Figure 2.2: Diagrams contributing to the large N_f limit. At leading order (LO) of the order $O(N_f)$ there is only the fermion loop (A) contributing. At next-to-leading order (NLO) of order $O(1)$ there is an infinite number of diagrams contributing (B) which can be resummed by the Schwinger-Dyson method.

At small temperatures $T \ll \mu$ we enter the region of a non-Fermi-liquid behavior, which will be studied in detail in the next chapter.

Further discussions on the large N_f limit can be found in the literature by Peshier [80] on the quasiparticle picture [81, 82, 83], who points out the large differences between large and small N_f QCD with respect to the different strong coupling behavior and questions the immediate significance of a comparison within large N_f NLO. A detailed discussion of the HTL-quasiparticle picture of QCD with respect to large N_f and its implications on 2PI ϕ -derivable approximations [45] is given by Rebhan [84].

2.2 Pressure at Large- N_f QCD

In the following we want to calculate the thermal pressure in the large N_f limit. As we already already mentioned there are indeed two quantities that are involved in the limit: The number of flavors N_f and the coupling g . By forming the limit $N_f \rightarrow \infty$ we actually keep the effective coupling $g_{\text{eff}}^2 \sim g^2 N_f$ of order 1. In this sense, a suppression by a factor $1/N_f$ is equivalent to a suppression by a factor g^2 . We will see how this provides a very strong ordering principle for diagrams in the large N_f expansion. There are no special assumptions on the number of colors. We will calculate the pressure at next-to-leading order (NLO) where the theory can be solved exactly, that is to all orders in the effective coupling, apart from possible difficulties introduced by a Landau pole that we will discuss later. We will

follow the original approach of references [66, 67] and define the effective coupling as

$$g_{\text{eff}}^2 \equiv \frac{g^2 N_f C_F d_F}{d_A} = \begin{cases} \frac{g^2 N_f}{2}, & \text{QCD,} \\ g^2 N_f, & \text{QED.} \end{cases} \quad (2.2.1)$$

where C_F is the quadratic Casimir of the representation containing the fermions and d_F and d_A are the dimensions of the fermionic and adjoint representations. This allows us to treat the two cases of massless QCD and ultrarelativistic QED the theory at the same time. Since the coupling runs in these theories, we need to know the β function. The one-loop β function for QCD, that is a $SU(N)$ gauge theory with N_f fermions in the fundamental representation, is given by

$$2g \frac{\mu dg}{d\mu} = \frac{\mu d(g^2)}{d\mu} = \beta(g^2) = -\frac{2g^4}{(4\pi)^2} \left(\frac{11}{3}N - \frac{2}{3}N_f \right). \quad (2.2.2)$$

For sufficiently small N_f , that is $N_f < \frac{11}{2}N$, the β function is negative, which means that QCD is asymptotically free. In the limit of $N_f \rightarrow \infty$ we see that this behavior changes as the sign of $\beta(g)$ gets positive and large N_f therefore is no more an asymptotically free theory. The β function then becomes

$$\beta(g_{\text{eff}}^2) = \frac{\mu dg_{\text{eff}}^2}{d\mu} = \frac{(g_{\text{eff}}^2)^2}{6\pi^2}. \quad (2.2.3)$$

This relation turns out to be exact at leading order in $1/N_f$, even if we add higher loop beta function contributions (see for example reference [85]) to the one-loop result (2.2.2) because they are diagrammatically suppressed at least by a factor of $1/N_f \propto g^2$. We can solve the renormalization scale dependence exactly, giving

$$\frac{1}{g_{\text{eff}}^2(\mu)} = \frac{1}{g_{\text{eff}}^2(\mu')} + \frac{\ln(\mu'/\mu)}{6\pi^2}. \quad (2.2.4)$$

This theory contains a Landau pole of the order of $\Lambda_L \sim \mu \exp(6\pi^2/g_{\text{eff}}^2)$. Following reference [66] we define the Landau scale Λ_L such that the vacuum gauge field propagator diverges at $Q^2 = \Lambda_L^2$. The vacuum gauge field propagator is defined as $D_{\text{vac}}^{-1} = q^2 - q_0^2 + \Pi_{\text{vac}}$ with Π_{vac} from equation (2.2.9) below, which leads to

$$\Lambda_L = \bar{\mu}_{\text{MS}} e^{5/6} e^{6\pi^2/g_{\text{eff}}^2(\bar{\mu}_{\text{MS}})}. \quad (2.2.5)$$

This Landau singularity means that the exact definition of the theory is ambiguous unless the UV completion is specified. But that should not hinder us from doing finite temperature calculations since the ambiguity for the

thermal pressure at NLO is suppressed by a factor $(\max(T, \mu)/\Lambda_L)^4$. As long as we stay well below the Landau pole with temperature T and chemical potential μ , we can expect to get results which are not afflicted by the UV incompleteness of the large N_f theory.

The pressure can be calculated by computing the diagrams contributing to the free energy, which is the trace of the sum of all 1PI vacuum bubble graphs. At leading order in the $1/N_f$ expansion we only have one diagram - that is the bare fermion loop in figure 2.2. To obtain the thermal pressure, we subtract off the vacuum part of the diagrams. The leading order pressure is thus given by

$$P_{\text{LO}} = N_f \text{Tr} \left(T \sum_{n, \text{odd}} \int \frac{d^3 \mathbf{q}}{(2\pi)^3} \ln \mathcal{Q} - \int \frac{d^4 Q}{(2\pi)^4} \ln \mathcal{Q} \right) \quad (2.2.6)$$

It is well-known how to calculate this contribution for finite temperature and chemical potential and the pressure is given by

$$P_{\text{LO}} = NN_f \left(\frac{7\pi^2 T^4}{180} + \frac{\mu^2 T^2}{6} + \frac{\mu^4}{12\pi^2} \right) \quad (2.2.7)$$

The leading order contribution in the pressure is thus of order N_f and strictly speaking infinitely large in the limit of $N_f \rightarrow \infty$. Of course, we can always think of this as the leading contribution to an expansion in terms of $1/N_f$ with large but finite N_f .

The next-to-leading order (NLO) of this expansion is proportional to $N_f^0 = 1$. We can calculate it from the gauge boson loop with an arbitrary number of fermion loop insertions (plus corresponding counterterm insertions), which are all of order N_f^0 . For each fermion loop insertion we get a factor N_f and a factor g^2 from the two vertices, thus just our effective coupling $g^2 N_f \propto g_{\text{eff}}^2 \sim O(1)$. Any additional bosonic or ghost insertion would give factors of g^2 or higher, without introducing new fermion loop factors of N_f , and are thus suppressed by at least a factor of $g^2 \propto 1/N_f$. Therefore this gauge boson loop is all there is to NLO. It can be resummed by the standard Schwinger-Dyson resummation. Its contribution to the pressure is (again subtracting the vacuum part)

$$P_{\text{NLO}} = -\frac{1}{2} \text{Tr} \left(T \sum_{n, \text{even}} \int \frac{d^3 \mathbf{q}}{(2\pi)^3} \ln([D_0^{-1}]^{\mu\nu}(Q) + \Pi_{\text{th}}^{\mu\nu}(Q)) - \int \frac{d^4 Q}{(2\pi)^4} \ln([D_0^{-1}]^{\mu\nu}(Q) + \Pi_{\text{vac}}^{\mu\nu}(Q)) \right) \quad (2.2.8)$$

where the trace runs over group and Lorentz indices. The vacuum part of the gauge-boson self energy is given by

$$\Pi_{\text{vac}}^{\mu\nu}(Q) = -\frac{g_{\text{eff}}^2}{12\pi^2} (\eta^{\mu\nu} Q^2 - Q^\mu Q^\nu) \left(\ln \frac{Q^2}{\bar{\mu}^2} - \frac{5}{3} \right), \quad (2.2.9)$$

and the one-loop bosonic self-energy can be calculated via

$$\tilde{\Pi}_G(Q) \equiv \eta_{\mu\nu}\Pi^{\mu\nu}(Q) - [\text{vac}] = 2\Pi_T(Q) + \Pi_L(Q), \quad (2.2.10)$$

$$\tilde{\Pi}_H(Q) \equiv \Pi^{00}(Q) - [\text{vac}] = \frac{q^2}{Q^2}\Pi_L(Q) \quad (2.2.11)$$

where $\tilde{\Pi}_G$ and $\tilde{\Pi}_H$ will be calculated in the next section in equations (2.3.21), (2.3.22), and (2.3.26). These cannot be given in closed form except for their imaginary parts [67], but are represented by one-dimensional integrals involving the fermionic distribution function n_f . Using this decomposition of the self energy, the trace of the resummed propagator can be rewritten as

$$\text{Tr} \ln([D_0^{-1}]^{\mu\nu}(Q) + \Pi_{\text{th}}^{\mu\nu}(Q)) = 2 \ln(Q^2 + \Pi_T + \Pi_{\text{vac}}) + \ln(Q^2 + \Pi_L + \Pi_{\text{vac}}) - \ln(Q^2) \quad (2.2.12)$$

if we choose an appropriate gauge in which D_0^{-1} factorizes in the same way as Π , as for example in the Feynman gauge $[D_0^{-1}]^{\mu\nu}(Q) = \eta^{\mu\nu}Q^2$. Any gauge dependence drops out to our order of interest, since we only regard the difference between thermal and vacuum contributions. We can now perform the sum over Matsubara frequencies in the usual way of replacing it by a contour integral that is deformed appropriately. The result is then given by [66]

$$\begin{aligned} \frac{P_{\text{NLO}}}{N_g} = & - \int \frac{d^3q}{(2\pi)^3} \int_0^\infty \frac{dq_0}{\pi} \left[2 \left(\left[n_b + \frac{1}{2} \right] \text{Im} \ln(q^2 - q_0^2 + \Pi_T + \Pi_{\text{vac}}) \right. \right. \\ & \left. \left. - \frac{1}{2} \text{Im} \ln(q^2 - q_0^2 + \Pi_{\text{vac}}) \right) \right. \\ & \left. + \left(\left[n_b + \frac{1}{2} \right] \text{Im} \ln\left(\frac{q^2 - q_0^2 + \Pi_L + \Pi_{\text{vac}}}{q^2 - q_0^2}\right) - \frac{1}{2} \text{Im} \ln\left(\frac{q^2 - q_0^2 + \Pi_{\text{vac}}}{q^2 - q_0^2}\right) \right) \right] \end{aligned} \quad (2.2.13)$$

with the bosonic distribution function $n_b(\omega) = 1/(e^{\omega/T} - 1)$ coming directly from the sum over even frequencies $q_0 = 2n\pi T$. When evaluating the integrals above exactly by numerical means, we can safely integrate parts proportional to n_b in Minkowski space, since those are exponentially ultra-violet safe. For terms without n_b more care is required. We will refer to the former contributions as “ n_b ”-parts and the latter as “non- n_b ” contributions. The “non- n_b ” contributions are potentially logarithmically divergent, unless a Euclidean invariant cutoff is introduced [66]. We will discuss this point in more detail in section 2.4.

For non-vanishing chemical potential μ we use the fermionic distribution function

$$n_f(k, T, \mu) = \frac{1}{2} \left(\frac{1}{e^{(k-\mu)/T} + 1} + \frac{1}{e^{(k+\mu)/T} + 1} \right) \quad (2.2.14)$$

which enters via the gauge boson self-energy expressions Π_T and Π_L .

2.3 Leading-order gauge boson self-energy

The leading-order gauge boson self-energy in the large N_f limit is diagrammatically represented by a gauge boson propagator containing one fermion loop insertion. In the imaginary time formalism it can be written as

$$\begin{aligned} \tilde{\pi}\Pi^{\mu\nu}(i\omega_n, \mathbf{p}) &= 2N_f \tilde{g}^2 g^2 \int \frac{d^3k}{(2\pi)^3} \int_{-\infty}^{\infty} \frac{dk_0}{2\pi} \int_{-\infty}^{\infty} \frac{dq_0}{2\pi} \rho_0(k_0, \mathbf{k}) \rho_0(q_0, \mathbf{q}) \\ &\quad \times \frac{n(k_0) - n(q_0)}{k_0 - q_0 - i\omega_n} (k^\mu q^\nu + q^\mu k^\nu - g^{\mu\nu} k^\alpha k_\alpha + g^{\mu\nu} m^2) \end{aligned} \quad (2.3.1)$$

with $\mathbf{q} \equiv \mathbf{k} - \mathbf{p}$. The constants \tilde{g} and $\tilde{\pi}$ can be adjusted to fit various author's conventions (see also the conventions used in appendix B). We follow Weldon's conventions [86] by setting $\tilde{g}^2/\tilde{\pi} = -1$. The fermionic Boltzmann-factor is given by $n(k_0) = 1/(e^{k_0/T} + 1)$ and the spectral function is given by $\rho_0(k_0, \mathbf{k}) = 2\pi\epsilon(k_0)\delta(k_0^2 - \mathbf{k}^2 - m^2) = \frac{\pi}{\epsilon_k}(\delta(k_0 - \epsilon_k) - \delta(k_0 + \epsilon_k))$ with $\epsilon(k_0) = k_0/|k_0|$ and $\epsilon_k \equiv \sqrt{\mathbf{k}^2 + m^2}$. We can find a spectral form of the self energy by using

$$\Pi_{\mu\nu}(z, \mathbf{p}) = \int_{-\infty}^{\infty} \frac{dp_0}{2\pi} \frac{\pi_{\mu\nu}(p_0, \mathbf{p})}{z - p_0} \quad (2.3.2)$$

which is valid for any complex z [87, eq (3.1.36)]. The spectral density is then given by

$$\begin{aligned} \tilde{\pi}\pi^{\mu\nu}(p_0, \mathbf{p}) &= -2N_f \tilde{g}^2 g^2 \int \frac{d^3k}{(2\pi)^3} \int_{-\infty}^{\infty} \frac{dk_0}{2\pi} \int_{-\infty}^{\infty} \frac{dq_0}{2\pi} \rho_0(k_0, \mathbf{k}) \rho_0(q_0, \mathbf{q}) \\ &\quad \times (n(k_0) - n(q_0)) 2\pi\delta(p_0 - k_0 + q_0) I^{\mu\nu} \end{aligned} \quad (2.3.3)$$

with

$$I^{\mu\nu} = (k^\mu q^\nu + q^\mu k^\nu - g^{\mu\nu} k^\alpha k_\alpha + g^{\mu\nu} m^2).$$

The spectral density is manifestly real which will simplify our calculations. Since the spectral density will play an important role, we will try to push its calculation as far as we can. After integrating over q_0 , we are left with with an expression depending only on $k^\mu = (k_0, \mathbf{k})$ and $p^\mu = (p_0, \mathbf{p})$. A transformation of variables $k^\mu \rightarrow -k'^\mu + p^\mu$ in the part proportional to $n(q_0) = n(k_0 - p_0)$ leaves all other parts invariant up to minus signs. It basically replaces $n(k_0 - p_0)$ by $-n(-k'_0) = n(k'_0) - 1$ so that we can replace $(n(k_0) - n(q_0))$ by $(2n(k_0) - 1)$ in equation (2.3.3). If we use $z = \cos\theta$ as the angle between $\mathbf{pk} = pkz$, we can express

$$\rho_0(k_0 - p_0, \mathbf{k} - \mathbf{p}) = 2\pi\epsilon(k_0 - p_0) \frac{1}{2kp} \delta\left(z - \frac{k^2 + p^2 - (k_0 - p_0')^2}{2kp}\right) \quad (2.3.4)$$

and integrate over z in $\int \frac{d^3 k}{(2\pi)^3} = \frac{1}{(2\pi)^2} \int_{-1}^1 dz \int_0^\infty k^2 dk$. Analogous to Weldon [86] we can then define

$$\begin{aligned} I_G &\equiv g^{\mu\nu} I_{\mu\nu} = -k_0^2 + k^2 + p_0^2 - p^2, \\ I_H &\equiv u^\mu u^\nu I_{\mu\nu} = \frac{1}{2} (k^2 - p^2 + (k_0 - p_0)(3k_0 - p_0)) \end{aligned} \quad (2.3.5)$$

with $u^\mu = (1, 0, 0, 0)$ and integrate over k_0 . This is the last integral that we can do analytically. The spectral density turns out to be antisymmetric in k_0 meaning $\pi(k_0, \mathbf{k}) = -\pi(-k_0, \mathbf{k})$. The final result for the spectral density of the self-energy can then be written as a sum of two parts that only differ by the sign of p_0

$$\pi_X(p_0, \mathbf{p}) = \pi_X^+(p_0, p) - \pi_X^+(-p_0, p), \quad (2.3.6)$$

$$\begin{aligned} \pi_X^+(p_0, p) &= -\frac{\tilde{g}^2 g^2 N_f}{\tilde{\pi} 2\pi p} \int_0^\infty dk \left(n(k) - \frac{1}{2} \right) \bar{I}_X \\ &\quad \times \epsilon(k - p_0) \theta(|k - p| \leq |k - p_0| \leq |k + p|) \end{aligned} \quad (2.3.7)$$

with $X = G$ or H as in

$$\begin{aligned} \bar{I}_G &\equiv I_G(k_0 = k) = p_0^2 - p^2, \\ \bar{I}_H &\equiv I_H(k_0 = k) = \frac{1}{2} (2k + p - p_0)(2k - p - p_0). \end{aligned} \quad (2.3.8)$$

The θ -function stems from the integration over z with $-1 \leq z \leq 1$ and its usage here means $\theta(\text{true expression}) = 1$ and $\theta(\text{false expression}) = 0$.

Self-energy in the complex energy plane

Starting from the spectral form (2.3.2) we can calculate the self-energy in Minkowski or in Euclidean metric or anywhere between in the complex plane. To compare our results to the real-time formalism we start with the self-energy with Feynman prescription

$$\tilde{\Pi}_F(p_0, \mathbf{p}) \equiv \Pi(p_0 + ip_0\epsilon, \mathbf{p}). \quad (2.3.9)$$

Separating $\frac{1}{x+i\epsilon} = \frac{P}{x} - i\pi\delta(x)$ with P denoting the principal value, and knowing that $\pi(k_0, \mathbf{k})$ is a real function, we can easily separate this equation into real and imaginary parts

$$\text{Re}\tilde{\Pi}_F(p_0, \mathbf{p}) = \int_{-\infty}^{\infty} \frac{dp'_0}{2\pi} \pi(p'_0, p) \frac{P}{p_0 - p'_0}, \quad (2.3.10)$$

$$\text{Im}\tilde{\Pi}_F(p_0, \mathbf{p}) = -\frac{1}{2} \epsilon(p_0) \pi(p_0, p). \quad (2.3.11)$$

In the general case we can write

$$\begin{aligned}\Pi(a + ib, \mathbf{p}) &= \int_{-\infty}^{\infty} \frac{dp_0}{2\pi} \pi(p_0, p) \frac{1}{a + ib - p_0} \\ &= \int \frac{dp_0}{2\pi} \pi(p_0, p) \left(\frac{a - p_0}{(a - p_0)^2 + b^2} - i \frac{b}{(a - p_0)^2 + b^2} \right) \quad (2.3.12)\end{aligned}$$

where we separated real- and imaginary parts. By using the antisymmetry property of the spectral density (2.3.6) we can finally write

$$\begin{aligned}\Pi(a + ib, \mathbf{p}) &= \int \frac{dp_0}{2\pi} \pi^+(p_0, p) \left(\frac{a - p_0}{(a - p_0)^2 + b^2} - \frac{a + p_0}{(a + p_0)^2 + b^2} \right) \\ &\quad - i \int \frac{dp_0}{2\pi} \pi^+(p_0, p) \left(\frac{b}{(a - p_0)^2 + b^2} - \frac{b}{(a + p_0)^2 + b^2} \right) \quad (2.3.13)\end{aligned}$$

where all integrals to be evaluated are real. Particularly for the case $a \rightarrow 0$ and $b = \omega \neq 0$ we recover the result for the Euclidean metric

$$\tilde{\Pi}_{Eucl}(i\omega, \mathbf{p}) \equiv \Pi(i\omega + \varepsilon, \mathbf{p}), \quad (2.3.14)$$

$$\begin{aligned}\text{Re} \tilde{\Pi}_{Eucl}(i\omega, \mathbf{p}) &= \int_{-\infty}^{\infty} \frac{dp_0}{2\pi} \pi^+(p_0, p) \frac{-2p_0}{\omega^2 + p_0^2} \\ &= \int_{-\infty}^{\infty} \frac{dp_0}{2\pi} \pi(p_0, p) \frac{-p_0}{\omega^2 + p_0^2}, \quad (2.3.15)\end{aligned}$$

$$\text{Im} \tilde{\Pi}_{Eucl}(i\omega, \mathbf{p}) = 0. \quad (2.3.16)$$

Minkowski space results

Plugging our self-energy (2.3.6) in the expressions (2.3.10) above we get the Minkowski space results. First we note that we can write the integral over p_0 that we have to deal with in a simple way since p and k are positive:

$$\begin{aligned}&\int_{-\infty}^{\infty} dp_0 \epsilon(k - p_0) \theta(|k - p| \leq |k - p_0| \leq |k + p|) f(p_0) \\ &= \theta(k - p) \left(\int_{-p}^p dp_0 f(p_0) - \int_{2k-p}^{2k+p} dp_0 f(p_0) \right) \\ &\quad + \theta(p - k) \left(\int_{-p}^{2k-p} dp_0 f(p_0) - \int_p^{2k+p} dp_0 f(p_0) \right) \\ &= \int_{-p}^p dp_0 f(p_0) - \int_{2k-p}^{2k+p} dp_0 f(p_0). \quad (2.3.17)\end{aligned}$$

The resulting integral for the real part can then be written as

$$\begin{aligned} \text{Re}\tilde{\Pi}_X(p_0, \mathbf{p}) &= -\frac{\tilde{g}^2 g^2 N_f}{\tilde{\pi} 2\pi p} \int_0^\infty dk \left(n(k) - \frac{1}{2} \right) \\ &\times \left[\int_{-p}^p dp'_0 - \int_{2k-p}^{2k+p} dp'_0 \right] \left(\frac{P}{p_0 - p'_0} - \frac{P}{p_0 + p'_0} \right) \bar{I}_X(k, p'_0, p). \end{aligned} \quad (2.3.18)$$

Using

$$\begin{aligned} &\int dp'_0 \left(\frac{P}{p_0 - p'_0} - \frac{P}{p_0 + p'_0} \right) \bar{I}_G(k, p'_0, p) \\ &= -p_0'^2 - (p_0'^2 - p^2) (\log(|p'_0 - p_0|) + \log(|p'_0 + p_0|)) \end{aligned} \quad (2.3.19)$$

and

$$\begin{aligned} &\int dp'_0 \left(\frac{P}{p_0 - p'_0} - \frac{P}{p_0 + p'_0} \right) \bar{I}_H(k, p'_0, p) \\ &= \frac{1}{2} [8kp'_0 - p_0'^2 - (2k - p - p_0)(2k + p - p_0) \log(|p'_0 - p_0|) \\ &\quad - (2k - p + p_0)(2k + p + p_0) \log(|p'_0 + p_0|)] \end{aligned} \quad (2.3.20)$$

we finally arrive at the real part of the self-energy that is stated in Weldon's paper [86]

$$\begin{aligned} \text{Re}\tilde{\Pi}_G(p_0, \mathbf{p}) &= \left(-\frac{\tilde{g}^2}{\tilde{\pi}} \right) \frac{g^2 N_f}{2\pi^2} \int_0^\infty dk \left(n(k) - \frac{1}{2} \right) \\ &\times \left[4k + \frac{p_0^2 - p^2}{2p} \log \left| \frac{2k + p_0 + p}{2k + p_0 - p} \frac{2k - p_0 + p}{2k - p_0 - p} \right| \right] \end{aligned} \quad (2.3.21)$$

and

$$\begin{aligned} \text{Re}\tilde{\Pi}_H(p_0, \mathbf{p}) &= \left(-\frac{\tilde{g}^2}{\tilde{\pi}} \right) \frac{g^2 N_f}{2\pi^2} \int_0^\infty dk \left(n(k) - \frac{1}{2} \right) \\ &\times \left[2k \left(1 - \frac{p_0}{p} \log \left| \frac{p_0 + p}{p_0 - p} \right| \right) \right. \\ &\quad + \frac{(2k + p_0 + p)(2k + p_0 - p)}{4p} \log \left| \frac{2k + p_0 + p}{2k + p_0 - p} \right| \\ &\quad \left. - \frac{(2k - p_0 - p)(2k - p_0 + p)}{4p} \log \left| \frac{2k - p_0 - p}{2k - p_0 + p} \right| \right]. \end{aligned} \quad (2.3.22)$$

Note that Weldon already subtracted the $T = 0$ vacuum part and replaced $n(k) - \frac{1}{2}$ by $n(k)$. For the imaginary part no further calculation is necessary

and we can simply relate the imaginary part of the self-energy to its spectral density (2.3.6)

$$\text{Im}\tilde{\Pi}_X(p_0, \mathbf{p}) = -\frac{1}{2}\epsilon(p_0) (\pi_X^+(p_0, p) - \pi_X^+(-p_0, p)). \quad (2.3.23)$$

We are left with integrals over k that can be solved analytically. We rewrite the integral over k for the sign- and the θ -function as

$$\begin{aligned} & \int_{-\infty}^{\infty} dk \epsilon(k - p_0) \theta(|k - p| \leq |k - p_0| \leq |k + p|) f(k) \\ &= \theta(p^2 - p_0^2) \int_{\frac{p_0+p}{2}}^{\infty} f(k) dk - \theta(p_0 - p) \int_{\frac{p_0-p}{2}}^{\frac{p_0+p}{2}} f(k) dk. \end{aligned} \quad (2.3.24)$$

The function $f(k)$ is one of the following $f(k) = n(k)$, $kn(k)$, or $k^2n(k)$ if we already subtract the vacuum part from $n(k) - \frac{1}{2}$. This leaves us with the following integrals

$$\begin{aligned} F_1(x) &\equiv \int_x^{\infty} n(k) dk = -x + T \log(e^{x/T} + 1), \\ F_2(x) &\equiv \int_x^{\infty} kn(k) dk = \frac{\pi^2 T^2}{6} - \frac{x^2}{2} + xT \log(e^{x/T} + 1) + T^2 \text{Li}_2(-e^{x/T}), \\ F_3(x) &\equiv \int_x^{\infty} k^2 n(k) dk = -\frac{x^3}{3} + x^2 T \log(e^{x/T} + 1) \\ &\quad + 2xT^2 \text{Li}_2(-e^{x/T}) - 2T^3 \text{Li}_3(-e^{x/T}) \end{aligned} \quad (2.3.25)$$

with $\text{Li}_n(x)$ being the polylogarithm function. The functions $F_i(x)$ have the property that $F_i(x \rightarrow \infty) \rightarrow 0$ and $F_i(x > 0, T \rightarrow 0) \rightarrow 0$. The thermal contribution to the imaginary part of the self-energy can then be written as

$$\begin{aligned} \text{Im}\tilde{\Pi}_X(p_0, \mathbf{p}) &= -\frac{1}{2}\epsilon(p_0) \left(-\frac{\tilde{g}^2}{\tilde{\pi}} \right) \frac{g^2 N_f}{2\pi p} \\ &\quad \times \left[\theta(p^2 - p_0^2) \left(F_X^+\left(\frac{p_0+p}{2}\right) - F_X^-\left(\frac{-p_0+p}{2}\right) \right) \right. \\ &\quad + \theta(p_0 - p) \left(F_X^+\left(\frac{p_0+p}{2}\right) - F_X^+\left(\frac{p_0-p}{2}\right) \right) \\ &\quad \left. - \theta(-p_0 - p) \left(F_X^-\left(\frac{-p_0+p}{2}\right) - F_X^-\left(\frac{-p_0-p}{2}\right) \right) \right] \end{aligned} \quad (2.3.26)$$

with $X = G$ or H and

$$F_G^{\pm}(x) = \int_x^{\infty} n(k) \bar{I}_G dk = (p_0^2 - p^2) F_1(x), \quad (2.3.27)$$

$$F_H^\pm(x) = \int_x^\infty n(k) \bar{I}_H(\pm p_0, p, k) dk = \frac{p_0^2 - p^2}{2} F_1(x) \mp 2p_0 F_2(x) + 2F_3(x). \quad (2.3.28)$$

Using symmetric and antisymmetric versions of these functions $F_X^S \equiv (F_X^+ + F_X^-)/2$ and $F_X^A \equiv (F_X^+ - F_X^-)/2$ we can rewrite equation (2.3.26) as

$$\begin{aligned} \text{Im} \tilde{\Pi}_X(p_0, \mathbf{p}) &= -\frac{1}{2} \epsilon(p_0) \left(-\frac{\tilde{g}^2}{\tilde{\pi}} \right) \frac{g^2 N_f}{2\pi p} \\ &\times \left[F_X^S\left(\frac{|p_0 + p|}{2}\right) - F_X^S\left(\frac{|p_0 - p|}{2}\right) \right. \\ &\quad \left. + \epsilon(p_0 + p) F_X^A\left(\frac{|p_0 + p|}{2}\right) - \epsilon(p_0 - p) F_X^A\left(\frac{|p_0 - p|}{2}\right) \right]. \end{aligned} \quad (2.3.29)$$

This way of writing is especially convenient for calculating the G -part of the self-energy, since $F_G^A = 0$ vanishes.

Euclidean space results

To obtain the results in Euclidean space we start from equation (2.3.15) with π^+ . As in the case for the Minkowski metric, we can simplify the integral over p_0 with sign- and θ -function according to equation (2.3.17) and we are left with real integrals of the basic form

$$\int dp_0 \frac{-2p_0}{\omega^2 + p_0^2} \bar{I}_G(k, p_0, p) = -p_0^2 + (\omega^2 + p_0^2) \log(\omega^2 + p_0^2) \quad (2.3.30)$$

and

$$\begin{aligned} \int dp_0 \frac{-2p_0}{\omega^2 + p_0^2} \bar{I}_H(k, p_0, p) &= \frac{1}{2} p_0 (8k - p_0) - 4k\omega \arctan\left(\frac{p_0}{\omega}\right) \\ &\quad - \frac{1}{2} (4k^2 - p^2 - \omega^2) \log(\omega^2 + p_0^2). \end{aligned} \quad (2.3.31)$$

For $\omega^2 + p_0^2 > 0$ there is no danger of running into singularities. Using the integral limits for p_0 from $-p$ to p and $2k - p$ to $2k + p$ as in (2.3.17) we can write the self-energy in the Euclidean metric as

$$\begin{aligned} \text{Re} \tilde{\Pi}_G(i\omega, \mathbf{p}) &= \left(-\frac{\tilde{g}^2}{\tilde{\pi}} \right) \frac{g^2 N_f}{2\pi^2} \int_0^\infty dk \left(n(k) - \frac{1}{2} \right) \\ &\times \left(4k + \frac{\omega^2 + p^2}{2p} \log \frac{\omega^2 + (2k - p)^2}{\omega^2 + (2k + p)^2} \right), \end{aligned} \quad (2.3.32)$$

$$\begin{aligned} \text{Re}\tilde{\Pi}_H(i\omega, \mathbf{p}) &= \left(-\frac{\tilde{g}^2}{\pi}\right) \frac{g^2 N_f}{2\pi^2} \int_0^\infty dk \left(n(k) - \frac{1}{2}\right) \\ &\times \left[2k + \frac{\omega^2 + p^2 - 4k^2}{4p} \log \frac{\omega^2 + (2k-p)^2}{\omega^2 + (2k+p)^2} \right. \\ &\left. - \frac{2k\omega}{p} \left(\arctan \frac{2k-p}{\omega} + 2 \arctan \frac{p}{\omega} - \arctan \frac{2k+p}{\omega} \right) \right]. \end{aligned} \quad (2.3.33)$$

This is in principle the result given by reference [66] up to the appearance of the arc tangents in the last line. The expression given there can be fully recovered by using $\arctan(z) = \frac{1}{2}i \log(1-iz) - \frac{1}{2}i \log(1+iz)$ for complex z and gathering the sum of logarithms into one logarithmic expression

$$\arctan \frac{2k-p}{\omega} + 2 \arctan \frac{p}{\omega} - \arctan \frac{2k+p}{\omega} \simeq -\frac{i}{2} \log \frac{1 + \frac{4k^2}{(\omega-ip)^2}}{1 + \frac{4k^2}{(\omega+ip)^2}}. \quad (2.3.34)$$

However this expression should be used with care. If one takes the principal branch of the logarithmic expression on the r.h.s., one obtains results that might differ from the arc tangent expression by some multiple of π . Solving for the branch-cut, that is where the expression inside the logarithm equals -1 , one finds that expression for real ω , p , and k can be written as

$$\sum \arctan = -\frac{i}{2} \log \frac{1 + \frac{4k^2}{(\omega-ip)^2}}{1 + \frac{4k^2}{(\omega+ip)^2}} + \pi \epsilon(p\omega) \theta(p^2 - \omega^2) \theta(|k| - \frac{p^2 + \omega^2}{2\sqrt{p^2 - \omega^2}}) \quad (2.3.35)$$

where one should take the principal value of the arctan and log expressions involved. As shown in equation (2.3.16) the imaginary part of the self-energy in the Euclidean space vanishes.

Complex Result

The result in the complex plane allows us to link results in Minkowski space and Euclidean space by great arcs. The safest way to obtain the result in the complex plane is to start with equation (2.3.13), where all integrals involved are real, and the result for the self-energy is separated into real and imaginary part. Starting point are the following indefinite integrals

$$\begin{aligned} F_G^{Re}(p_0) &\equiv \int dp_0 \left(\frac{a-p_0}{(a-p_0)^2 + b^2} - \frac{a+p_0}{(a+p_0)^2 + b^2} \right) \bar{I}_G \\ &= -p_0^2 - 2ab \left(\arctan \frac{a-p_0}{b} + \arctan \frac{a+p_0}{b} \right) \\ &\quad - \frac{1}{2}(a^2 - b^2 + p^2) (\log(b^2 + (a-p_0)^2) + \log(b^2 + (a+p_0)^2)), \end{aligned} \quad (2.3.36)$$

$$\begin{aligned}
F_G^{Im}(p_0) &\equiv \int dp_0 \left(\frac{b}{(a-p_0)^2+b^2} - \frac{b}{(a+p_0)^2+b^2} \right) \bar{I}_G \quad (2.3.37) \\
&= -(a^2-b^2-p^2) \left(\arctan \frac{a-p_0}{b} + \arctan \frac{a+p_0}{b} \right) \\
&\quad + ab (\log(b^2+(a-p_0)^2) + \log(b^2+(a+p_0)^2)).
\end{aligned}$$

Analogous results for F_H^{Re} and F_H^{Im} can be easily derived with any symbolic integrator. We combine these integrals according to equation (2.3.17) to form the result in general complex plane ($X = G$ or H):

$$\begin{aligned}
\text{Re}\Pi_X(a+ib, \mathbf{p}) &= \left(-\frac{\tilde{g}^2}{\pi} \right) \frac{g^2 N_f}{2\pi^2} \int_0^\infty dk \left(n(k) - \frac{1}{2} \right) \frac{1}{2p} \quad (2.3.38) \\
&\quad \times (F_X^{Re}(p) - F_X^{Re}(-p) - F_X^{Re}(2k+p) + F_X^{Re}(2k-p)),
\end{aligned}$$

$$\begin{aligned}
\text{Im}\Pi_X(a+ib, \mathbf{p}) &= -\left(-\frac{\tilde{g}^2}{\pi} \right) \frac{g^2 N_f}{2\pi^2} \int_0^\infty dk \left(n(k) - \frac{1}{2} \right) \frac{1}{2p} \quad (2.3.39) \\
&\quad \times (F_X^{Im}(p) - F_X^{Im}(-p) - F_X^{Im}(2k+p) + F_X^{Im}(2k-p)).
\end{aligned}$$

For $b \neq 0$ the expressions in the logarithms are positive, and the arc tangent functions stay finite, so that there is no danger of crossing a branch cut or encountering other singularities. Therefore these expressions are safe to be used in calculating the arc between Minkowski and Euclidean space.

Again, to subtract the vacuum part, just replace $(n(k) - \frac{1}{2})$ by $n(k)$.

2.4 Landau pole ambiguity

In the pressure formula (2.2.13) that we intend to integrate, we had two different kinds of contributions that we called “ n_b ” and “non- n_b ”. We already mentioned that the former are safe to be calculated in Minkowski space: for large q_0 the bosonic distribution function suppresses the integrand exponentially by $O(\exp(-q_0/T))$, while for large q but moderate q_0 , the thermal self-energy has an exponentially small imaginary part $\text{Im}\Pi \sim \exp(-(q-q_0)/2T)$ as can be seen from the exact result for the imaginary part of the self energy in Minkowski space (2.3.26), knowing that the functions F_i from (2.3.25) vanish exponentially as their argument increases. For the “non- n_b ” parts in (2.2.13) the situation is more subtle.

The “non- n_b ” parts are not exponentially suppressed for large q_0 . Also, in the region where $q_0 \sim q$, the self-energy functions are only suppressed by $1/q$ so that they might cause UV divergencies that should be studied. It is best to go into Euclidean space and study the relevant terms of the pressure function (2.2.13). In the limit of small T^2/Q^2 , the logarithms involved can

be expanded, giving

$$\begin{aligned} 2 \ln \frac{Q^2 + \Pi_{\text{vac}} + \Pi_T}{Q^2 + \Pi_{\text{vac}}} + \ln \frac{Q^2 + \Pi_{\text{vac}} + \Pi_L}{Q^2 + \Pi_{\text{vac}}} &= \\ &= \frac{2\Pi_T + \Pi_L}{Q^2 + \Pi_{\text{vac}}} - \frac{2\Pi_T^2 + \Pi_L^2}{2(Q^2 + \Pi_{\text{vac}})^2} + \dots \end{aligned} \quad (2.4.1)$$

The functions Π_T and Π_L can be expanded using (2.2.10) and (2.2.11) and the expressions for $\text{Re}\tilde{\Pi}_G(i\omega, \mathbf{p})$ (2.3.32) and $\text{Re}\tilde{\Pi}_H(i\omega, \mathbf{p})$ (2.3.33). One can expand the two functions in the limit $T^2 \ll Q^2$ by series expansion of the expression within the brackets in terms of small k and then performing the k integration for each order of k separately. The result is given by [66]

$$\left. \frac{\text{Re}\tilde{\Pi}_G(i\omega, \mathbf{p})}{2g_{\text{eff}}^2} \right|_{Q \gg T} = \frac{7\pi^2(3\omega^2 - q^2)}{45(Q^2)^2} T^4 - \frac{248\pi^4(5\omega^4 - 10\omega^2q^2 + q^4)}{315(Q^2)^4} T^6 + O(T^8), \quad (2.4.2)$$

$$\left. \frac{\text{Re}\tilde{\Pi}_H(i\omega, \mathbf{p})}{2g_{\text{eff}}^2} \right|_{Q \gg T} = \frac{7\pi^2q^2}{45(Q^2)^2} T^4 - \frac{248\pi^4q^2(5\omega^2 - q^2)}{945(Q^2)^4} T^6 + O(T^8). \quad (2.4.3)$$

The integration over the first term of the series (2.4.1) with the vacuum self-energy from (2.2.9) then gives

$$\frac{1}{2} \int \frac{d^4Q}{(2\pi)^4} \frac{2\Pi_T + \Pi_L}{Q^2 + \Pi_{\text{vac}}} \simeq \frac{7\pi^2 T^4 g_{\text{eff}}^2}{45} \int \frac{d^4Q}{(2\pi)^4} \frac{3\omega^2 - q^2}{(Q^2)^3} \frac{1}{1 - g_{\text{eff}}^2 \ln(Q^2/\bar{\mu}_{\text{MS}}^2)/12\pi^2}. \quad (2.4.4)$$

By simple power counting we see that this integral is potentially logarithmically divergent. However, if we perform the angular integral over the 4-sphere first, we see that the contribution $\int d\Omega_4(3\omega^2 - q^2) = 0$ vanishes for any distance $|Q|$. Since the rest of (2.4.4) is a function of Q^2 only, any regularization or cutoff which respects Euclidean invariance will be UV well behaved. It is important to average over the Euclidean four spheres first, before integrating over the radius $|Q|$. If we first perform one of the integrations ω or q first, and then integrate over the other variable without respecting Euclidean invariance, we might get spurious logarithmic divergencies. Of course, as long as we choose the upper integration limits such that in the end we integrate over the complete 4-sphere, nothing should happen (except for numerical cancellations to become more demanding). Integrating over a 4-dimensional cylinder in the ω/q space, or cutting out a four-dimensional cube might bring in potentially logarithmic contributions for a large cutoff Q . But numerically it is easiest to integrate over the surface of the 4-sphere for a fixed Q , and then integrate over the radius up to the cutoff.

Introducing a cutoff might cause gauge fixing dependence. For Lorentz and Coulomb gauges this turns out not to be the case because the self-energy

is gauge invariant as large N_f is basically an Abelian theory up to NLO. By the very same procedure as above, it can furthermore be shown that the introduction of an Euclidean invariant cutoff can be applied safely also to finite chemical potential.

As in references [66, 67] we apply a cutoff and stop the d^4Q integration at $Q^2 = a\Lambda_L^2$, varying the value of a between 1/4 and 1/2 to estimate the irreducible ambiguity.

In reference [66], the “ n_b ” terms from equation (2.2.13) were calculated in Minkowski space. Terms without n_b were computed along a complex frequency contour which ran up the Minkowski axis to $\omega_{\max} < \Lambda_{\text{Landau}}\sqrt{a}$ for some $a < 1$, then along the great arc to Euclidean space, and back down to $q_0 = \sqrt{q_{\max}^2 - q^2}$; finally, a Euclidean integration of the n_b free term was performed over 4-spheres in Euclidean space up to $Q^2 < \Lambda_{\text{Landau}}^2 a$. In reference [67] a simpler way of calculating the integral was pursued: all pieces linear in n_b were calculated in Minkowski space, and all terms without n_b were calculated in Euclidean space. By actually performing calculations in both ways, we had a rather non-trivial numerical check on the result which finally helped to reveal a coding error in the original result published [67, 66]. In the numerical implementation both ways turned out to agree within numerical errors of about 10^{-5} . The term after the vanishing leading term in equation (2.4.1) is of the order $(\Pi_T^2 + \Pi_L^2)/(Q^2 + \Pi_{\text{vac}})^2 \sim T^8$ so that the ambiguity introduced by the Landau pole is of the order $O(T^8/\Lambda_{\text{Landau}}^4)$.

2.5 Results and discussion

In Fig. 2.3 we display our exact results² for the interaction pressure $P - P_0 \propto N_f^0$, where the ideal-gas limit

$$P_0 = NN_f \left(\frac{7\pi^2 T^4}{180} + \frac{\mu^2 T^2}{6} + \frac{\mu^4}{12\pi^2} \right) + N_g \frac{\pi^2 T^4}{45} \quad (2.5.1)$$

has been subtracted, for the entire μ - T plane (but reasonably below the scale Landau pole). For this we introduce an angle $\phi = \arctan \frac{\pi T}{\mu}$ and encode the magnitudes T/Λ_L and μ/Λ_L through the running coupling $g_{\text{eff}}^2(\bar{\mu}_{\text{MS}})$ with $\bar{\mu}_{\text{MS}}^2 = \pi^2 T^2 + \mu^2$ according to (2.2.5).

We found that the ambiguity arising from the presence of a Landau pole reaches the percent level for $g_{\text{eff}}^2 \gtrsim 28$, where $\Lambda_L/\sqrt{\pi^2 T^2 + \mu^2} \lesssim 19$. At larger coupling (corresponding to larger T and/or μ), this ambiguity grows rapidly and will be shown in the two-dimensional plots below by a (tiny) red area.

In the following we shall compare the exact large- N_f result with known results from perturbation theory at high temperature and small chemical

² Tabulated results are available on-line at <http://hep.itp.tuwien.ac.at/~ipp/data/>.

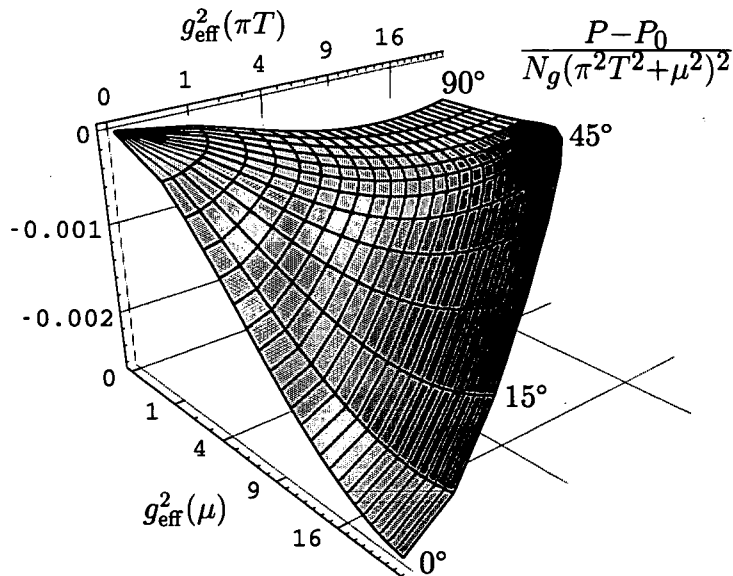


Figure 2.3: Exact result for the large- N_f interaction pressure $P - P_0$ normalized to $N_g(\pi^2 T^2 + \mu^2)^2$ as a function of $g_{\text{eff}}^2(\bar{\mu}_{\text{MS}})$ with $\bar{\mu}_{\text{MS}}^2 = \pi^2 T^2 + \mu^2$, which is the radial coordinate, and $\phi = \arctan \frac{\pi T}{\mu}$.

potential, where dimensional reduction is an effective organizing principle, and with results at zero temperature, where dimensional reduction does not apply. We also investigate to what extent quark number susceptibilities at vanishing chemical potential determine the behavior at larger chemical potential.

2.5.1 Comparison to dimensional reduction

Dimensional reduction is a method of expressing the static properties of a (3+1)-dimensional field theory at high temperature in terms of an effective field theory in 3 space dimensions [22, 60]. In the imaginary time formalism, all nonstatic modes involve the temperature scale, so integrating them out to obtain an effective field theory on scales $\ll T$ leaves only the static modes with zero Matsubara frequency. The dimensionally reduced theory involves the color-electric screening scale gT and a dimensionful coupling $g^2 T$ which is also the scale of color-magnetic screening. The perturbative result for the thermal pressure of hot gauge theories with fermions has been obtained by using this approach in reference [62] at zero chemical potential to order g^5 . The analytic result of dimensional reduction through order g^5 with complete analytic dependence on arbitrary T and μ was calculated by [65] and in the

large N_f limit this reduces to

$$\begin{aligned} \frac{P - P_0}{N_g} \Big|_{\text{DR}} &= - \left(\frac{5}{9} T^4 + \frac{2}{\pi^2} \mu^2 T^2 + \frac{\mu^4}{\pi^4} \right) \frac{g_{\text{eff}}^2}{32} \\ &\quad + T \frac{1}{12\pi} m_E^3 + \frac{g_{\text{eff}}^4}{(48\pi)^2} \bar{\alpha}_{\text{E3}} + O(g_{\text{eff}}^6 T^4) \end{aligned} \quad (2.5.2)$$

where the effective field theory parameter m_E^2 is given by

$$\frac{m_E^2}{T^2} = \left(1 + \frac{3\mu^2}{\pi^2 T^2} \right) \left[\frac{g_{\text{eff}}^2}{3} - \frac{g_{\text{eff}}^4}{(6\pi)^2} \left(2 \ln \frac{\bar{\mu}_{\text{MS}}}{4\pi T} - 1 - \aleph(z) \right) \right] + O(g_{\text{eff}}^6) \quad (2.5.3)$$

and the coefficient of order g^4 is analytic in T and μ and given by

$$\begin{aligned} \bar{\alpha}_{\text{E3}} &= 12 \left\{ \frac{5}{9} T^4 + \frac{2}{\pi^2} \mu^2 T^2 + \frac{\mu^4}{\pi^4} \right\} \ln \frac{\bar{\mu}_{\text{MS}}}{4\pi T} \\ &\quad + 4T^4 \left\{ \frac{1}{12} + \gamma - \frac{16}{15} \frac{\zeta'(-3)}{\zeta(-3)} - \frac{8}{3} \frac{\zeta'(-1)}{\zeta(-1)} \right\} \\ &\quad + \frac{\mu^2 T^2}{\pi^2} \left\{ 14 + 24\gamma - 32 \frac{\zeta'(-1)}{\zeta(-1)} \right\} + \frac{\mu^4}{\pi^4} (43 + 36\gamma) \\ &\quad - 96T^4 \{ 3\aleph(3, 1) + 8\aleph(3, z) + 3\aleph(3, 2z) - 2\aleph(1, z) \} \\ &\quad + \frac{48i\mu T^3}{\pi} \{ \aleph(0, z) - 12\aleph(2, z) - 12\aleph(2, 2z) \} \\ &\quad + \frac{96\mu^2 T^2}{\pi^2} \{ 4\aleph(1, z) + 3\aleph(1, 2z) \} + \frac{144i\mu^3 T}{\pi^3} \aleph(0, z) \end{aligned} \quad (2.5.4)$$

with the definitions from [65]

$$z \equiv \frac{1}{2} - i \frac{\mu}{2\pi T}, \quad (2.5.5)$$

$$\zeta'(x, y) \equiv \partial_x \zeta(x, y), \quad (2.5.6)$$

$$\aleph(n, w) \equiv \zeta'(-n, w) + (-1)^{n+1} \zeta'(-n, w^*), \quad (2.5.7)$$

$$\aleph(w) \equiv \Psi(w) + \Psi(w^*). \quad (2.5.8)$$

Here, n is assumed to be a non-negative integer and w a general complex number. ζ is the Riemann zeta function and Ψ is the digamma function $\Psi(w) \equiv \Gamma'(w)/\Gamma(w)$. Note that despite the appearance of complex quantities in (2.5.4) the coefficient $\bar{\alpha}_{\text{E3}}$ is real as it has to be.

For later usage we also present the effective field theory parameter of the coupling from dimensional reduction

$$g_{\text{eff}E}^2 = T \left[g_{\text{eff}}^2 + \frac{g_{\text{eff}}^4}{3(2\pi)^2} \left(2 \ln \frac{\bar{\mu}_{\text{MS}}}{4\pi T} - \aleph(z) \right) \right] + O(g_{\text{eff}}^6). \quad (2.5.9)$$

The expansion of the pressure in terms of small μ/T is given by

$$\begin{aligned} \frac{P - P_0}{N_g} \Big|_{T \gg \mu} = & - \left[\frac{5}{9} T^4 + \frac{2}{\pi^2} \mu^2 T^2 + \frac{1}{\pi^4} \mu^4 \right] \frac{g_{\text{eff}}^2}{32} \\ & + \frac{1}{12\pi} T m_E^3 + \left[\left(\frac{20}{3} T^4 + \frac{24}{\pi^2} T^2 \mu^2 \right) \ln \frac{\bar{\mu}_{\text{MS}}}{4\pi T} \right. \\ & + \left(\frac{1}{3} - \frac{88}{5} \ln 2 + 4\gamma - \frac{8}{3} \frac{\zeta'(-3)}{\zeta(-3)} + \frac{16}{3} \frac{\zeta'(-1)}{\zeta(-1)} \right) T^4 \\ & - \frac{26 + 32 \ln 2 - 24\gamma}{\pi^2} T^2 \mu^2 \\ & \left. + \frac{12\mu^4}{\pi^4} \left[\ln \frac{\bar{\mu}_{\text{MS}}}{4\pi T} + \gamma + C_4 \right] + \dots \right] \frac{g_{\text{eff}}^4}{(48\pi)^2} + O(g_{\text{eff}}^6 T^4), \quad (2.5.10) \end{aligned}$$

where the terms $\propto g_{\text{eff}}^4$ and involving μ have been first obtained by Vuorinen [71]. The contribution to order g_{eff}^5 arises from the NLO correction to the effective-field-theory parameter m_E^2 , which at finite μ was first computed in reference [69]. An alternative way of writing (2.5.3) is given by

$$\frac{m_E^2}{T^2} = \left(\frac{1}{3} + \frac{\mu^2}{\pi^2 T^2} \right) g_{\text{eff}}^2 \left\{ 1 - \frac{g_{\text{eff}}^2}{6\pi^2} \left[\ln \frac{\bar{\mu}_{\text{MS}}}{e^{1/2-\gamma}\pi T} + \frac{1}{2} \mathcal{D}\left(\frac{\mu}{\pi T}\right) \right] \right\} + O(g_{\text{eff}}^6) \quad (2.5.11)$$

with the function

$$\mathcal{D}(x) = -2\gamma - 4 \ln 2 - 2 \operatorname{Re} \Psi\left(\frac{1}{2}(1 + ix)\right). \quad (2.5.12)$$

For small x this function can be expanded as

$$\mathcal{D}(x) = 4 \sum_{n=1}^{\infty} (-1)^n \left(1 - \frac{1}{2^{2n+1}} \right) \zeta(2n+1) x^{2n}, \quad (2.5.13)$$

with a radius of convergence of 1, which corresponds to $\mu = \pi T$. The only nonanalytic terms in g_{eff}^2 to the pressure in the dimensionally reduced effective field theory at large N_f stem from the ‘‘plasmon term’’ $\propto m_E^3$. As can be seen from the expansion in figure 2.1 of the perturbative QCD pressure, the logarithms $\ln(g)$ do not survive the large N_f limit.

In figure 2.4 we plot the result obtained from dimensional reduction by Vuorinen [65] in the large N_f limit. In this plot we choose a naive renormalization scale of $\bar{\mu}_{\text{MS}} = \sqrt{(\pi T)^2 + \mu^2}$. By comparison to figure 2.3 we see that the small coupling range is well reproduced for couplings $g_{\text{eff}}^2 \lesssim 9$ for smaller μ/T but deviates considerably for larger μ/T . This is partly due to the choice of the renormalization scale which apparently is not the best. The exact result is independent of the choice of the initial renormalization scale. More precisely the scale dependence of the exact result enters only via the coupling $g_{\text{eff}}(\bar{\mu}_{\text{MS}})$ and results can be easily converted from one renormalization scale to another by applying the renormalization scale dependence

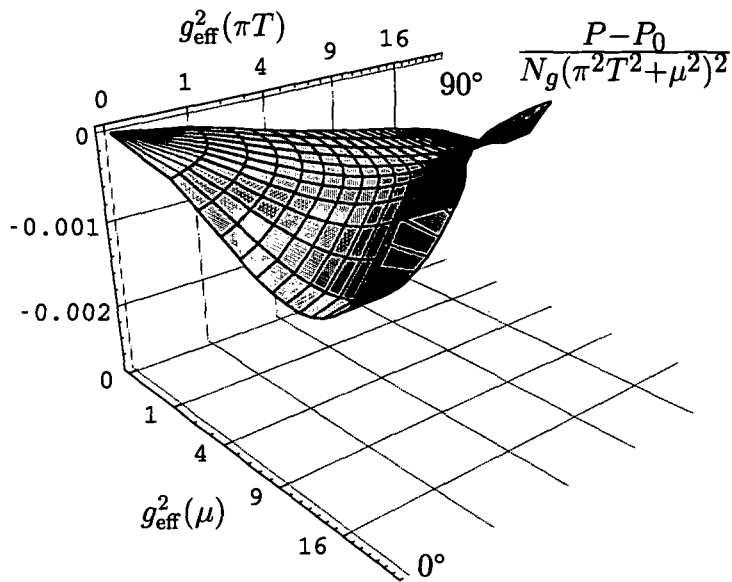


Figure 2.4: Dimensional reduction (DR) result of the pressure $(P_{\text{DR}} - P_0)/(N_g(\pi^2 T^2 + \mu^2)^2)$ in the large N_f limit in the same range as in figure 2.3. The renormalization scale is chosen as $\bar{\mu}_{\text{MS}} = \sqrt{(\pi T)^2 + \mu^2}$ for $\pi T = \bar{\mu}_{\text{MS}} \sin \phi$ and $\mu = \bar{\mu}_{\text{MS}} \cos \phi$.

relation (2.2.4). In the perturbative result this holds true only up to the order of perturbative accuracy. Numerically, due to truncation to a certain order in the coupling, the pressure not only depends on the renormalization scale indirectly via the coupling $g_{\text{eff}}(\bar{\mu}_{\text{MS}})$, but also directly, since higher order contributions that would fix the renormalization scale dependence are not taken into account. The result will therefore in general differ whether we started from a renormalization scale $\bar{\mu}_1$ and rescaled the resulting pressure according to (2.2.4) to a renormalization scale $\bar{\mu}_1 \rightarrow \bar{\mu}_2$, or if we directly calculated the perturbative result with the latter renormalization scale $\bar{\mu}_2$. Therefore, for perturbative results there is this additional question of which renormalization scale to choose.

A possible optimization is provided by the FAC (fastest apparent convergence) scale, which is derived by demanding that the effective-field-theory parameter m_E^2 from (2.5.11) vanishes to order g_{eff}^4 and all higher orders. This means solving $\ln \frac{\bar{\mu}_{\text{MS}}}{e^{1/2-\gamma}\pi T} + \frac{1}{2}\mathcal{D}(\frac{\mu}{\pi T})$ so that we obtain

$$\bar{\mu}_{\text{MS}}(\text{FAC-m}) = \pi T \exp \left[\frac{1}{2} - \gamma_E - \frac{1}{2}\mathcal{D}\left(\frac{\mu}{\pi T}\right) \right]. \quad (2.5.14)$$

For $\mu = 0$ this expression reduces to $\bar{\mu}_{\text{MS}}(\text{FAC-m}) = \pi T e^{\frac{1}{2}-\gamma_E}$ while for $T = 0$ it is given by $\bar{\mu}_{\text{MS}}(\text{FAC-m}) = 2\mu e^{\frac{1}{2}}$.

In figure 2.5 we see the difference between the pressure obtained from dimensional reduction to the exact large N_f result for this FAC-m renormalization scale. As in the three-dimensional plots we vary temperature T and chemical potential μ depending on the angle $\phi = \arctan \frac{\pi T}{\mu}$. The result is given for values of the coupling $0 \leq g_{\text{eff}}^2 \leq 24$ where the ambiguity introduced by the Landau pole is negligible numerically. In the plot we rescaled the dimensionally reduced pressure by the exact renormalization scale dependence (2.2.4) to the scale $\bar{\mu}_{\text{MS}} = \sqrt{(\pi T)^2 + \mu^2}$ to allow for unified comparison. The lines enclose those areas where the difference is less than $\pm 10^{-5}$, $\pm 10^{-4}$, or $\pm 10^{-3}$ in units of the normalized pressure. 10^{-3} is about the size of the NLO results, and thus marks the breakdown of the agreement between the two approaches (100% deviation). Notice that there is always a factor 10 of increase of the inaccuracy between neighboring lines of the contour plot. We have very good agreement for $g_{\text{eff}}^2 \lesssim 7$, but this value slowly decreases as the ratio μ/T is increased. Only for small angles $\phi \lesssim 20^\circ$ the behavior changes considerably and the ranges of good agreement shrink faster with decreasing μ/T . For the FAC-m scale dimensional reduction gives lower values of pressure than the exact large N_f result for $\phi \gtrsim 25^\circ$ and higher predictions for smaller μ/T . In between there is a transition from negative to positive differences which of course is of no real relevance to the error ranges in the plot.

Another natural choice for scale might be to apply FAC to g_E^2 . This

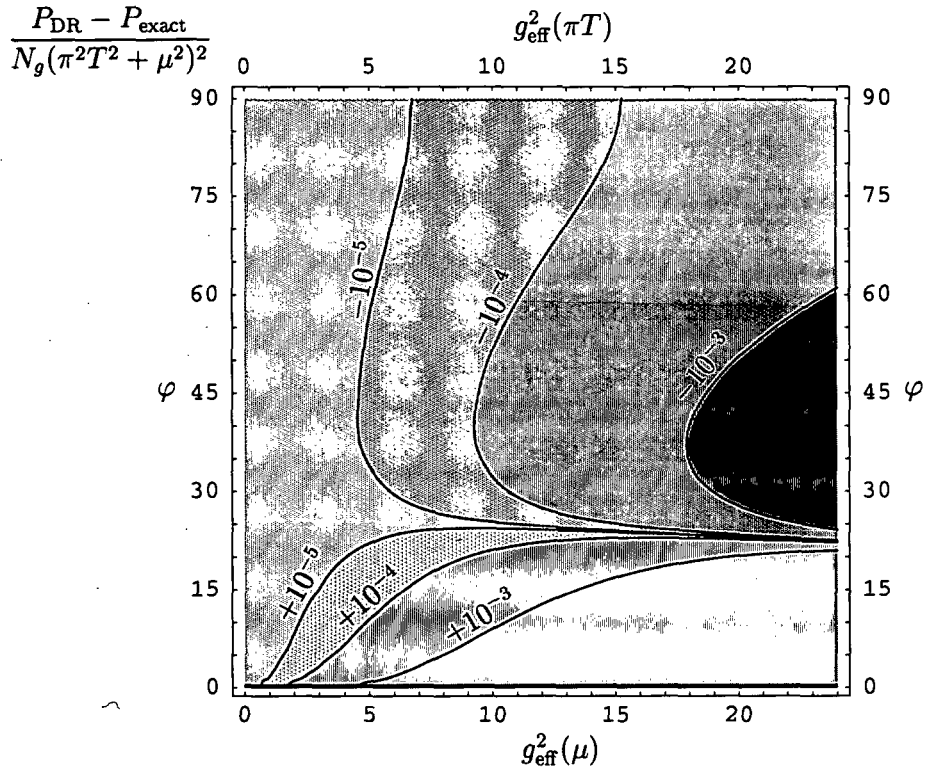


Figure 2.5: Difference between the pressure obtained from dimensional reduction to the exact large N_f result for the FAC (fastest apparent convergence) renormalization scale $\bar{\mu}_{\text{MS}}(\text{FAC-m}) = \pi T \exp(\frac{1}{2} - \gamma_E - \frac{1}{2}\mathcal{D}(\frac{\mu}{\pi T}))$ for different values of $\phi = \arctan \frac{\pi T}{\mu}$ and g_{eff}^2 , normalized to $N_g(\pi^2 T^2 + \mu^2)^2$. The result of the dimensionally reduced pressure is rescaled by the exact renormalization scale dependence (2.2.4) to the scale $\bar{\mu}_{\text{MS}} = \sqrt{(\pi T)^2 + \mu^2}$ to allow for unified comparison.

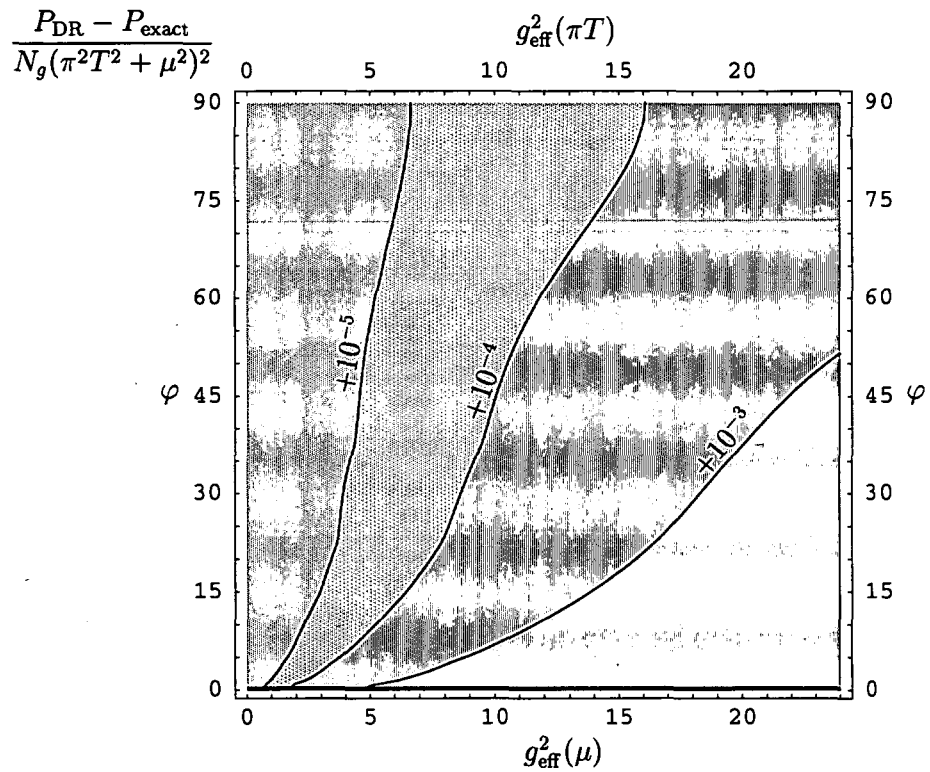


Figure 2.6: Same as figure 2.5 except that the scale is now FAC-g instead of FAC-m, that is applying fastest apparent convergence to g_E^2 . Contrary to the FAC-m scale, the error is now always positive, meaning that dimensional reduction at this renormalization scale always overestimates the exact result. Apart from that the error of the FAC-g scale is comparable to the one of the FAC-m scale.

produces in the $N_f \rightarrow \infty$ limit

$$\bar{\mu}_{\text{MS}}(\text{FAC-g}) = \pi T \exp \left[-\gamma_E - \frac{1}{2} \mathcal{D} \left(\frac{\mu}{\pi T} \right) \right] \quad (2.5.15)$$

which curiously is just a factor $1/\sqrt{e}$ smaller than the FAC-m scale but shows otherwise exactly the same functional dependence on μ and T .

Figure 2.6 shows the difference of the pressures now for the FAC-g scale. It is conspicuous that this time there is no sign change in the plot. Indeed, contrary to what we saw in figure 2.5 for the FAC-m scale, the difference between P_{DR} and $P_{\text{exact}} = P_{\text{NLO}}$ is now always positive, meaning that dimensional reduction at this renormalization scale always overestimates the exact result. But apart from that, the absolute value of the errors of the FAC-g scale plot is comparable to the one of the FAC-m scale. One should not be irritated by the horizontal line in figure 2.5 at $\phi \approx 25^\circ$ where the range of small error is extended to larger values of the coupling g_{eff}^2 : This merely indicates the change of sign of the error.

Having such good agreement for a wide range of ϕ and g_{eff}^2 , it seems tempting to try to improve the result by averaging over the two scales: Taking the arithmetic mean of the two scales FAC-m and FAC-g we obtain a scale that is a factor $(1 + 1/\sqrt{e})/2 \approx 0.803265..$ smaller than the FAC-m scale. Remember that the FAC-m and FAC-g scale are directly proportional to each other with $\bar{\mu}_{\text{MS}}(\text{FAC-g}) = \bar{\mu}_{\text{MS}}(\text{FAC-m})/\sqrt{e} \approx 0.606531 \bar{\mu}_{\text{MS}}(\text{FAC-m})$ so that the arithmetic mean scale is also proportional to them.

Figure 2.7 shows the remarkable agreement that follows from this choice of scale: The thermal pressure of dimensional reduction agrees to the exact large N_f result for $\phi \gtrsim 65^\circ$ over the whole range of couplings. If we look at smaller couplings $g_{\text{eff}}^2 \lesssim 10$, the two results agree perfectly down to $\phi \gtrsim 35^\circ$. Only below $\phi \lesssim 30^\circ$ the spreading of errors does not differ much from that of the scales FAC-m and FAC-g separately. One should note however, that this might be a mere coincidence in the large N_f limit and that no real conclusion can be inferred from this result for finite, smaller N_f . After all, for finite N_f FAC-m and FAC-g are not necessarily proportional to each other (except for $\mu = 0$ where both are simply proportional to the temperature T).

2.5.2 Pressure at zero chemical potential

At zero chemical potential we shall study in more detail the convergence properties and renormalization scale dependences of perturbation theory on the one hand, and the Landau pole ambiguity of our large N_f result on the other hand. In figure 2.8 we give the numerical result of the thermal pressure as a function of $g_{\text{eff}}^2(\bar{\mu} = \pi e^{-\gamma_E} T)$. The perturbative results depend on the value of the renormalization point $\bar{\mu}$, which we vary between πT and $4\pi T$. In order to compare the different perturbative results with the exact large N_f result, we use the exact running coupling (2.2.4) to rescale everything

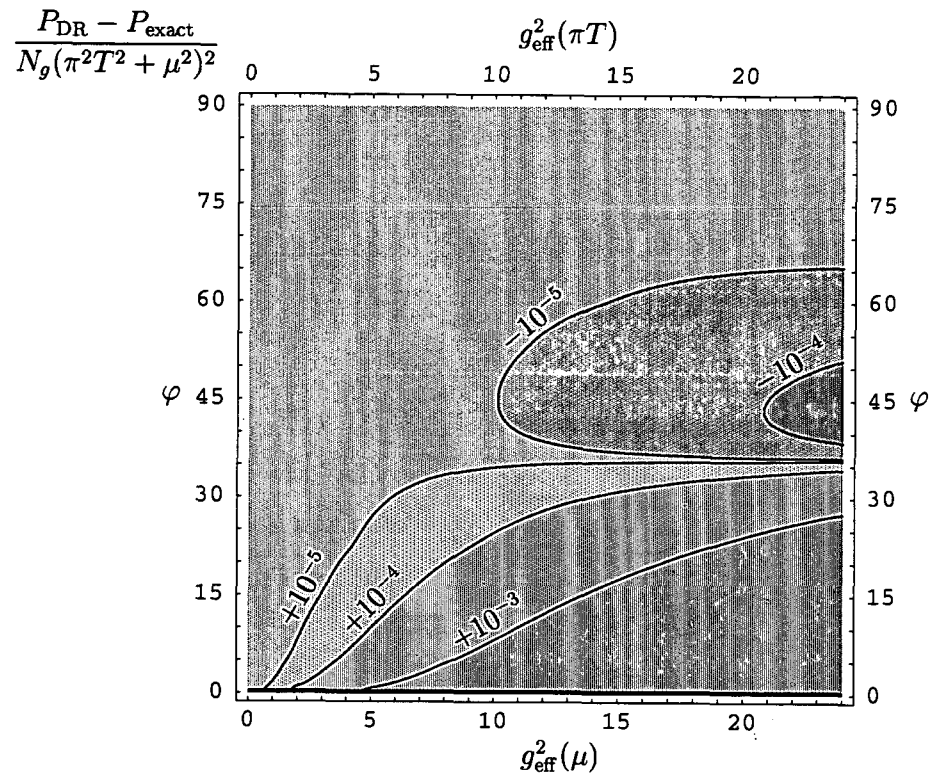


Figure 2.7: Same as figures 2.5 and 2.6 except that the scale is now chosen as the arithmetic mean of the two scales FAC-m and FAC-g. We see remarkable agreement for $\phi \gtrsim 65^\circ$ over the whole range of couplings down to $\phi \gtrsim 35^\circ$ for $g_{\text{eff}}^2 \lesssim 10$. Below $\phi \lesssim 30^\circ$ the spreading of errors does not differ much from that of the scales FAC-m and FAC-g separately.

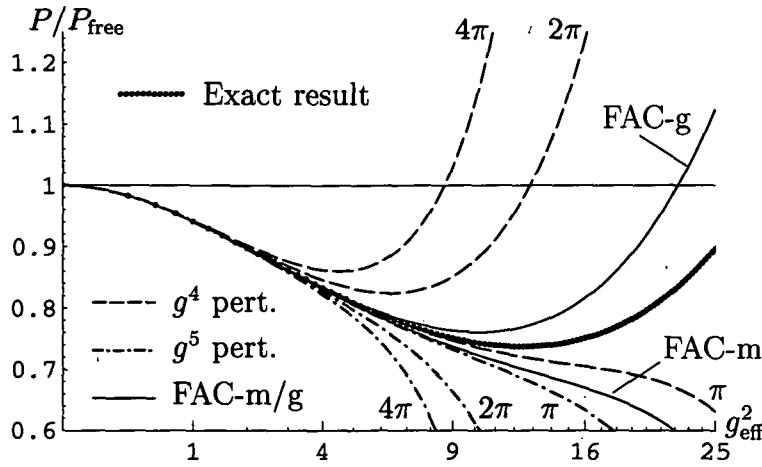


Figure 2.8: Exact result for $P_{\text{NLO}}/P_{\text{free}}$ as a function of g_{eff}^2 ($\bar{\mu} = \pi e^{-\gamma_E T}$), rendered with an abscissa linear in g_{eff} , in comparison with and two sets of perturbative results through order g^4 and g^5 with renormalization point chosen within a power of 2 of $2\pi T$; The line marked “FAC-m” corresponds $\bar{\mu} = \pi e^{\frac{1}{2}-\gamma_E T}$ where the perturbative result to order g^4 coincides with the one to order g^5 . The line marked “FAC-g” corresponds to the renormalization point $\bar{\mu} = \pi e^{-\gamma_E T}$ and shows the result through order g^5 .

to $\bar{\mu} = \pi e^{-\gamma_E T}$. We see that the perturbative result through order g^5 gives reliable results only for effective couplings $g_{\text{eff}}^2 \lesssim 4$. If the perturbative result to order g^5 is optimized by fastest apparent convergence of m_E^2 (FAC-m) from equation (2.5.14) which for $\mu = 0$ means the scale $\bar{\mu} = \pi e^{\frac{1}{2}-\gamma_E T}$, the agreement with perturbation theory is improved and extends to $g_{\text{eff}}^2 \approx 7$. Figure 2.8 shows for comparison also the FAC-g scale.

Figure 2.9 shows the same thermal pressure as figure 2.8, but with the perturbative results varied between μ/e and μe where $\mu = \pi e^{-\gamma_E T}$ which is in fact the FAC-g scale. The central line of the g^5 result is just the FAC-g line from the previous plot. The central line of the g^4 result also corresponds to the FAC-g scale. Different from the FAC-m scale, the FAC-g scale stays not the same from order g^4 to order g^5 , but instead changes noticeably. Remember that the FAC-m scale was just chosen such that the g^4 and the g^5 results lie on top of each other. Figure 2.9 also includes the arithmetic mean of the two FAC scales which is $\frac{1}{2}(\text{FAC-m} + \text{FAC-g}) = \frac{1}{2}(1 + 1/\sqrt{e})\text{FAC-m} = \frac{1}{2}(\sqrt{e} + 1)\text{FAC-g}$. It turns out that this line is almost indistinguishable from the exact result. Only for larger values of g_{eff}^2 can one see a tiny deviation from the exact result.

The exact large N_f result flattens out for higher values of g_{eff}^2 and reaches a minimum at $g_{\text{eff}}^2 \approx 12$. For this coupling, $\Lambda_{\text{Landau}} \simeq 480T$ and the ambiguity introduced by the Landau singularity is completely negligible. For still

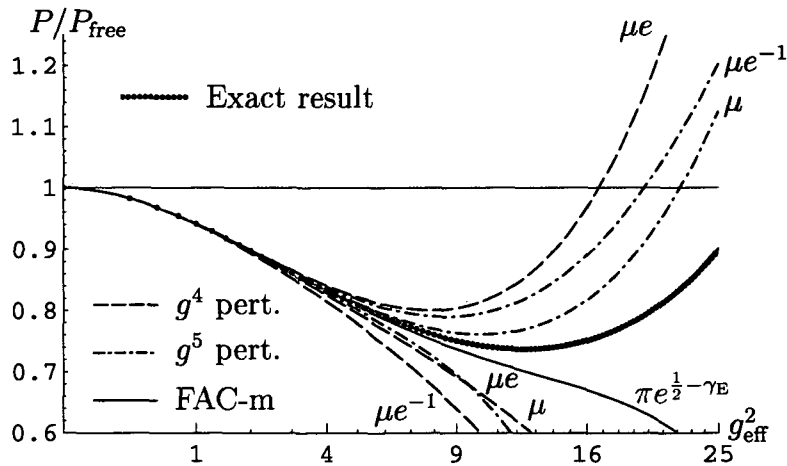


Figure 2.9: Same as figure 2.8 only with renormalization point chosen within a power of e of $\mu = \pi e^{-\gamma_E T}$. The FAC-g result is not explicitly marked, but coincides with the scale choice of μ in this plot. Therefore the central line of the g^5 result shows the FAC-g up to order g^5 , and the central line of the g^4 result shows the FAC-g result up to order g^4 . Note that unlike the FAC-m result, the FAC-g result differs considerably from order g^4 to order g^5 . Plotted in this graph is also the arithmetic mean of the two FAC scales as described in the text. This line is almost indistinguishable from the exact result.

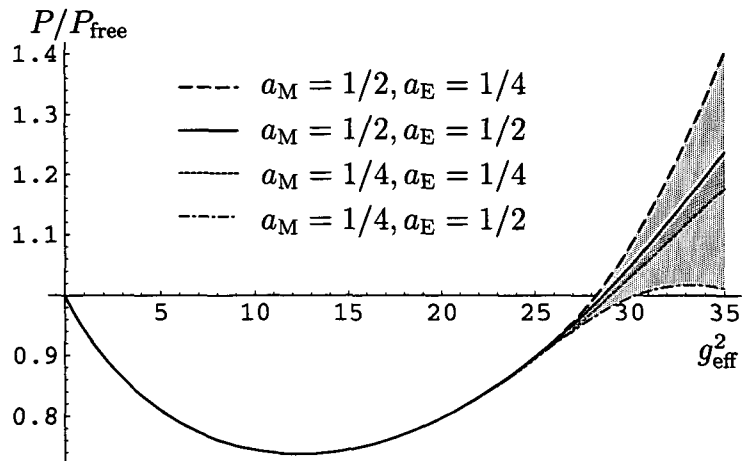


Figure 2.10: The result for P_{NLO}/P_{free} up to $g_{\text{eff}}^2 = 35$ and with different cutoffs.

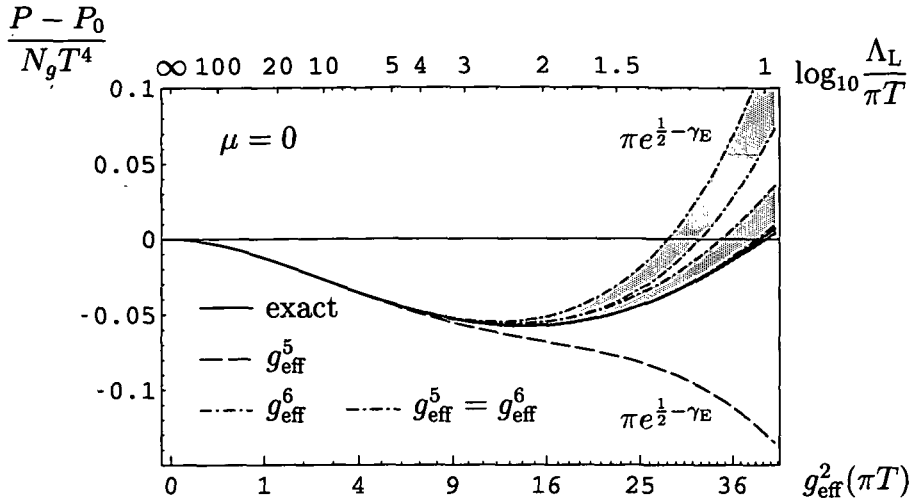


Figure 2.11: Exact result for the interaction pressure at zero chemical potential as in references [66, 67] but as a function of $g_{\text{eff}}^2(\bar{\mu}_{\text{MS}} = \pi T)$ or, alternatively, $\log_{10}(\Lambda_L/\pi T)$. The dashed line is the perturbative result when the latter is evaluated with renormalization scale $\bar{\mu}_{\text{MS}} = \bar{\mu}_{\text{FAC}} \equiv \pi e^{1/2-\gamma T}$; the dash-dotted lines include the numerically determined coefficient to order g_{eff}^6 (with its estimated error) at the same renormalization scale. The result marked “ $g_{\text{eff}}^5 = g_{\text{eff}}^6$ ” corresponds to choosing $\bar{\mu}_{\text{MS}}$ such that the order- g_{eff}^6 coefficient vanishes and retaining all higher-order terms contained in the plasmon term $\propto m_E^3$. In this and the following plots the (tiny) red band appearing around the exact result at large coupling displays the effect of varying the cut-off from 50% to 70% of the Landau scale Λ_L .

higher values the pressure rises and starts to exceed the free theory pressure at $g_{\text{eff}}^2 > 28$, as can be seen in figure 2.10. This occurs at a coupling for which $\Lambda_{\text{Landau}}/T < 34$. While this still seems to be a reasonably large number, the numerical result starts to become sensitive to the cutoff just where the pressure approaches the free one. The four curves displayed in figure 2.10 show the result of varying the parameter a in the UV cutoff $\sqrt{a}\Lambda_{\text{Landau}}$ in the Minkowski and Euclidean parts of the calculation (a_M and a_E respectively) from $a = 1/4$ to $a = 1/2$. The numerical result is rather insensitive to this below $g_{\text{eff}}^2 \approx 25$, but very sensitive in the region where the pressure starts to exceed the free one.

In figure 2.11 we show the pressure at $\mu = 0$ and compare with even higher orders of perturbation theory. Here the result is presented as a function of $g_{\text{eff}}^2(\bar{\mu}_{\text{MS}} = \pi T)$ and not divided by the free NLO contribution from the pressure, but with the ideal-gas limit from equation (2.5.1) subtracted. In the plots we also give the corresponding values of the Landau pole $\log_{10}(\Lambda_L/\pi T)$ to different values of the effective coupling g_{eff}^2 . This plot also contains the

result up to g_{eff}^6 which is not known analytically yet, but obtained from our numerical results at small coupling. For small coupling the agreement of our numerical results with perturbation theory is sufficiently accurate so that we can numerically extract coefficients to this order as follows: From the pressure in dimensional reduction (2.5.10) we can infer by applying the exact running coupling of large N_f (2.2.4) that the g_{eff}^6 -term in the pressure at $\mu = 0$ has the form

$$\begin{aligned} \frac{1}{N_g} P \Big|_{g_{\text{eff}}^6, \mu=0} &= \left(\frac{g_{\text{eff}}}{4\pi} \right)^6 T^4 \left[C_6 + 10 \ln^2 \frac{\bar{\mu}_{\text{MS}}}{\pi T} \right. \\ &\quad \left. - \frac{16\pi^2}{81} \left(1 + 12\gamma - \frac{464 \ln 2}{5} - 8 \frac{\zeta'(-3)}{\zeta(-3)} + 16 \frac{\zeta'(-1)}{\zeta(-1)} \right) \ln \frac{\bar{\mu}_{\text{MS}}}{\pi T} \right]. \end{aligned} \quad (2.5.16)$$

Notice the appearance of the (as yet) unknown constant C_6 . For small values of g_{eff}^2 , perturbation theory is expected to give excellent agreement with the exact result, so that we can actually use our (numerically obtained) exact result to determine unknown coefficients in the perturbative series. By least-square fitting we obtain numerically the estimate $C_6 = +20(2)$.

In real, finite- N_f QCD this result corresponds to the $N_f^3 g^6 T^4$ coefficient of the pressure. As we saw in figure 2.1, the purely gluonic contribution $\propto N_f^0 g^6 T^4$ of the same coupling order g^6 is completely nonperturbative.

In the figures 2.8 and 2.9 the agreement between exact result and perturbative result up to order g_{eff}^5 was limited to a range of about $g_{\text{eff}}^2 \lesssim 9$. In figure 2.11 we show the improved result that remains accurate up to $g_{\text{eff}}^2 \sim 16$ by including our numerical estimate of the g_{eff}^6 -coefficient and using $\bar{\mu}_{\text{FAC}}$. The agreement with the exact result can even be further improved by fixing the renormalization point such that the g_{eff}^6 coefficient vanishes and keeping all orders of the odd terms in g_{eff} by leaving the plasmon term $\propto m_E^3$ unexpanded in g_{eff}^2 . The result of this procedure is indicated by the gray area in figure 2.11. Obviously the result now gets very close to the exact result. Of course, this procedure does by no means guarantee that an analogous scheme for real QCD with finite N_f will produce similarly convincing results, but we can take it as another indication of the observation that keeping the parameters of the dimensionally reduced theory unexpanded can improve the convergence of thermal perturbation theory [88].

Figure 2.12 shows a comparison of the Φ -derivable 2-loop result in the HTL approximation (full lines) and in the next-to-leading approximation (full lines ending in dashed lines) as performed by Rebhan [84]. In the Φ -derivable approach of reference [46], a fermionic gap equation had been assumed that turned out not to be compatible with the limit of large N_f . As is shown in [84], the originally quadratic gap equation for the fermions does not comply with the Casimir scaling in the large N_f limit and that this limit would favor a linear dependence on the asymptotic mass \bar{M}_∞ . The new gap equation (16) in reference [84] reproduces qualitatively the nonmonotonic

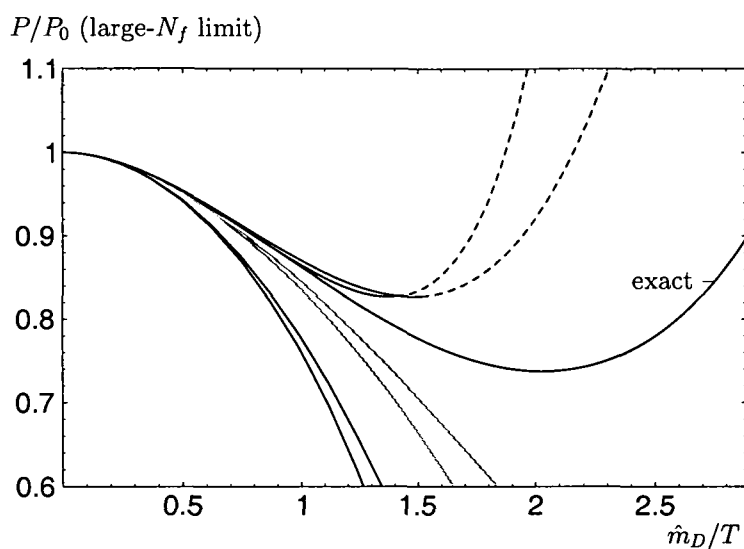


Figure 2.12: Comparison (taken from reference [84]) of the Φ -derivable 2-loop result in the HTL approximation (full lines) and in the next-to-leading approximation (full lines ending in dashed lines), for $\bar{\mu} = T$ and $4\pi T$, and the exact result for the pressure in the limit of large N_f . The gray lines denote the next-to-leading approximation with quadratic fermionic gap equation considered in reference [46], but which Rebhan argues in reference [84] needs to be replaced by equation (16) therein. The Debye mass appearing on the lower axis of the plot is related to the effective coupling via $\hat{m}_D/T \equiv g_{\text{eff}}(\mu_{\text{DR}})/\sqrt{3}$.

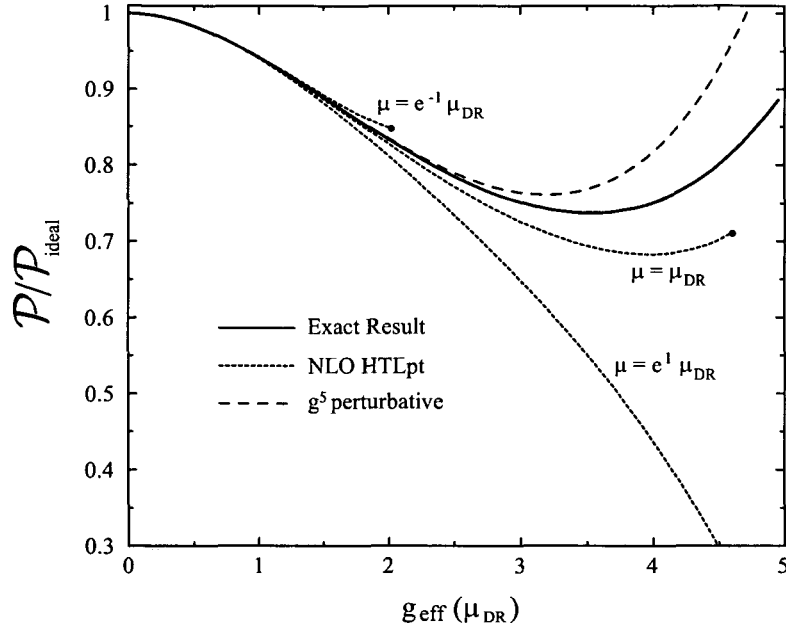


Figure 2.13: Comparison (taken from reference [89]) of the NLO HTLpt prediction for the $O(N_f^0)$ contribution to the free energy, the exact numerical in the large N_f limit, and the perturbative prediction accurate to g^5 as a function of $g_{\text{eff}}(\mu_{\text{DR}}) = \sqrt{s_f} g(\mu_{\text{DR}}) = 2\pi \sqrt{s_f \alpha_s(\mu_{\text{DR}})}$ where $\mu_{\text{DR}} = \pi e^{-\gamma} T$. Dots indicate the point at which there is no longer a real-valued solution to the gap equation for m_D . The renormalization scale μ is varied by a factor of e around μ_{DR} and the perturbative g^5 result is evaluated at the central scale.

behavior in g_{eff}^2 of the exact result. By a curious coincidence, for $N = 3$ and $N_f = 3$ the revised gap equation has exactly the same solutions as the uncoupled quadratic gap equations that have been previously in use. Only for $N_f > 3$ there exists a coupling where the fermionic mass ceases to grow monotonically with g . Because of this coincidence, the numerical changes in the previous results of [46] are almost completely negligible.

Figures 2.13 and 2.14 show the HTLpt (Hard Thermal Loop - perturbation theory) comparison to the large N_f limit by Andersen et al. [89]. The plots show the NLO HTLpt prediction for the $O(N_f^0)$ contribution to the free energy, the perturbative prediction accurate to g^5 , and the exact result up to NLO in the large N_f limit. It should be noted, however, that both the HTLpt and the 2-loop Φ -derivable results are perturbatively accurate only up to and including order g_{eff}^3 , where the perturbative result is rather ill-behaved. As noticed in [89], the HTLpt predictions for both the free energy and the Debye mass (which was also discussed in [89]) seemed to diverge from the exact result around $g_{\text{eff}} \sim 2$ regardless of the scale that was chosen;

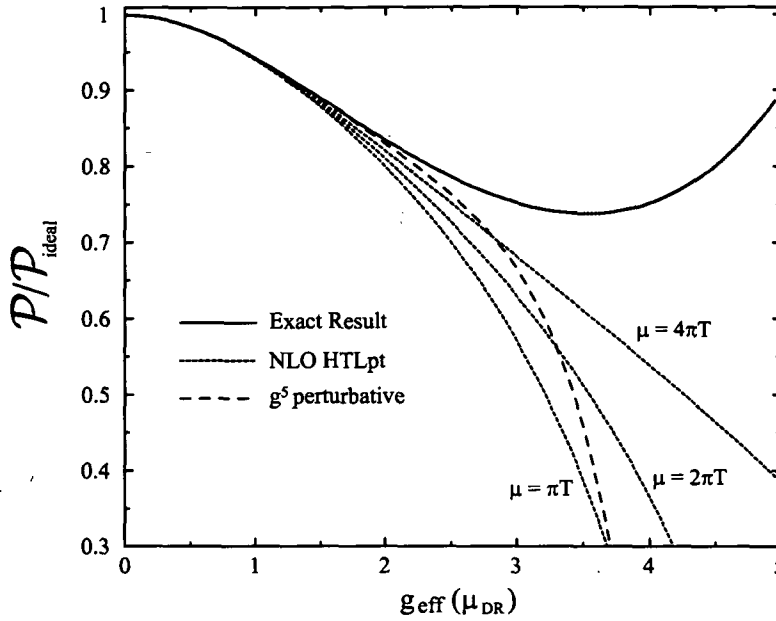


Figure 2.14: Same as figure 2.13 only with the renormalization scale μ varied by a factor of 2 around $2\pi T$. The perturbative g^5 result is again evaluated at the central scale. [89]

however, for both quantities, choosing the scale to be $\mu = \mu_{\text{DR}} = \pi e^{-\gamma} T$ seemed to reasonably reproduce the exact results. The authors of [89] concluded that their result is comparable to the performance of the Φ -derivable approach in the large N_f limit in figure 2.12.

2.5.3 Quark number susceptibilities

Linear quark number susceptibility

The (linear) quark number susceptibility is defined as the first derivative of the quark number density $\mathcal{N} \equiv N/V$ with respect to chemical potential (see also appendix C.2),

$$\chi = \frac{\partial \mathcal{N}}{\partial \mu} = \frac{\partial^2 P}{\partial \mu^2}. \quad (2.5.17)$$

Figure 2.15 displays the exact large- N_f result for the interaction part of χ at zero chemical potential as a function of g_{eff} (or alternatively $\log_{10}(\Lambda_L/\pi T)$). Similar to the thermal pressure, the result is nonmonotonic, but the minimum already occurs at $g_{\text{eff}}^2(\pi T) \approx 8.6$, and the free-theory value is recovered at $g_{\text{eff}}^2(\pi T) \approx 22.5$, where the Landau ambiguity is still well under control since $\Lambda_L/T \approx 100$ at that coupling.

The perturbative (dimensional reduction) result can be read from the

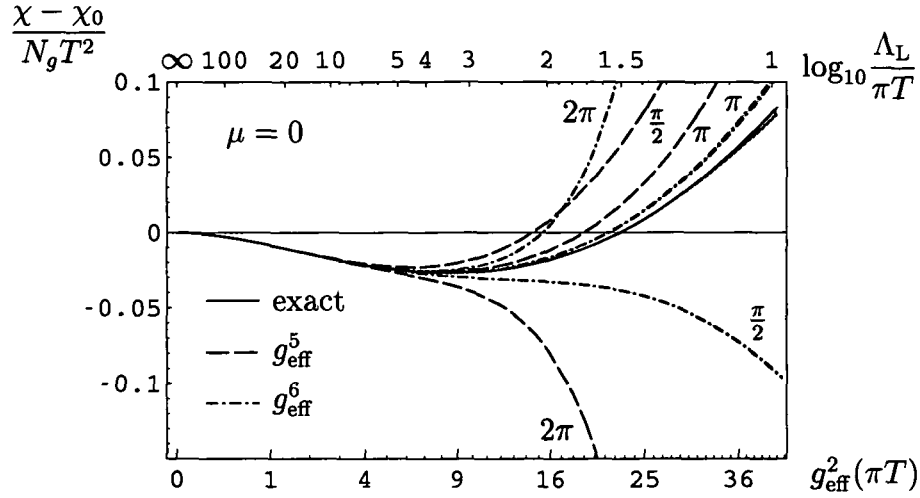


Figure 2.15: The interaction part of the quark number susceptibility at $\mu = 0$ compared with strict perturbation theory to order g_{eff}^5 and g_{eff}^6 , respectively, with renormalization scale varied about πT by a factor of 2.

linear term in μ^2 of (2.5.10) and gives

$$\begin{aligned} \frac{\chi - \chi_0}{N_g T^2} &= 2 \frac{\partial}{\partial(\mu^2)} \frac{P - P_0}{N_g} \Big|_{\mu=0} = -\frac{g_{\text{eff}}^2}{8\pi^2} + \frac{g_{\text{eff}}^3}{4\pi^3\sqrt{3}} \\ &+ \frac{g_{\text{eff}}^4}{48\pi^4} \left[\ln \frac{\bar{\mu}_{\text{MS}}}{4\pi e^{-\gamma} T} - \frac{13}{12} - \frac{4}{3} \ln 2 \right] \\ &+ \frac{g_{\text{eff}}^5}{16\pi^5\sqrt{3}} \left[-\ln \frac{\bar{\mu}_{\text{MS}}}{e^{1/2-\gamma}\pi T} + \frac{7}{18} \zeta(3) \right]. \end{aligned} \quad (2.5.18)$$

The coefficient of g_{eff}^4 has only recently been obtained in [71] in a three-loop calculation. We can confirm its closed-form value by a numerical fit, which gives agreement with an accuracy of 2×10^{-4} , thus providing a good check on both our numerics and the analytical calculations of [71]. This level of accuracy allows us to also extract the order- g^6 term as (for $\mu_{\text{MS}} = \pi T$)

$$\frac{\chi|_{g_{\text{eff}}^6}}{N_g T^2} = -4.55(9) \times \left(\frac{g_{\text{eff}}}{4\pi} \right)^6. \quad (2.5.19)$$

In Fig. 2.15 we show the perturbative results to order g_{eff}^5 and g_{eff}^6 , varying the renormalization scale about πT by a factor of 2 (now without the improvement of keeping effective-theory parameters unexpanded). The value $\bar{\mu}_{\text{MS}} = \pi T$ is in fact close to $\bar{\mu}_{\text{FAC}}$ where it makes no difference whether m_E^2 is kept unexpanded or not. We find that the quality of the perturbative result for the susceptibility is comparable to that observed in the pressure, with $\bar{\mu}_{\text{MS}} = \pi T$ being close to the optimal choice.

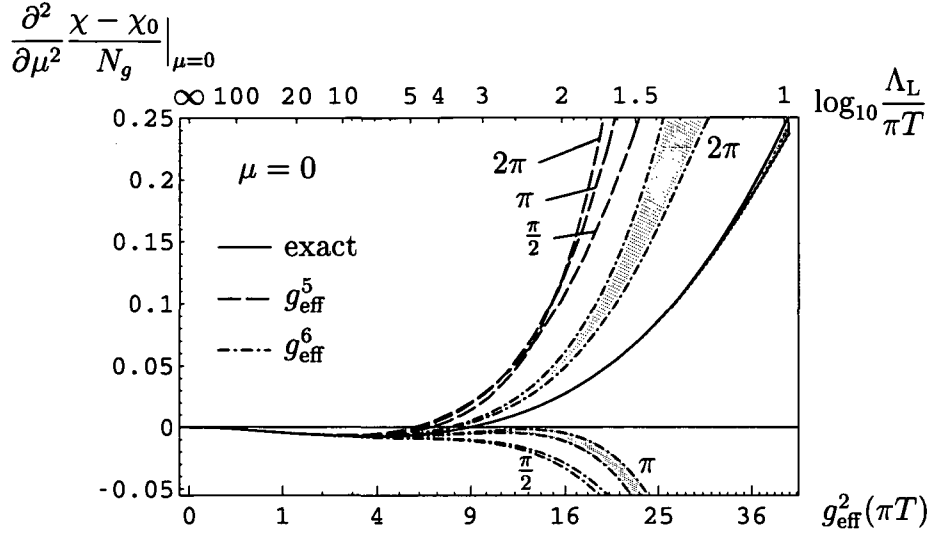


Figure 2.16: The interaction part of the higher-order quark number susceptibility $\frac{\partial^2}{\partial \mu^2}(\chi - \chi_0)$ at $\mu = 0$ compared with strict perturbation theory to order g_{eff}^5 and g_{eff}^6 , respectively, with renormalization scale varied about πT by a factor of 2. The coloured bands of the g_{eff}^6 -results cover the estimated error of the numerically extracted perturbative coefficients.

Higher-order quark susceptibility

We also computed explicitly the higher-order susceptibility $\partial^4 P / \partial \mu^4 \Big|_{\mu=0}$ (which has been investigated in lattice QCD with $N_f = 2$ in reference [79]).

Our exact result in the large- N_f limit is shown in figure 2.16. In this quantity, we find that the nonmonotonic behavior observed above in the pressure and the linear susceptibility is much more pronounced. The minimum now occurs at $g_{\text{eff}}^2 \approx 3.7$, where perturbation theory is still in good shape, and the free-theory value is exceeded for $g_{\text{eff}}^2 \gtrsim 9$. Using (2.5.10) we find to order g^5

$$\begin{aligned}
 \frac{\partial^2}{\partial \mu^2} \frac{\chi - \chi_0}{N_g} \Big|_{\mu=0} &= \frac{\partial^4}{\partial \mu^4} \frac{P - P_0}{N_g} \Big|_{\mu=0} = 12 \frac{\partial^2}{(\partial \mu^2)^2} \frac{P - P_0}{N_g} \Big|_{\mu=0} & (2.5.20) \\
 &= -\frac{3g_{\text{eff}}^2}{4\pi^4} + \frac{3\sqrt{3}g_{\text{eff}}^3}{4\pi^5} + \frac{g_{\text{eff}}^4}{8\pi^6} \left[\ln \frac{\bar{\mu}_{\text{MS}}}{4\pi T} + \gamma + C_4 \right] \\
 &\quad + \frac{3\sqrt{3}g_{\text{eff}}^5}{16\pi^7} \left[-\ln \frac{\bar{\mu}_{\text{MS}}}{e^{1/2-\gamma}\pi T} + \frac{7}{3} \zeta(3) - \frac{31}{54} \zeta(5) \right] + O(g_{\text{eff}}^6).
 \end{aligned}$$

In the original publication of these results [68] the coefficient appearing at order g_{eff}^4 has been numerically extracted as $C_4 = -7.02(3)$. In the meantime, the complete μ dependence of the dimensional reduction result to order g_{eff}^4

has been worked out in reference [65] from where one can obtain the exact result

$$C_4 = -\frac{1}{12} - 12 \ln 2 + \frac{7}{6} \zeta(3) = -6.9986997796998 \dots \quad (2.5.21)$$

The complete agreement with reference [65] provided on the one hand an independent check on the correctness of the 3-loop calculations of [65] and on the other hand a check on the accuracy of our numerical analysis.

Using (2.5.21) we can extract the term of order g_{eff}^6 in equation (2.5.20) as $-39(1)g_{\text{eff}}^6/(128\pi^8)$ for $\bar{\mu} = \pi T$. The perturbative results to order g_{eff}^5 and to order g_{eff}^6 are compared with the exact result in figure 2.16. This shows that the accuracy of the perturbative result again improves by going from order g_{eff}^5 to order g_{eff}^6 , but the renormalization scale dependence increases sharply at large coupling.

Pressure at larger chemical potential from susceptibilities

With regard to the attempts to explore QCD at finite chemical potential by means of lattice gauge theory [75, 76, 77, 78], it is of interest how well the pressure at larger chemical potential can be approximated by the first few terms of a Taylor series in μ^2 .

In reference [75] it has been observed that the ratio of $\Delta P = P(T, \mu) - P(T, \mu = 0)$ over the corresponding free-theory quantity ΔP_0 is practically independent of μ for the range of chemical potentials explored. This is also realized when quasi-particle models are used for a phenomenological extrapolation of lattice data [90, 91] in a method introduced by Peshier et al. [83]. In figure 2.17 we show the deviation from this ‘‘scaling’’ at higher values of μ/T by considering the quantity $\delta P = P(T, \mu) - P(T, 0) - \frac{1}{2}\chi|_{\mu=0}(\mu^2 + \mu^4/(2\pi^2 T^2))$ divided by $P_{\text{NLO}}^{\text{free}} = N_g \pi^2 T^4 / 45$. The combination $(\mu^2 + \mu^4/(2\pi^2 T^2))$ appearing therein is such that a replacement of P and χ by their interaction-free values P_0 and χ_0 makes δP vanish identically. (As can be seen from the above perturbative results, δP also vanishes for the leading-order interaction parts $\propto g_{\text{eff}}^2$.) In the exact large- N_f results of figure 2.17 we observe that for coupling $g_{\text{eff}}^2 \lesssim 4$ the deviation δP is at most a few percent of $P_{\text{NLO}}^{\text{free}}$ for $\mu/T \lesssim \pi$, but it rapidly grows for $\mu/T \gtrsim \pi$. This is in fact also nicely illustrated by the 3-dimensional plot of the pressure in figure 2.3, which has a rather conspicuous kink at $\phi = 45^\circ$ corresponding to $\mu = \pi T$.

It turns out that including the exact higher-order susceptibility at $\mu = 0$ does not lead to a better approximation of the pressure at larger chemical potential. The dashed lines in Fig. 2.17 correspond to $\delta P = P(T, \mu) - P(T, 0) - \frac{\mu^2}{2}\chi|_{\mu=0} - \frac{\mu^4}{4!}\frac{\partial^4 P}{\partial \mu^4}|_{\mu=0}$. While this slightly improves matters at small μ/T , it results into even quicker deviations for larger μ/T .

It is of course impossible to say whether this behavior would also appear in real QCD, but since it occurs already at comparatively small g_{eff} in the

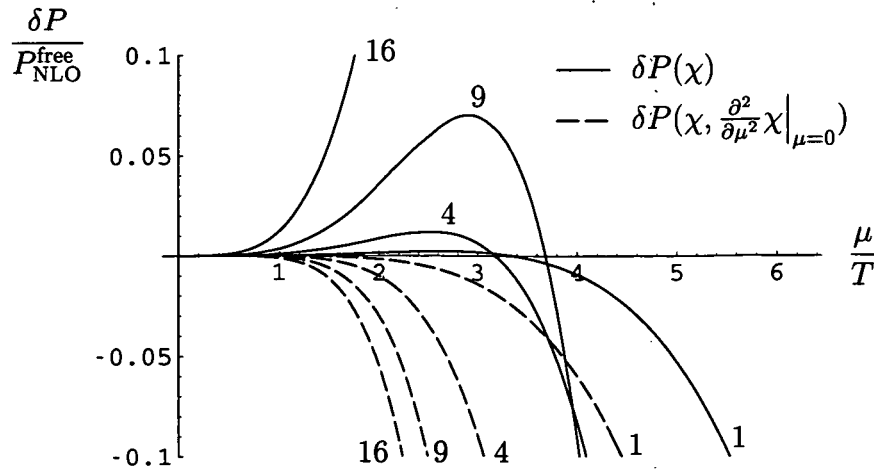


Figure 2.17: Deviation from the scaling observed in Ref. [75] in lattice QCD for small chemical potential in the quantity $\delta P = P(T, \mu) - P(T, 0) - \frac{1}{2}\chi|_{\mu=0}(\mu^2 + \mu^4/(2\pi^2 T^2))$ (full lines) and in $\delta P = P(T, \mu) - P(T, 0) - \frac{\mu^2}{2}\chi|_{\mu=0} - \frac{\mu^4}{4!}\frac{\partial^4 P}{\partial \mu^4}|_{\mu=0}$ (dashed lines), both normalized to $P_{\text{NLO}}^{\text{free}} = N_g \pi^2 T^4 / 45$, for $g_{\text{eff}}^2(\pi T) = 1, 4, 9, 16$.

large- N_f limit, where the peculiar nonmonotonic behavior of the pressure as a function of g_{eff} does not yet arise (the minimum in the normalized interaction pressure occurs at $g_{\text{eff}}^2(\pi T) \approx 14$), it may be taken as an indication that extrapolations of lattice data on the equation of state from small chemical potential to large μ/T are generally problematic. If anything, real QCD should be more complicated because of the existence of phase transitions which are absent at NLO in the large- N_f limit.

2.5.4 Pressure at zero temperature

Our exact result for the thermal pressure at zero temperature and finite chemical potential is given in figure 2.18 as a function of $g_{\text{eff}}^2(\bar{\mu}_{\text{MS}} = \mu)$. In contrast to the pressure at zero chemical potential and finite temperature, the interaction pressure divided by μ^4 is monotonically decreasing essentially all the way up to the point where the Landau ambiguity becomes noticeable.

The thermal pressure at zero temperature and large chemical potential for QED and QCD has been obtained to order g^4 long ago by Freedman and McLerran [72, 73]. At this order, there is a non-analytic zero-temperature plasmon term $\propto g^4 \ln(g)$, whose prefactor is known exactly, but the constant under the logarithm only numerically. The transposition of their result, which has been obtained in a particular momentum-subtraction scheme, to the gauge-independent $\overline{\text{MS}}$ scheme can be found in references [46, 92]. The

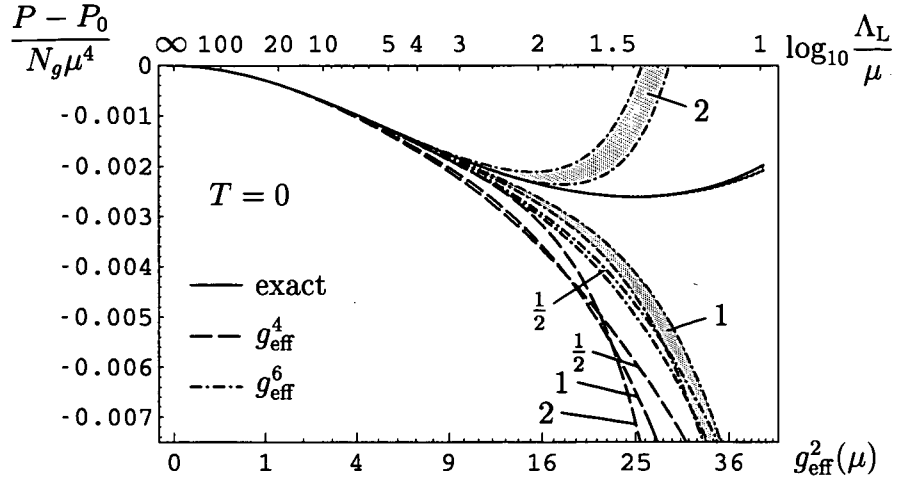


Figure 2.18: The interaction part of the pressure at zero temperature and finite chemical potential as a function of $g_{\text{eff}}^2(\bar{\mu}_{\text{MS}} = \mu)$ or, alternatively, $\log_{10}(\Lambda_L/\mu)$, compared with the perturbative result of Freedman and McLerran [72, 73] to order g_{eff}^4 , and our numerically extracted order- g_{eff}^6 result, both with renormalization scale in the perturbative results varied around $\bar{\mu}_{\text{MS}} = \mu$ by a factor of 2. The coloured bands of the g_{eff}^6 -results cover the error of the numerically extracted perturbative coefficients.

large- N_f limit of this result reads

$$\left. \frac{P - P_0}{N_g \mu^4} \right|_{T=0} = -\frac{g_{\text{eff}}^2}{32\pi^4} - \left[\ln \frac{g_{\text{eff}}^2}{2\pi^2} - \frac{2}{3} \ln \frac{\bar{\mu}_{\text{MS}}}{\mu} - \tilde{C}_4 \right] \frac{g_{\text{eff}}^4}{128\pi^6} + O(g_{\text{eff}}^6 \ln g_{\text{eff}}) \quad (2.5.22)$$

and involves one of the numerical constants computed in reference [72],

$$\tilde{C}_4 = \frac{79}{18} - \frac{\pi^2}{3} - \frac{7 \log(2)}{3} - \frac{2b}{3} \approx 0.536, \quad (2.5.23)$$

where b has an integral representation, given in equation (II.3.25)³ of reference [72], that apparently cannot be evaluated in closed form. With better computer equipment, b can however be evaluated numerically to higher accuracy than that given in [72] as $b = -1.581231511\dots$, which leads to $\tilde{C}_4 = 0.5358316747\dots$

The accuracy of our numerical results is sufficiently high to confirm the correctness of the result for \tilde{C}_4 with an accuracy of $\sim 2 \times 10^{-4}$. With the knowledge of the exact value of \tilde{C}_4 we can also extract, with lower precision,

³ Note that there is a typo in the equation mentioned: Comparison with equation (II.3.24) shows that there is a missing exponent 2 after the second set of large round parenthesis in equation (II.3.25) of [72] as pointed out by [68].

the next coefficients at order g_{eff}^6 , which again involve a logarithmic term:

$$\begin{aligned} \frac{P - P_0}{N_g \mu^4} \Big|_{T=0} = & -\frac{g_{\text{eff}}^2}{32\pi^4} - \left[\ln \frac{g_{\text{eff}}^2}{2\pi^2} - \frac{2}{3} \ln \frac{\bar{\mu}_{\text{MS}}}{\mu} - \tilde{C}_4 \right] \frac{g_{\text{eff}}^4}{128\pi^6} \\ & - \left[\left(3.18(5) - \frac{16}{3} \ln \frac{\bar{\mu}_{\text{MS}}}{\mu} \right) \ln \frac{g_{\text{eff}}^2}{2\pi^2} \right. \\ & \left. + \frac{16}{9} \ln^2 \frac{\bar{\mu}_{\text{MS}}}{\mu} + \frac{16}{3} \left(\tilde{C}_4 - \frac{1}{2} \right) \ln \frac{\bar{\mu}_{\text{MS}}}{\mu} - 3.4(3) \right] \frac{g_{\text{eff}}^6}{2048\pi^8} + \dots \end{aligned} \quad (2.5.24)$$

In figure 2.18 we also study the renormalization scale dependence and apparent convergence of the perturbative result. We have varied $\bar{\mu}_{\text{MS}}$ about μ by a factor of 2, and it emerges that the larger values are somewhat favored.

At low temperature $T \ll \mu$, dimensional reduction does not occur. If one nevertheless considers the effective-field-theory parameter m_E^2 of (2.5.11) in this limit, one finds that the function $\mathcal{D}(x)$ therein approaches $-2(\ln 2x + \gamma)$, so that the $T \rightarrow 0$ limit of m_E^2 exists and reads

$$m_E^2 \rightarrow \mu^2 \frac{g_{\text{eff}}^2}{\pi^2} \left\{ 1 - \frac{g_{\text{eff}}^2}{6\pi^2} \left[\ln \frac{\bar{\mu}_{\text{MS}}}{2\mu} - \frac{1}{2} \right] \right\} + O(g_{\text{eff}}^6). \quad (2.5.25)$$

Fastest apparent convergence applied to this quantity would suggest $\bar{\mu}_{\text{MS}} = 2e^{\frac{1}{2}}\mu \approx 3.3\mu$. This turns out to be not as good as the choice of 2μ , though slightly better than $\bar{\mu}_{\text{MS}} = \mu$.

The region of low temperature $T \ll \mu$ might be readily explored in the large N_f limit, where it gives rise to anomalous contributions of the pressure in the context of non-Fermi liquid. We will study this region in the next chapter.

Chapter 3

Non-Fermi Liquid

3.1 Introduction

3.1.1 From ideal gas to non-Fermi liquid

What is a non-Fermi liquid? The straightforward answer is to start from the ideal gas and extend the model layer by layer: The ideal gas is a statistical description of non-interacting point-like particles. If we go to low temperatures, we cannot neglect quantum mechanics and we have the choice of describing either bosons, which leads to the Bose-gas and to Bose-Einstein condensation at very low temperatures, or fermions, called (ideal) Fermi gas. Still, the Fermi gas is an accumulation of non-interacting fermions. If we turn on short-range interaction we get to the description of a (Landau-) Fermi-liquid. Thermodynamic quantities will mostly show the same order of dependence on the temperature T as in a Fermi gas, but their magnitude might change drastically. Finally, if the interactions we introduce change the dependence on T qualitatively, which is the case for long-range quasi-static interactions, the system cannot be described by the quasi-particle picture of the Landau-Fermi-liquid theory, and is therefore called a non-Fermi-liquid. Thus, a non-Fermi liquid is a cold gas/liquid of fermions with long-range interactions that change the behavior of a Landau-Fermi liquid qualitatively.

The ideal gas of not too dense, not too cold, and “non-interacting” (actually only interacting by elastic impact for thermalization) particles obeys the ideal gas law $pV = Nk_B T$. While simple and universal, this law is not sufficient to calculate all thermodynamic quantities like energy or entropy of the system. To calculate the energy for a fixed number of particles $E(S, V)$, we need an additional quantity, for example the specific heat $C_V \equiv T \left(\frac{\partial S}{\partial T} \right)_V$, which depends on the inner degrees of the ideal gas. Each degree of freedom in every particle of a system will contain the same energy on average so that the specific heat is given by

$$C_V(T) = \frac{f}{2} N k_B \quad (\text{ideal gas}) \quad (3.1.1)$$

for f degrees of freedom per particle and the Boltzmann constant k_B . For pointlike particles in three dimensions $f = 3$, for molecules of two atoms for example there is one additional degree of freedom for rotation and one for the change of bond length so that $f = 5$. The specific heat is an extensive quantity, but we can divide by the volume $C_V \equiv C_V/V = \frac{f}{2}nk_B$ which now depends on the particle density $n \equiv N/V$. Note that the specific heat for an ideal gas is independent of temperature. The entropy of the system can be calculated for example by integrating $(\frac{\partial S}{\partial T})_V = C_V/T$ and the Maxwell relation $(\frac{\partial S}{\partial V})_T = (\frac{\partial p}{\partial T})_V = Nk_B/V$ which for the ideal gas gives $S(T, V) = C_V \ln(T/T_0) + Nk_B \ln(V/V_0) + S(T_0, V_0)$. Statistical distribution of quantities like the mean velocity is given by the Maxwell-Boltzmann distribution function, which is not valid anymore for small temperatures where quantum mechanics starts to play a role. Here we have to use Bose-Einstein statistics for bosons or Fermi-Dirac statistics for fermions.

The ideal Fermi gas is a description of cold, non-interacting fermions [93, 94]. Examples include electrons in metals and semiconductors (when the Coulomb interaction between them is neglected), as well as neutrons in a neutron star (again when neglecting the interaction). Fermions obey the Pauli principle: no two fermions with the same quantum numbers can be in the same energy state. As a consequence, fermions will fill up the Fermi sphere in momentum space - if one possible momentum is occupied by a fermion, the next fermion has to go to the next higher momentum. (If they differ by a quantum number, e.g. the spin, then they might occupy the same energy level.) The particle density corresponding to a completely filled Fermi sphere of radius p_F in momentum space for a spin 1/2 fermion gas is given by $n = N/V = p_F^3/(3\pi^2\hbar^3)$ at zero temperature. The number-density distribution for $T = 0$ is a step-function: 1 for energy states below the Fermi energy, and 0 for energy states above. For non-zero temperature, the number-density distribution is given by the Fermi-Dirac distribution $n = (e^{(\epsilon-\mu)/(k_B T)} + 1)^{-1}$, where the chemical potential is just the energy on the Fermi surface at zero temperature $\mu|_{T=0} = \epsilon_F \equiv \epsilon(p_F)$. The specific heat can be calculated from the energy change due to the Fermi-Dirac distribution at non-zero temperature. It is given by

$$\begin{aligned} C_V(T) &\approx \frac{\pi^2}{3} k_B^2 D(\epsilon_F) T + O(T^3) && \text{(ideal Fermi gas)} \\ &= V \frac{m p_F}{3\hbar^3} k_B^2 T + O(T^3) \\ &= \frac{\pi^2}{2} N k_B \frac{T}{T_F} + O(T^3) \end{aligned} \tag{3.1.2}$$

with a density of states factor $D(\epsilon) = \frac{\sqrt{2}}{\pi^2} V (m/\hbar^2)^{3/2} \epsilon^{1/2}$ and the Fermi energy $\epsilon_F = \frac{\hbar^2}{2m} (3\pi^2 N/V)^{2/3} = p_F^2/(2m) = k_B T_F$. We see that the specific

heat of the ideal Fermi gas grows linearly in T for small temperatures. This is in contrast to the specific heat of an ideal gas (3.1.1) that is independent of temperature. Another striking difference to the ideal gas is the pressure: Since the fermions fill up the Fermi sphere, only a small fraction of fermions can be in the ground state. As a consequence, the pressure of a Fermi gas is nonzero even at zero temperature. This is in contrast to the pressure of an ideal gas that would be zero ($pV = Nk_B T$). This so-called degeneracy pressure stabilizes a neutron star (Fermi gas of neutrons) or a White Dwarf star (Fermi gas of electrons) against the inward pull of gravity.

If we include (short-range) interactions between the fermions, we call the system a Fermi liquid. A description of Fermi liquid was first given in 1956 by Landau [95, 96] and is thus commonly dubbed Landau-Fermi-liquid theory. It can be applied to liquid ${}^3\text{He}$ (which contains 2 protons, 1 neutron and 2 electrons - an odd number of fermions per atom - such that the atom itself is a fermion¹), as well as to the electrons in a normal metal. Landau-Fermi-liquid theory is qualitatively very similar to the theory of an ideal Fermi gas in which quasi-particles take the role of the non-interacting particles of the Fermi gas. Quasi-particles are collective excitations of the macroscopic system with certain energy ϵ and momentum p . The properties of quasiparticles are mainly characterized by the dispersion relation $\epsilon(p)$. Quasi-particles might have finite lifetime which gets sufficiently long in the vicinity of the Fermi surface to allow for a description similar to the particles in a Fermi gas. Strictly speaking, only certain kinds of interaction lead to the Landau-Fermi liquid, for example quasi-particles should still be fermions. (If there are attractive forces that favor a pairing of the fermions into bosons, the description of the Landau-Fermi-liquid is not applicable anymore.) Since the quasi-particles are fermions, they also fill up the Fermi sphere in momentum space. Quasi-particles always have a spin 1/2 spectrum. If the underlying particles had spins different from 1/2, this would lead to a degeneracy of the energies of the quasi-particles so that each branch corresponds to a spin 1/2 quasiparticle. The velocity of a quasiparticle is defined as $v_F = (\partial\epsilon/\partial p)|_{p=p_F}$. In the non-relativistic case one can introduce the effective mass of the quasiparticle as $m^* = p_F/v_F$. With this definition, the specific heat can be derived as

$$C_V(T) \approx V \frac{m^* p_F}{3\hbar^3} k_B^2 T + O(T^3 \ln T). \quad (\text{Landau-Fermi liquid}) \quad (3.1.3)$$

The only difference to the formula (3.1.2) in the leading order contribution is that the particle mass m is replaced by the effective mass m^* of the

¹Note that liquid ${}^4\text{He}$ with an even number of fermions per atom forms a boson gas and is a superfluid below 2.17 K. At this temperature, ${}^3\text{He}$ behaves like a Landau-Fermi liquid. Only at much smaller temperatures, around 2.7 mK, two atoms of ${}^3\text{He}$ align themselves to give an overall spin $s = 1$ and angular momentum $l = 1$ and also form a superfluid. This effect was found in 1971 by Osheroff, Lee, and Richardson who in 1996 received the Nobel prize for their work.

quasi-particle. We still have the same linear dependence on temperature² [97]. Note also that the next order contribution changes from $O(T^3)$ for the Fermi gas to $O(T^3 \ln T)$ for the Landau-Fermi liquid [98]. Not only the specific heat, but also other thermodynamic quantities like compressibility or spin-susceptibility show the same qualitative temperature dependence as in the Fermi gas, but might have different coefficients. The classical Landau Fermi liquid theory was extended to relativistic Fermi systems, enabling the study of high density matter with weak interaction via scalar and vector meson exchange [99]. As mentioned, not every kind of interaction leads to a Landau-Fermi liquid: If the interaction favors a pairing of the fermions, we effectively deal with a Bose gas. (In fact, in a Fermi gas arbitrarily small attractive forces lead to Cooper pairing of fermions.) If we have long-range, quasi-static interactions, the quasi-particle description is also not valid any more, and we obtain non-Fermi-liquid behavior.

Anomalous contributions to the specific heat were first calculated by Holstein et al. [100] who found a deviation from the linear dependence on T by a term proportional to $T \ln T^{-1}$. For very small temperatures T , the temperature dependence will actually be dominated by the $T \ln T^{-1}$ term. For QCD, quasi-static transverse gauge boson interactions further lead to a series with fractional powers of T . The specific heat of this non-Fermi liquid is given by (now with the usual quantum-mechanical natural units of $k_B = \hbar = 1$)

$$C_V \equiv C_V/V \approx \mu_q^2 T \frac{NN_f}{3} + ..T \ln ..T^{-1} \quad (\text{non-Fermi liquid})$$

$$+ ..T^{5/3} + ..T^{7/3} + O(T^3 \ln T) \quad (3.1.4)$$

where the coefficients were first calculated in 2003 [101] and will be presented in the following sections.

3.1.2 Non-Fermi liquid

A “non-Fermi liquid” is in principle any thermodynamic system of fermions that goes beyond the classical Landau-Fermi liquid description (including for example Cooper pairing of fermions and color superconductivity). Here we will narrow its usage to a Landau-Fermi liquid that is changed qualitatively by the introduction of long-range interactions. It was noticed by Holstein et al. [100] in 1973 when studying the de Haas-van Alphen effect³

²For a Bose liquid the specific heat grows proportional to the cube of the temperature $C_V = V 2\pi^2 T^3 / (15(\hbar u)^3)$ with the sound velocity $u = \epsilon/p$ [96].

³The de Haas-van Alphen effect states that magnetization shows an oscillatory dependence on the inverse magnetic field if the magnetic field is strong enough, $T \lesssim \mu_B B \ll \mu$ with the Bohr magneton $\mu_B = e\hbar/(2m_e)$ times the magnetic induction B still smaller than the chemical potential μ [96, 102]. A determination of oscillations in the magnetization M as a function of the inverse magnetic field $1/H$ (the de Haas-van Alphen effect) for

that long-range interactions lead to a deviation from the linear temperature dependence of the specific heat for small T . In order to explain the special de Haas-van Alphen oscillations in some noble metals in a slight modification of the original model, a current-current interaction, which in contrast to the Coulomb potential is not screened at zero frequency, leads to an anomalous contribution to the specific heat of the form $T \ln T^{-1}$. The coefficient of this term is of the order $\sim \alpha(v_F/c)(m^*/m)^2 \sim 10^{-5}$ smaller than that of the dominant term linear in T for non-relativistic QED applications, so originally it was argued that this anomalous contribution cannot be the cause for measurable effects. (A factor of 4 that was missing in the original calculation was corrected by [103] so that the leading log correction to the specific heat is $C_V = (g_0^2 p_F^2 / 36\pi^2) T \ln T^{-1}$). While this contribution implies that the entropy of the non-Fermi liquid exceeds the entropy of a Landau-Fermi liquid below some temperature, it is not possible to infer at which temperature this happens without complete knowledge of the argument of the logarithm: As long as we take the logarithm of a dimensionful quantity $\ln T$, we are missing the information on the relevant scale for the appearance of the anomalous behavior.

Long-range interactions are generally screened in the presence of a large Fermi sea. The reason why this does not happen for transverse gauge bosons like photons is that gauge invariance prevents them from acquiring a mass, unless gauge invariance is spontaneously broken (as in superconductors). An electron gas interacting via transverse gauge bosons shows non-Fermi liquid behavior depending on the number of space dimensions D . The specific heat is proportional to $C_V \sim T \ln T^{-1}$ only in $D = 3$ dimensions. For $D < 3$ dimensions, $C_V \sim T^{D/3}$ while for $D > 3$ the system behaves like an ordinary Landau-Fermi liquid [103, 104]. In this sense $D = 3$ corresponds to a quantum critical point with respect to variation of the dimension.

A recent calculation of non-Fermi-liquid corrections using renormalization group resummation techniques in reference [105] suggests a different leading nonanalytic behavior of the specific heat proportional to $T^3 \ln T$, which actually is of the same order as ordinary Landau-Fermi liquid corrections coming for example from electron-phonon interactions [98, 106, 107, 108]. However, the starting point of reference [105] already neglected diagrammatic contributions which would give $T \ln T^{-1}$ corrections.

It is sometimes assumed that the anomalous contributions to entropy or specific heat will hardly play any role at all, since color superconductivity (CSC) will dominate dense quark matter long before non-Fermi liquid behavior becomes effective [109, 110]. The argument is based on simple dimensional analysis of the energy scale, and compares the critical temperature of color superconductivity to the scale where the leading log correction be-

different orientations of the field has been the most successful method for mapping out the shape of the Fermi surface of metals [102].

comes as large as the leading contribution, that is where non-Fermi liquid becomes *nonperturbative*. Using the known formulae for the CSC critical temperature and our complete leading logarithm contribution presented in the following, we can calculate the *perturbative* correction stemming from non-Fermi liquid effects. As we will see in figure 3.6 of section 3.6.2, perturbative NFL corrections to the specific heat are of the order of 10%-20% at the CSC critical temperature for $g \sim O(1)$ and of the order of $g/(3\sqrt{2})$ for small g . Moreover, quark components which do not participate in the formation of diquark condensates will produce non-Fermi-liquid behavior even in the color superconducting phase.

Non-Fermi liquid behavior may therefore occur in astrophysical situations, for example the cooling rate of proto-neutron stars [16] if they involve a normal (non-superconducting) degenerate quark matter component.

In solid state physics experiments, non-Fermi-liquid behavior has been measured in so-called heavy-fermion metals [111], for example in the specific heat of the recently analyzed YbRh₂Si₂ crystal [17, 18]. There, $T \ln T^{-1}$ has been demonstrated experimentally over more than an order of magnitude in the vicinity of the quantum critical point for non-Fermi liquid behavior. At ambient pressure there are only a few undoped compounds that show non-Fermi-liquid behavior, like UBe₁₃ [112], CeNi₂Ge₂ [113], or CeCu₂Si₂ [114]. Other heavy fermion metals can be tuned to a quantum critical point by varying for example doping, pressure, or magnetic field.

In the following we will show how the specific heat for ultradegenerate QED and QCD can be calculated from the pressure integral we used for calculating the large N_f limit. Non-analytic contributions in T come from transverse gauge boson contributions. We will complete the leading logarithmic contribution $T \ln T^{-1}$ in that we calculate the argument of the logarithm. Beyond this contribution, dynamical screening gives rise to anomalous fractional powers $T^{(3+2n)/3}$, for which we calculate the coefficients up to and including order $T^{7/3}$.

3.2 Entropy at small temperatures

We want to study thermodynamic quantities in the region of small temperature $T \ll \mu$. The anomalous contributions that we would like to calculate, can be located in the entropy density

$$S \equiv S/V = \left(\frac{\partial P}{\partial T} \right)_\mu, \quad (3.2.1)$$

from which the specific heat can be derived. One might expect that the “ n_b ” contributions containing the Bose-Einstein distribution in the pressure (2.2.13) are negligible compared to the “non- n_b ” contributions, because $n_b(\omega) = 1/(e^{\omega/T} - 1)$ will vanish exponentially with small T for each (fixed)

ω . However, we will see that “ n_b ” contributions actually cannot be neglected for a region with $\omega \lesssim T$ and that they are the source of anomalous terms in the low-temperature series.

Looking at the “non- n_b ” contributions first (which are those parts of the calculation that we have to integrate in Euclidean space and which require the introduction of a cutoff due to the Landau pole), the corresponding part of the entropy is given by

$$\begin{aligned} \mathcal{S}_{\text{non-}n_b} = T \left\{ -\frac{g_{\text{eff}}^2}{8\pi^2} + \frac{g_{\text{eff}}^4}{32\pi^4} \left[\frac{2}{3} \ln \frac{\bar{\mu}_{\text{MS}}}{\mu} \right. \right. \\ \left. \left. - 0.328(1) \times \ln \frac{g_{\text{eff}}^2}{2\pi^2} + 0.462(5) \right] + O(g_{\text{eff}}^6 \ln g_{\text{eff}}) \right\} + O(T^3). \end{aligned} \quad (3.2.2)$$

We see that the coefficient at order g_{eff}^2 is the same as the g_{eff}^2 part of the strictly perturbative result for the pressure. The latter is also known as the exchange term [20] and coincides with the g_{eff}^2 part of (2.5.10). Here we have also numerically extracted the order- $g^4 \ln(g)$ corrections from the exact large N_f result of $\mathcal{S}_{\text{non-}n_b}$ at small coupling.

The dash-dotted lines in figure 3.1 show the exact (NLO large N_f) result for $\mathcal{S}_{\text{non-}n_b}$ for different couplings $g_{\text{eff}}^2(\bar{\mu}_{\text{MS}} = \mu) = 1, 4, \text{ and } 9$ and small temperatures $0 < T/\mu < 0.15$. In this range of temperatures, $\mathcal{S}_{\text{non-}n_b}$ is well approximated by the linear term (3.2.2). The dashed lines in figure 3.1 show the “ n_b ” contributions to the specific heat in the large N_f limit evaluated numerically. For small T we see that these parts cannot be neglected. For sufficiently small T/μ , \mathcal{S}_{n_b} is positive and even dominates so that the total result for the entropy turns out to exceed its free-theory value for a certain range of T/μ . The size of the range where the anomalous contribution dominates in the entropy gets larger with increasing g_{eff}^2 . The largest part of the positive and nonlinear contributions at small T/μ in fact comes from the transverse vector-boson modes. These are only weakly dynamically screened at small frequencies and completely unscreened in the static limit because of gauge invariance. We will see that it is the transverse part of the “non- n_b ” term that will fully contain the temperature-dependent anomalous contribution. The large N_f limit will allow us to calculate the anomalous contributions in a very straightforward manner, so let us start by looking more closely at the transverse contribution.

3.3 Transverse contribution

We started our large N_f calculation from equation (2.2.13) which gives the pressure associated with the gauge boson loop with a resummed fermion loop insertion. All interesting non-Fermi liquid ($T \ln T$, $T^{5/3}$, and $T^{7/3}$) behavior to the specific heat arise from the thermal part, the “non- n_b ” part, of the

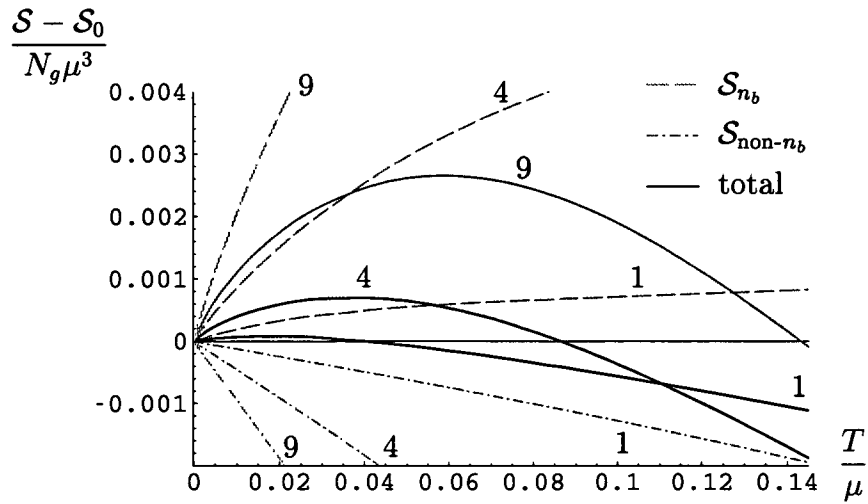


Figure 3.1: The interaction part of the entropy at small T/μ for $g_{\text{eff}}^2 (\bar{\mu}_{\text{MS}} = \mu) = 1, 4, \text{ and } 9$. The “non- n_b ” contributions (dash-dotted lines) are negative and approximately linear in T with a coefficient agreeing with the exchange term $\propto g_{\text{eff}}^2$ in the pressure at small coupling; the “ n_b ” contributions (dashed lines) are positive and nonlinear in T such that the total entropy exceeds the free-theory value at sufficiently small T/μ . Transverse gauge boson modes dominate the anomalous contribution in the “non- n_b ” part.

transverse propagator. In the following, we will calculate the contribution to the pressure coming from the transverse part

$$\frac{P_{T,n_b}}{N_g} = - \int \frac{d^3q}{(2\pi)^3} \int_0^\infty \frac{dq_0}{\pi} 2n_b \text{Im} \ln(q^2 - q_0^2 + \Pi_T + \Pi_{\text{vac}}). \quad (3.3.1)$$

We will start with a motivating calculation for the leading logarithmic contribution to the pressure and systematically extend this calculation to finally obtain the anomalous Fermi liquid contributions up to and including order $T^{7/3}$.

3.3.1 Leading log contribution

To calculate the pressure at small T , we start from equation (3.3.1) where we can write the argument function as $\text{Im} \ln x = \arctan(\text{Im} x / \text{Re} x)$ as long as $\text{Re} x$ is positive. Keeping this in mind, we use the following low-temperature approximations: We first neglect the real part of $\text{Re}(\Pi_T + \Pi_{\text{vac}}) \simeq 0 + O(q_0^2)$ so that the main contribution comes from q^2 . For the imaginary part we only go through order $O(q)$ (the complete results for real and imaginary parts of Π_T are given in appendix D) so that we use the following expression

$$\text{Im} \ln(q^2 - q_0^2 + \Pi_T + \Pi_{\text{vac}}) \simeq \arctan \frac{-g_{\text{eff}}^2 4\mu^2 q_0 \theta(\mu - \frac{q}{2}) / (16\pi q)}{q^2}. \quad (3.3.2)$$

We first apply the q -integration of the form

$$\begin{aligned} \int_0^{q_m} dq q^2 \arctan \frac{q_0}{q^3} &= \frac{1}{6} \left(\pi q_m^3 - 2q_m^3 \arctan \frac{q_m^3}{q_0} + q_0 \ln \left(1 + \frac{q_m^6}{q_0^2} \right) \right) \\ &\simeq \frac{1}{3} q_0 \left(1 + \ln \frac{q_m^3}{q_0} \right) + O(q_0^3) \end{aligned} \quad (3.3.3)$$

for a maximum upper bound q_m . From the imaginary part we see that $q_m = 2\mu$. We are left with the following q_0 integration which gives

$$\begin{aligned} \frac{P_{T,n_b}}{N_g} &= \frac{4\pi}{8\pi^3} \int_0^\infty \frac{dq_0}{\pi} \frac{2}{e^{q_0/T} - 1} \frac{g_{\text{eff}}^2 \mu^2}{12\pi} q_0 \left(1 + \ln \frac{4\pi q_m^3}{g_{\text{eff}}^2 \mu^2 q_0} \right) \\ &= \frac{g_{\text{eff}}^2 \mu^2 T^2}{72\pi^2} \left(\ln \frac{4\pi q_m^3}{g_{\text{eff}}^2 \mu^2 T} + \gamma_E - \frac{6}{\pi^2} \zeta'(2) \right) \\ &= \frac{g_{\text{eff}}^2 \mu^2 T^2}{72\pi^2} \left(\ln \frac{32\pi\mu}{g_{\text{eff}}^2 T} + \gamma_E - \frac{6}{\pi^2} \zeta'(2) \right) \end{aligned} \quad (3.3.4)$$

with $\gamma_E - \frac{6}{\pi^2} \zeta'(2) \simeq 1.14718$. One does not have to worry about first expanding in small q_0 and then integrating q_0 from 0 to ∞ : The bosonic distribution function $n_b = 1/(\exp(q_0/T) - 1)$ ensures that for small T only

small values of $q_0 \lesssim T$ are sampled in the integrand - larger q_0 contributions are suppressed exponentially. We find the contribution to the entropy density $\mathcal{S} \equiv S/V = (\partial P/\partial T)_{V,\mu}$ as

$$\frac{\mathcal{S}_{T,n_b}}{N_g} = \frac{g_{\text{eff}}^2 \mu^2 T}{36\pi^2} \left(\ln \frac{32\pi\mu}{g_{\text{eff}}^2 T} - \frac{1}{2} + \gamma_E - \frac{6}{\pi^2} \zeta'(2) \right). \quad (3.3.5)$$

We can also form the specific heat $\mathcal{C}_V \equiv C_V/V$ at constant volume and number density which for unit-volume is given by [115]

$$\mathcal{C}_V = T \left\{ \left(\frac{\partial \mathcal{S}}{\partial T} \right)_\mu - \left(\frac{\partial \mathcal{N}}{\partial T} \right)_\mu^2 \left(\frac{\partial \mathcal{N}}{\partial \mu} \right)_T^{-1} \right\}. \quad (3.3.6)$$

where \mathcal{N} is the number density $\mathcal{N} \equiv N/V = (\partial P/\partial \mu)_{T,V}$. The application of this formula including the leading-order contribution is given in equation (C.1.5) from appendix C. We find that to leading order the coefficient of the logarithm remains the same for entropy and specific heat. There is only a shift by -1 in the sublogarithmic term

$$\frac{\mathcal{C}_{V,T,n_b}}{N_g} = \frac{g_{\text{eff}}^2 \mu^2 T}{36\pi^2} \left(\ln \frac{32\pi\mu}{g_{\text{eff}}^2 T} - \frac{3}{2} + \gamma_E - \frac{6}{\pi^2} \zeta'(2) \right). \quad (3.3.7)$$

This first version of the result already includes the correct pre-factor of the leading logarithmic contribution of the specific heat as given in the literature. It confirms the calculation of reference [103] who also found the leading log contribution $C_V = (g_0^2 p_F^2 / 36\pi^2) T \ln T^{-1}$ as the specific heat correction, and even goes beyond this known result in that dimensional dependence and the constants "under" the logarithm are determined. But the term proportional to T (the argument of the logarithm) still calls for improved approximations and should not be trusted yet: It will change by inclusion of higher order terms as we will see in the next section.

3.3.2 Straightforward improvements

It is possible to retain another term and replace $4\mu^2$ by $(4\mu^2 + q^2)$ in (3.3.2). This will enable us to obtain the correct leading contribution to the q -integration even for larger q . The integral over the arc tangent involves roots of some cubic equation, but it is still solvable. After performing the small- q_0 expansion, the result is almost the same, up to an additional term.

$$\int_0^{q_m} dq q^2 \arctan \frac{q_0(4\mu^2 + q^2)}{q^3} \simeq \frac{4\mu^2}{3} q_0 \left(1 + \ln \frac{q_m^3}{q_0 4\mu^2} + \frac{3}{2} \frac{q_m^2}{4\mu^2} \right) + O(q_0^{5/3}). \quad (3.3.8)$$

Using $q_m = 2\mu$, this term only contributes by a shift of $+3/2$ inside the braces. The second integral is straightforward and leads to the following pressure

$$\frac{P_{T,n_b}}{N_g} = \frac{g_{\text{eff}}^2 \mu^2 T^2}{72\pi^2} \left(\ln \frac{32\pi\mu}{g_{\text{eff}}^2 T} + \frac{3}{2} + \gamma_E - \frac{6}{\pi^2} \zeta'(2) \right) \quad (3.3.9)$$

and its corresponding entropy

$$\frac{S_{T,n_b}}{N_g} = \frac{g_{\text{eff}}^2 \mu^2 T}{36\pi^2} \left(\ln \frac{32\pi\mu}{g_{\text{eff}}^2 T} + 1 + \gamma_E - \frac{6}{\pi^2} \zeta'(2) \right). \quad (3.3.10)$$

It is also possible to add the vacuum term which also contains a part proportional to q^2 : Instead of q^2 in the denominator of (3.3.2) we could start with

$$q^2 - q_0^2 + \Pi_T + \Pi_{\text{vac}} \simeq q^2 + q^2 \frac{g_{\text{eff}}^2}{6\pi^2} \ln \frac{\bar{\mu}_{\text{MS}}}{2\mu} + O(q_0^2) + O(q^3). \quad (3.3.11)$$

The calculation will be almost unaffected, only in the final step we need to change $g_{\text{eff}}^2 \rightarrow g_{\text{eff}}^2 / (1 + \frac{g_{\text{eff}}^2}{6\pi^2} \ln \frac{\bar{\mu}_{\text{MS}}}{2\mu})$. It is clear that this only gives corrections subleading in g_{eff}^2 . In fact, this substitution is nothing else than a change in scale as given by the exact scale dependence of g_{eff} in (2.2.4).

Another extension that we should consider is the T -dependence of the self-energies. Up to now we tacitly assumed constant self-energies $\Pi_T(T) = \Pi_T(0)$ at small T , but this is a simplification which might affect the next-to-leading order in temperature. We find the following temperature dependencies:

$$\text{Im}\Pi_T(q_0, q, T) = \text{Im}\Pi_T(q_0, q, 0) - T^2 \frac{g_{\text{eff}}^2 \pi}{12q} q_0 \theta(2\mu - q) + O(q_0^2), \quad (3.3.12)$$

$$\text{Re}\Pi_T(q_0, q, T) = \text{Re}\Pi_T(q_0, q, 0) + T^2 \frac{g_{\text{eff}}^2 q^2}{36\mu^2} + O(q_0^2) + O(q^3). \quad (3.3.13)$$

The leading order contributions turn out to have the same order as the $T = 0$ terms, so that our calculation does not change qualitatively. Introducing new variables

$$X = 1 + \frac{\pi^2 T^2}{3\mu^2}, \quad (3.3.14)$$

$$Y = 1 + \frac{g_{\text{eff}}^2 T^2}{36\mu^2} - \frac{g_{\text{eff}}^2}{6\pi^2} \ln \frac{2\mu}{\bar{\mu}_{\text{MS}}} \quad (3.3.15)$$

we can write the resulting pressure as

$$\frac{P_{T,n_b}}{N_g} = \frac{g_{\text{eff}}^2 \mu^2 T^2}{72\pi^2} \left(\ln \frac{32\pi\mu}{g_{\text{eff}}^2 T} + \ln \frac{Y}{X} + \gamma_E - \frac{6}{\pi^2} \zeta'(2) + \frac{3}{2X} \right) \frac{X}{Y}. \quad (3.3.16)$$

effectively adding T^4 contributions to the pressure (or equivalently T^3 contributions to the entropy or the specific heat). This expression reduces to (3.3.9) if we set $T \rightarrow 0$ in X and Y .

We should also consider consistently including higher order terms of q and q_0 in the arctan arguments of (3.3.2) or (3.3.8). In the next section we will see how this will eventually lead to an integral with a tenth degree

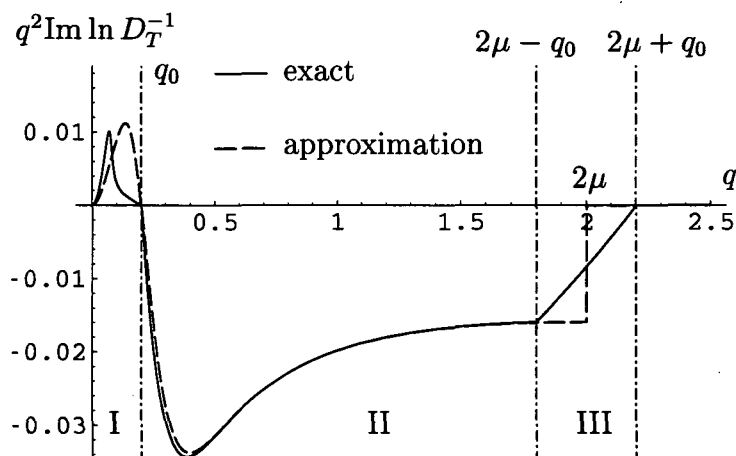


Figure 3.2: Integrand for the q -integration $q^2 \text{Im} \ln(q^2 - q_0^2 + \Pi_T + \Pi_{\text{vac}})$ for $\mu = \bar{\mu}_{\text{MS}}/2 = 1$, $q_0 = 0.2$, $g_{\text{eff}}^2 = 1$. The solid line shows the exact result that follows from the full $T = 0$ self energy expressions, the dashed line shows the result with $\text{Re} \Pi_T$ expanded through order $O(q_0^2)$ and $O(q^2)$ and $\theta(2\mu - |q \pm q_0|)$ replaced by $\theta(2\mu - q)$. The parameter $q_0 = 0.2$ is chosen this large as to clearly show the three different ranges. We will see that the error introduced by changing regions I and III by our approximation only contribute at order $O(q_0^3)$ or higher, whereas the main contribution for lower orders only comes from region II, if the dashed line is integrated from q_0 to 2μ .

polynomial in the denominator that cannot be readily solved. We have to introduce approximations in order to factorize the polynomial to obtain doable integrals, and we shall carefully check that we don't omit any vital contributions while applying our approximations.

3.3.3 Approximations to order T^3

We want to carefully examine the full integrand of (3.3.1) and study which kind of approximations can be applied consistently up to order T^3 . For $T = 0$ an exact solution of the real and imaginary parts of the gluon self energy Π_T and Π_L can be given (see appendix D, equations (D.1.8), (D.1.9), (D.1.15), and (D.1.16)). These solutions contain expressions like $\ln|q - q_0|$ or $\theta(2\mu - |q_0 \pm q|)$ so that the q -integration naturally splits into three regions. The full line in figure 3.2 shows the exact integrand. The dashed line in the figure shows the integrand that we want to use: We resolve all absolute values in the integral in a region $q_0 < q < 2\mu$, and expand the real part $\text{Re}(\Pi_T + \Pi_{\text{vac}})$ through order $O(q_0^2)$ and $O(q^2)$. Also, as before, we replace $\theta(2\mu - |q_0 \pm q|)$ by $\theta(2\mu - q)$ so that our inverse transverse propagator $D_T^{-1} =$

$q^2 - q_0^2 + \Pi_T + \Pi_{\text{vac}}$ for $T = 0$ reads

$$\begin{aligned} \text{Re } D_T^{-1} &= \left(q^2 - q^2 \frac{g_{\text{eff}}^2}{6\pi^2} \ln \frac{2\mu}{\bar{\mu}_{\text{MS}}} + O(q^4) \right) \\ &+ \left(\frac{g_{\text{eff}}^2 \mu^2}{\pi^2 q^2} - 1 + \frac{g_{\text{eff}}^2}{6\pi^2} \left[\frac{1}{2} + \ln \frac{2\mu}{\bar{\mu}_{\text{MS}}} \right] + \frac{g_{\text{eff}}^2 q^2}{80\pi^2 \mu^2} + O(q^4) \right) q_0^2 \\ &+ O(q_0^4), \end{aligned} \quad (3.3.17)$$

$$\text{Im } D_T^{-1} = -\frac{g_{\text{eff}}^2 q_0}{48\pi q^3} (q^2 - q_0^2) (12\mu^2 + 3q^2 + q_0^2) \theta(2\mu - q). \quad (3.3.18)$$

All powers of higher order in q or q_0 in (3.3.18) are suppressed at least by a factor of g_{eff}^2 . The expansion in the first line of (3.3.18) in q is a priori only justifiable for anomalous contributions that arise from a region of small q_0 and small q . Actually, the q integral gives contributions all the way up to $0 < q < 2\mu$ and higher order contributions in q contribute to the argument of the leading logarithm $T \ln T^{-1}$. These corrections will be suppressed by g_{eff}^2 at least so that we neglect them for the moment.

Both real and imaginary part can be extended from region II between q_0 and $2\mu - q_0$ to the integration region q_0 to 2μ , and we should verify that this procedure does not introduce an error to the order of interest. In the following we will explicitly examine to what order the regions I and III will contribute.

In region I we can argue by the maximum upper bound of the integrand: The arc tangent function limits the integrand to $\pi/2$ so that the integral can maximally contribute with $\int_0^{q_0} q^2 \frac{\pi}{2} dq = \pi q_0^3/6$. This is a result of order q_0^3 that can be neglected if we expect results of the order $q_0 \ln q_0$, $q_0^{5/3}$, or $q_0^{7/3}$.

In region III the argumentation is more subtle. If we expand the exact self energy functions in a region $2\mu - q_0 < q < 2\mu + q$ and integrate them in this interval, we obtain as a leading order contribution $-72\pi g_{\text{eff}}^2 \pi \mu^2 q_0^2 / (4\mu(72\pi^2 + 13g_{\text{eff}}^2 - 12g_{\text{eff}}^2 \ln \frac{4\mu}{\bar{\mu}_{\text{MS}}})) + O(q_0^3)$. This result is quadratic in the leading order of q_0 and could therefore not be neglected as such. However, it turns out that this contribution exactly matches the quadratic contribution that one would obtain from extending the approximating formula from region II to region III and integrating it between $2\mu - q_0$ and 2μ . This is also suggested by figure 3.2 where the triangle in region III of the exact solution is replaced by a rectangle of half the width of our dashed approximate expression. So by integrating our region II formula from q_0 to 2μ , we actually reduce the error to order $O(q_0^3)$. In the following we can expect to obtain correct expansion terms below third order in q_0 by integrating out our approximating functions (3.3.17) and (3.3.18) from q_0 to 2μ .

3.3.4 Momentum integration

We will integrate (3.3.1) using our approximating functions (3.3.17) and (3.3.18), abbreviated conveniently as Re (containing only the explicit terms given in (3.3.17) omitting higher order contributions) and Im , using integration by parts.

$$\int_{q_0}^{2\mu} q^2 \arctan \frac{\text{Im}}{\text{Re}} dq = \frac{q^3}{3} \arctan \frac{\text{Im}}{\text{Re}} \Big|_{q_0}^{2\mu} - \int_{q_0}^{2\mu} \frac{q^3}{3} \frac{\text{Re Im}' - \text{Im Re}'}{\text{Re}^2 + \text{Im}^2} dq. \quad (3.3.19)$$

The first part of this integral poses no problem, and it is straightforward to expand the result in terms of small q_0 :

$$\frac{q^3}{3} \arctan \frac{\text{Im}}{\text{Re}} \Big|_{q_0}^{2\mu} = -\frac{g_{\text{eff}}^2 \mu^2 q_0}{6\pi} + O(q_0^3). \quad (3.3.20)$$

As it should be, this result is independent of whether we start the integration from q_0 or from 0. The second part of the integral is more demanding as we get a bulky polynomial in the denominator. (To simplify the following expressions, we will set $\bar{\mu}_{\text{MS}} = 2\mu$, thereby getting rid of logarithmic constants, and reintroduce them only in the final result):

$$\begin{aligned} & 57600\mu^4 \pi^4 q^6 (\text{Re}^2 + \text{Im}^2) \\ &= q^{10} (57600\mu^4 \pi^4 + 1440g_{\text{eff}}^2 \mu^2 \pi^2 q_0^2 + 9g_{\text{eff}}^2 q_0^4) \\ &+ q^8 (75\mu^4 \pi^2 [128g_{\text{eff}}^2 + 3g_{\text{eff}}^4 - 1536\pi^2] q_0^2 + 120g_{\text{eff}}^2 \mu^2 [g_{\text{eff}}^2 - 12\pi^2] q_0^4) \\ &+ q^6 (1800g_{\text{eff}}^2 [64 + g_{\text{eff}}^2] \mu^6 \pi^2 q_0^2 \\ &\quad - 20\mu^4 [480g_{\text{eff}}^2 \pi^2 - 2880\pi^4 + g_{\text{eff}}^4 (-92 + 15\pi^2)] q_0^4) \\ &+ q^4 (3600g_{\text{eff}}^4 \mu^8 \pi^2 q_0^2 - 600g_{\text{eff}}^2 \mu^6 [192\pi^2 + g_{\text{eff}}^2 (-16 + 5\pi^2)] q_0^4 \\ &\quad - 50g_{\text{eff}}^4 \mu^4 \pi^2 q_0^8) \\ &+ q^2 (-7200g_{\text{eff}}^4 \mu^8 [-8 + \pi^2] q_0^4 + 600g_{\text{eff}}^4 \mu^6 \pi^2 q_0^6 + 100g_{\text{eff}}^4 \mu^4 \pi^2 q_0^8) \\ &+ (3600g_{\text{eff}}^4 \mu^8 q_0^6 + 600g_{\text{eff}}^4 \mu^6 \pi^2 q_0^8 + 25g_{\text{eff}}^4 \mu^4 \pi^2 q_0^{10}). \end{aligned} \quad (3.3.21)$$

Bearing in mind that this is just the denominator of the integrand, a direct integration seems impossible: This is a polynomial of tenth degree in q , or given the fact that only even powers of q appear, we have to cope with a quintic at least. Performing rational integrals requires knowledge of the roots of the denominator (see appendix E.1, equation (E.1.6)). But for a quintic, solutions in form of root expressions can not be given anymore in general. However, all we need is an expansion of the final integral in terms of q_0 , that is for small q_0 . Can we therefore locate those terms of this polynomial that are important to low order terms of the q_0 expansion? A first naive approach of simply expanding the denominator in terms of small q_0 will certainly fail, because also our integration variable q can become small at the same time.

A possible solution might be found in the pole structure of this expression for small q_0 as plotted in figure 3.3. The location of the poles reveals some symmetry, and presumably only a few terms from the polynomial (3.3.21) determine this structure. In the following we will see how to extract these terms.

Pole structure

We obtain (what we will call) the "low-order front" of the polynomial by first retaining only the leading order in q_0 for each order of q separately, and then keeping only the leading order terms in q for each order of q_0 . Applying this procedure to our polynomial (3.3.21), we first get terms of the orders q^{10} , $q^8 q_0^2$, $q^6 q_0^2$, $q^4 q_0^2$, $q^2 q_0^4$, and q_0^6 which are the relevant terms for small q_0 . From the three terms proportional to q_0^2 we can omit $q^8 q_0^2$ and $q^6 q_0^2$ for small q and q_0 so that we are left with only four terms that fully determine the leading order behavior of the integrand denominator for small q and q_0 :

$$\text{Re}^2 + \text{Im}^2 \approx \frac{1}{q^6} \left(q^{10} + \frac{g_{\text{eff}}^4 \mu^4}{16\pi^2} q^4 q_0^2 - \frac{g_{\text{eff}}^4 \mu^4 (\pi^2 - 8)}{8\pi^4} q^2 q_0^4 + \frac{g_{\text{eff}}^4 \mu^4}{16\pi^2} q_0^6 \right). \quad (3.3.22)$$

This "low-order front" uniquely characterizes the small q_0 and small q pole structure. The first three terms will not change even if we include higher-order terms of q or q_0 from the beginning of the calculation in (3.3.17): higher order contributions in q_0 are shielded by the q_0^6 term, higher order terms in q are shielded by the q^{10} term (for small q where the small q_0 pole structure appears) and all other power mixtures in between are shielded by this low-order front of four terms. It should be noted however that in the expansion of (3.3.17) also negative powers of q appear for higher order q_0 corrections that add terms of the order $(q_0/q)^{2n}$ with $2n \geq 6$. Their omission turns out to be negligible since we restricted our integral to the region $q_0 \leq q$ and the coefficients of this series quickly get smaller.

Still, we are left with a quintic whose general solution cannot be given in form of root expressions. Let us see, if we can reproduce the pole structure suggested by figure 3.3. As a first guess we would start with

$$\text{Re}^2 + \text{Im}^2 \approx \frac{1}{q^6} (A + q^6) (F + q^4) \quad (3.3.23)$$

which would give four poles arranged in a square at a distance $F^{1/4}$ and six poles arranged in the shape of a honeycomb at a distance $A^{1/6}$. Expanded, this term gives $AF + Aq^4 + Fq^6 + q^{10}$. We can read off A from the q^4 term $A = g_{\text{eff}}^4 \mu^4 q_0^2 / (16\pi^2)$ which determines F from the constant term as $F = q_0^4$. This already explains the main features of the pole structures. Unfortunately, our low-order front is not correctly reproduced yet. This is not dramatic for the additional Fq^6 -term, because it is sub-leading to the

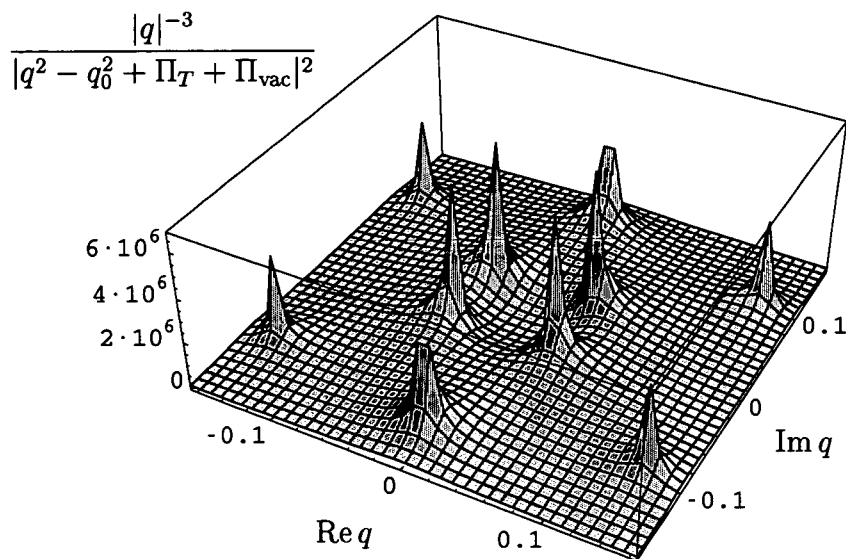


Figure 3.3: Pole structure of the *truncated* absolute squared transverse propagator $\text{Re}^2 + \text{Im}^2$ at $\mu = \bar{\mu}_{MS}/2 = 1$, $q_0 = 0.05$, $g_{\text{eff}}^2 = 1$ in the complex q -plane. This 10-pole structure arises from the special form of truncation that we chose in (3.3.17). For small q_0 the 10-pole structure naturally decomposes into a rectangular structure with the four poles in the middle at the order of $|q| \approx q_0$, while the six surrounding poles, prominently arranged in the shape of a honeycomb, stay at the order $|q| \approx (g_{\text{eff}}^2 \mu^2 q_0 / 4\pi)^{1/3}$. While the inner four poles basically contribute to the leading logarithmic contribution, it is these outer six poles that give rise to anomalous Fermi-liquid behavior of order $T^{5/3}$ and $T^{7/3}$. Corrections to this simple picture will be discussed in the text. The plot is multiplied by $|q|^{-3}$ which does not change the pole structure since the propagator contains an overall factor of q^6 , but merely makes the poles have similar heights in this plot.

low-order front, but the term proportional to q^2 is not reproduced at all. Therefore we have to extend our guess slightly:

$$\text{Re}^2 + \text{Im}^2 \approx \frac{1}{q^6} (A + q^6) (F + Gq^2 + q^4) \equiv D_0 \quad (3.3.24)$$

where we can determine $G = -2(\pi^2 - 8)q_0^2/\pi^2$. In this way we change the inner pole structure from a square to a rectangle. We can now calculate the integral. Since we know how to factor our denominator, we can apply partial fraction decomposition and reduce the integral (3.3.19) to doable simpler integrals

$$\int \frac{N}{D} dq \approx \int \frac{N}{D_0} dq = \int \frac{N_\alpha}{(q^6 + \dots)} dq + \int \frac{N_\beta}{(q^4 + \dots)} dq \quad (3.3.25)$$

where we abbreviated the numerator as $N = q^3(\text{Re Im}' - \text{Im Re}')/3$, the original denominator as $D = \text{Re}^2 + \text{Im}^2$, and its first factorization as D_0 from (3.3.24). Applying this procedure, we obtain the following result:

$$\begin{aligned} - \int_{q_0}^{2\mu} \frac{N}{D_0} dq &= - \frac{g_{\text{eff}}^2 \mu^2 q_0}{12\pi} \left(\frac{1}{2} + \ln \frac{32\pi\mu}{g_{\text{eff}}^2 q_0} \right) + \frac{2^{2/3} (g_{\text{eff}} \mu)^{4/3} q_0^{5/3}}{9\sqrt{3}\pi^{2/3}} \left(1 + \frac{g_{\text{eff}}^2}{64} \right) \\ &+ \frac{8 \cdot 2^{1/3} (g_{\text{eff}} \mu)^{2/3} q_0^{7/3}}{3\sqrt{3}\pi^{4/3}} \left(1 + \frac{g_{\text{eff}}^2}{72} \right) + O(q_0^3 \ln q_0). \end{aligned} \quad (3.3.26)$$

The result looks insofar good as we obtain the same leading order logarithm as from our first approach (3.3.8) if we take (3.3.20) into account, and we obtain anomalous $q_0^{5/3}$ and $q_0^{7/3}$ contributions. However, those are not complete yet, as we will see soon. This integral is only the first of a series that we can form: If we denote the terms we neglected in the denominator as $\delta D_0 = D - D_0$, we can write an expansion series that should contain the complete result:

$$\int \frac{N}{D} dq = \int \frac{N}{D_0 + \delta D_0} dq = \int \frac{N}{D_0} dq - \int \frac{N \delta D_0}{D_0^2} dq + \int \frac{N \delta D_0^2}{D_0^3} dq - + \dots \quad (3.3.27)$$

Again, as before, by partial fraction decomposition, all of the integrals on the right hand side are doable. Looking at the second term in this series, we again find contributions of the order $q_0^{5/3}$ and $q_0^{7/3}$:

$$\begin{aligned} \int \frac{N \delta D_0}{D_0^2} dq &= \frac{2 \cdot 2^{2/3} (g_{\text{eff}} \mu)^{4/3} q_0^{5/3}}{9\sqrt{3}\pi^{2/3}} \left(1 + \frac{g_{\text{eff}}^2}{64} \right) \\ &+ \frac{64 \cdot 2^{1/3} (g_{\text{eff}} \mu)^{2/3} q_0^{7/3}}{27\sqrt{3}\pi^{4/3}} \left(1 - \frac{3g_{\text{eff}}^2}{256} - \frac{5g_{\text{eff}}^4}{16384} \right) + (q_0^3 \ln q_0). \end{aligned} \quad (3.3.28)$$

Although we expect to calculate a correction contribution, the $q_0^{5/3}$ term turns out to be twice as big as the first one. Apparently the series does

not converge fast enough. The third term in the series $\int N \delta D_0^2 / D_0^3 dq$ again seems promising for it starts at order $O(q_0^{7/3})$ and does not contain a $q_0^{5/3}$ term anymore, but still we would like to find a more controlled kind of approximation.

Completing the hypercube

The problem of the series lies in the correction δD_0 which is of the order q_0^2 . This order is not enough to compensate negative orders of q_0 that are introduced by powers of the denominator D_0 . We could ask if it is possible to shuffle the q_0^2 terms from δD_0 into D_0 in such a way that D_0 remains a product of a fourth-order and a sixth-order polynomial. In this way we could form a new denominator D_1 with a corresponding $\delta D_1 = D - D_1 = O(q_0^4)$ and we could expect a faster converging series in terms of q_0 . It turns out that it is indeed possible to complete the square - or actually the 10-dimensional hypercube - up to a given order of q_0 so that corrections are higher-order in q_0 by the following procedure: We start from

$$\begin{aligned} \text{Re}^2 + \text{Im}^2 &= \frac{1}{q^6} \{a + bq^2 + cq^4 + dq^6 + eq^8 + fq^{10}\} \\ &\approx \frac{1}{q^6} M (A + Bq^2 + Cq^4 + q^6) (F + Gq^2 + q^4) \equiv D_1 \\ &= \frac{1}{q^6} M \{AF + (AG + BF)q^2 + (A + BG + CF)q^4 \\ &\quad + (B + CG + F)q^6 + (C + G)q^8 + q^{10}\} \quad (3.3.29) \end{aligned}$$

where $a, b, c, d, e,$ and f can be read off from (3.3.21). We already determined $A, F,$ and G before. δD_0 contains q_0^2 contributions for $q^{10}, q^8,$ and $q^6,$ and we have three variables left: $B, C,$ and M . This should not be too difficult, since the mixing terms BF, BG, CF, \dots naturally turn out to be of higher order in q_0 . We can summarize the procedure as follows:

$$\begin{aligned} M &\rightarrow f \sim 1 + O(q_0^2), \\ A &\rightarrow \frac{c}{M} \sim O(q_0^2), \\ F &\rightarrow \frac{a}{AM} \sim O(q_0^4), \\ G &\rightarrow \frac{b}{AM} \sim O(q_0^2), \\ C &\rightarrow \frac{e - MG}{M} \sim O(q_0^2), \\ B &\rightarrow \frac{d}{M} \sim O(q_0^2) \end{aligned} \quad (3.3.30)$$

where the coefficients are series expanded in q_0 and truncated to form polynomials. In our case we get the following assignments

$$\begin{aligned}
A &\rightarrow \frac{g_{\text{eff}}^4 \mu^4}{16\pi^2} q_0^2, \\
B &\rightarrow \frac{g_{\text{eff}}^2 \mu^2 (64 + g_{\text{eff}}^2)}{32\pi^2} q_0^2, \\
C &\rightarrow \frac{3g_{\text{eff}}^4 + 128g_{\text{eff}}^2 - 12288}{768\pi^2} q_0^2, \\
F &\rightarrow q_0^4, \\
G &\rightarrow -2 \frac{\pi^2 - 8}{\pi^2} q_0^2, \\
M &\rightarrow 1 + \frac{g_{\text{eff}}^2}{40\pi^2 \mu^2} q_0^2
\end{aligned} \tag{3.3.31}$$

Using these in (3.3.29) we obtain a correction term δD_1 of the order $O(q_0^4)$. It is possible to pursue the same strategy again to get rid of the $O(q_0^4)$ term in the δD_1 correction to form a D_2 result by the very same procedure as above, including the next order term in each variable. δD_2 would then be a correction of order $O(q_0^6)$.

Let us see how this new denominator D_1 changes the result. There are many terms involved in this calculation, so it is best to let a computer do all integrals each of which is doable just as before. Here is the final result:

$$\begin{aligned}
-\int_{q_0}^{2\mu} \frac{N}{D_1} dq &= -\frac{g_{\text{eff}}^2 \mu^2 q_0}{12\pi} \left(\frac{1}{2} + \ln \frac{32\pi\mu}{g_{\text{eff}}^2 q_0} \right) + \frac{2^{2/3} (g_{\text{eff}} \mu)^{4/3} q_0^{5/3}}{3\sqrt{3}\pi^{2/3}} \left(1 + \frac{g_{\text{eff}}^2}{64} \right) \\
&\quad - \frac{8 \cdot 2^{1/3} (g_{\text{eff}} \mu)^{2/3} q_0^{7/3}}{9\sqrt{3}\pi^{4/3}} \left(1 - \frac{g_{\text{eff}}^2}{32} - \frac{g_{\text{eff}}^4}{2048} \right) + O(q_0^3 \ln q_0). \tag{3.3.32}
\end{aligned}$$

Another calculation shows that the correction to this result $\int N \delta D_1 / D_1^2 dq$ is already of order $O(q_0^{13/3})$. Also, using the second correction $\int N / D_2 dq$ gives the same result up to $O(q_0^3)$ so that we can now trust the $q_0^{5/3}$ and $q_0^{7/3}$ coefficients.

Just to give an impression of how the series would continue, we give the q_0^3 coefficient of the expansion (3.3.32)

$$\begin{aligned}
O(q_0^3 \ln q_0) &\rightarrow \frac{q_0^3}{12\pi^3} \left\{ \frac{896}{3} - 8\pi^2 + \frac{10g_{\text{eff}}^2}{3} - \frac{123g_{\text{eff}}^4}{320} - \frac{67g_{\text{eff}}^6}{12288} \right. \\
&\quad \left. - 2(\pi^2 - 16)\sqrt{\pi^2 - 4} \left(\pi - 2 \arctan \frac{2}{\sqrt{\pi^2 - 4}} \right) \right. \\
&\quad \left. + \left(32\pi^2 - \frac{512}{3} - \frac{g_{\text{eff}}^2 \pi^2}{12} + \frac{g_{\text{eff}}^4}{30} + \frac{g_{\text{eff}}^6}{3072} \right) \ln \frac{32\pi\mu}{g_{\text{eff}}^2 q_0} \right. \\
&\quad \left. - 8(3\pi^2 - 16) \ln \frac{1024\pi}{g_{\text{eff}}^4} \right\} + O(q_0^{11/3}). \tag{3.3.33}
\end{aligned}$$

Note that this expansion results from the terms explicitly given in equations (3.3.17) and (3.3.18). Including higher order contributions of q_0 and q in (3.3.17) will change the higher order coefficients of g_{eff} given here.

3.3.5 Pressure, entropy and specific heat

As before, we calculate pressure by integrating over q_0 and entropy and specific heat from derivatives thereof. We introduce the following abbreviations

$$\tilde{c}_{\ln} = \frac{3}{2} + \gamma_E - \frac{6}{\pi^2} \zeta'(2), \quad (3.3.34)$$

$$\tilde{c}_{8/3} = -\frac{2^{2/3}(g_{\text{eff}}\mu)^{4/3}\Gamma(\frac{8}{3})\zeta(\frac{8}{3})}{3\sqrt{3}\pi^{11/3}}\left(1 + \frac{g_{\text{eff}}^2}{64}\right), \quad (3.3.35)$$

$$\tilde{c}_{10/3} = \frac{8 \cdot 2^{1/3}(g_{\text{eff}}\mu)^{2/3}\Gamma(\frac{10}{3})\zeta(\frac{10}{3})}{9\sqrt{3}\pi^{13/3}}\left(1 - \frac{g_{\text{eff}}^2}{32} - \frac{g_{\text{eff}}^4}{2048}\right). \quad (3.3.36)$$

Note that inclusion of higher order terms in q_0 and q in equation (3.3.17) may change the higher order coefficients in g_{eff} given here. The leading order in g_{eff} for each coefficient is complete though. The results are

$$\begin{aligned} \frac{P_{T,n_b}}{N_g} &= \frac{g_{\text{eff}}^2 \mu^2 T^2}{72\pi^2} \left(\ln \frac{32\pi\mu}{g_{\text{eff}}^2 T} + \tilde{c}_{\ln} \right) \\ &+ \tilde{c}_{8/3} T^{8/3} + \tilde{c}_{10/3} T^{10/3} + O(T^4 \ln T), \end{aligned} \quad (3.3.37)$$

$$\begin{aligned} \frac{S_{T,n_b}}{N_g} &= \frac{g_{\text{eff}}^2 \mu^2 T}{36\pi^2} \left(\ln \frac{32\pi\mu}{g_{\text{eff}}^2 T} + \tilde{c}_{\ln} - \frac{1}{2} \right) \\ &+ \frac{8}{3} \tilde{c}_{8/3} T^{5/3} + \frac{10}{3} \tilde{c}_{10/3} T^{7/3} + O(T^3 \ln T), \end{aligned} \quad (3.3.38)$$

$$\begin{aligned} \frac{C_{V,T,n_b}}{N_g} &= \frac{g_{\text{eff}}^2 \mu^2 T}{36\pi^2} \left(\ln \frac{32\pi\mu}{g_{\text{eff}}^2 T} + \tilde{c}_{\ln} - \frac{3}{2} \right) \\ &+ \frac{40}{9} \tilde{c}_{8/3} T^{5/3} + \frac{70}{9} \tilde{c}_{10/3} T^{7/3} + O(T^3 \ln T). \end{aligned} \quad (3.3.39)$$

Figure 3.4 shows a comparison between a full numerical result and the series expansion for small T for the transverse n_b -part of the entropy in the large N_f limit. Clearly, the leading order contribution of the curves is accurately reproduced by the small- T expansion for different g_{eff}^2 of 1, 4, or 9 in a region $T/\mu \lesssim g_{\text{eff}}/(2\pi^2)$. This is also the region where the complete large- N_f result for the low-temperature entropy exceeds the ideal-gas value in figure 3.1.

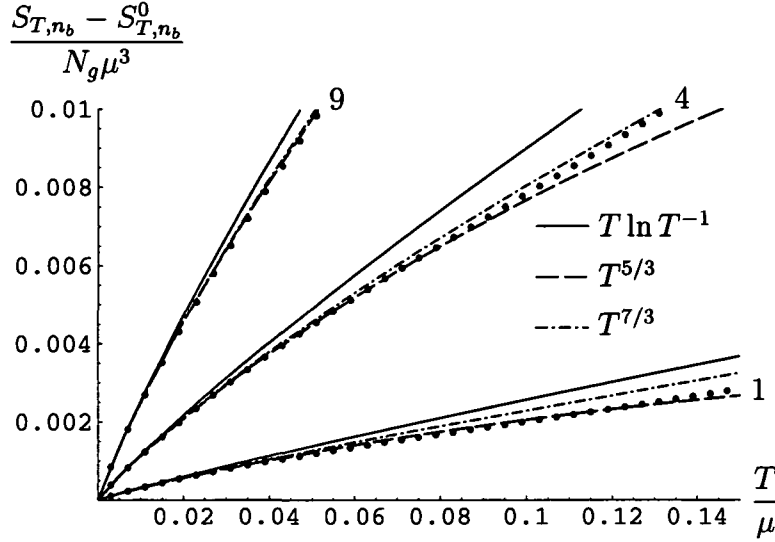


Figure 3.4: Transverse n_b -contribution to the interaction part of the low-temperature entropy density in the large- N_f limit for the three values $g_{\text{eff}}^2 = 1, 4, 9$. The heavy dots give the exact numerical results; the full, dashed, and dash-dotted lines correspond to our perturbative result up to and including the $T \ln T^{-1}$, $T^{5/3}$, and $T^{7/3}$ contributions.

3.3.6 Higher order corrections

We can now apply full temperature-dependence of the self energies and keep the renormalization scale $\bar{\mu}_{\text{MS}}$ explicitly in our formulae as in section 3.3.2. Our final result for the pressure reads as follows: Using the following dimensionless quantities

$$X = 1 + \frac{\pi^2 T^2}{3\mu^2}, \quad (3.3.40)$$

$$Y = 1 + \frac{g_{\text{eff}}^2 T^2}{36\mu^2} - \frac{g_{\text{eff}}^2}{6\pi^2} \ln \frac{2\mu}{\bar{\mu}_{\text{MS}}} \quad (3.3.41)$$

and the following abbreviations

$$\hat{c}_{\ln} = \frac{3}{2X} + \gamma_E - \frac{6}{\pi^2} \zeta'(2) + \ln \frac{Y}{X}, \quad (3.3.42)$$

$$\hat{c}_{8/3} = -\frac{2^{2/3} (g_{\text{eff}} \mu)^{4/3} \Gamma(\frac{8}{3}) \zeta(\frac{8}{3})}{3\sqrt{3} \pi^{11/3}} \left(1 + \frac{g_{\text{eff}}^2}{64Y}\right) \left(\frac{X}{Y}\right)^{2/3}, \quad (3.3.43)$$

$$\hat{c}_{10/3} = \frac{8 \cdot 2^{1/3} (g_{\text{eff}} \mu)^{2/3} \Gamma(\frac{10}{3}) \zeta(\frac{10}{3})}{9\sqrt{3} \pi^{13/3}} \left(1 - \frac{g_{\text{eff}}^2}{32Y} - \frac{g_{\text{eff}}^4}{2048Y^2}\right) \left(\frac{X}{Y}\right)^{1/3} \quad (3.3.44)$$

we can write the resulting pressure as

$$\begin{aligned} \frac{P_{T,n_b}}{N_g} &= \frac{g_{\text{eff}}^2 \mu^2 T^2}{72\pi^2} \left(\ln \frac{32\pi\mu}{g_{\text{eff}}^2 T} + \hat{c}_{\ln} \right) \frac{X}{Y} \\ &\quad + \hat{c}_{8/3} T^{8/3} + \hat{c}_{10/3} T^{10/3} + O(T^4 \ln T). \end{aligned} \quad (3.3.45)$$

The temperature corrections of X and Y only contribute to order $O(T^4)$ so that in a strict expansion sense, this expression reduces to (3.3.37) up to $\ln \bar{\mu}_{\text{MS}}$ terms.

Let us finally note that with the tools presented here, it seems a straightforward but tedious task to calculate the complete $O(T^4)$ contribution to the pressure (or the $O(T^3)$ contribution to entropy or specific heat). First, from the region II integral we expect a $T^3 \ln T$ contribution to the entropy as is suggested by the (still incomplete) contribution in equation (3.3.33). Then we have to take a careful look at regions I and III again, which could start contributing at this order. Finally, the temperature dependencies of the self-energies in equations (3.3.12) and (3.3.13) will also start contributing at this order via higher corrections similar to the X and Y functions above. In a full $O(T^3 \ln T)$ calculation of the entropy, all of these terms would have to be taken into account.

3.4 Longitudinal contribution

For the longitudinal “ n_b ”-part from our starting equation (2.2.13) we cannot neglect the real part of the self-energy Π_L compared to the vacuum self energy as we did in equation (3.3.2). We have to add a term

$$\text{Re}\Pi_L(q_0, q) = \frac{g_{\text{eff}}^2 \mu^2}{\pi^2} + O(q_0^2) + O(q^2) \quad (3.4.1)$$

which is absent in the transverse part. This contribution does not vanish for small q_0 and q and actually simplifies the calculation. This time we can expand the arc tangent for small argument $\arctan x \simeq x$ so that we can write

$$\text{Im} \ln(q^2 - q_0^2 + \Pi_L + \Pi_{\text{vac}}) \simeq \frac{g_{\text{eff}}^2 (4\mu^2 - q^2) q_0 \theta(\mu - \frac{q}{2}) / (8\pi q)}{q^2 + (g_{\text{eff}}^2 \mu^2) / \pi^2}. \quad (3.4.2)$$

Performing the q -integration as before we get

$$Q \equiv \int_0^{2\mu} dq q^2 \frac{g_{\text{eff}}^2 (4\mu^2 - q^2) q_0 / (8\pi q)}{q^2 + (g_{\text{eff}}^2 \mu^2) / \pi^2} \quad (3.4.3)$$

$$= \frac{g_{\text{eff}}^2 \mu^2}{4\pi} q_0 \left\{ \left(1 + \frac{g_{\text{eff}}^2}{4\pi^2} \right) \ln \left(1 + \frac{4\pi^2}{g_{\text{eff}}^2} \right) - 1 \right\}. \quad (3.4.4)$$

This integral can be performed exactly, so here and in the following step there is no need for any truncation so far. From this integral Q we get the

pressure as

$$\begin{aligned}\frac{P_{L,n_b}}{N_g} &= -\frac{4\pi}{8\pi^3} \int_0^\infty \frac{dq_0}{\pi} \frac{1}{e^{q_0/T} - 1} Q \\ &= -\frac{g_{\text{eff}}^2 \mu^2 T^2}{48\pi^2} \left\{ \left(1 + \frac{g_{\text{eff}}^2}{4\pi^2} \right) \ln \left(1 + \frac{4\pi^2}{g_{\text{eff}}^2} \right) - 1 \right\}\end{aligned}\quad (3.4.5)$$

and the entropy density as

$$\frac{S_{L,n_b}}{N_g} = -\frac{g_{\text{eff}}^2 \mu^2 T}{24\pi^2} \left\{ \left(1 + \frac{g_{\text{eff}}^2}{4\pi^2} \right) \ln \left(1 + \frac{4\pi^2}{g_{\text{eff}}^2} \right) - 1 \right\}.\quad (3.4.6)$$

The logarithm can be expanded giving

$$\frac{S_{L,n_b}}{N_g} = \frac{g_{\text{eff}}^2 \mu^2 T}{24\pi^2} \left(\ln \frac{g_{\text{eff}}^2}{4\pi^2} + 1 \right) + O(g_{\text{eff}}^4) + O(T^3).\quad (3.4.7)$$

3.5 Full result

Let us take together all the results we obtained so far. We have three main contributions to the entropy correction

$$S - S_0 = S_{\text{non-}n_b} + S_{T,n_b} + S_{L,n_b}\quad (3.5.1)$$

with $S_{\text{non-}n_b}$ from equation (3.2.2), S_{T,n_b} from (3.3.38), and S_{L,n_b} from (3.4.7). S_0 is the ideal-gas value per unit volume obtained from (2.5.1) and is given by

$$S_0 = \left(\frac{\partial P_0}{\partial T} \right)_{V,\mu} = NN_f \left(\frac{\mu^2}{3} T + \frac{7\pi^2}{45} T^3 \right) + N_g \frac{4\pi^2}{15} T^3.$$

Using the following abbreviations

$$c_{5/3} = -\frac{8 \cdot 2^{2/3} \Gamma(\frac{8}{3}) \zeta(\frac{8}{3})}{9\sqrt{3}\pi^{11/3}} (g_{\text{eff}} \mu)^{4/3},\quad (3.5.2)$$

$$c_{7/3} = \frac{80 \cdot 2^{1/3} \Gamma(\frac{10}{3}) \zeta(\frac{10}{3})}{27\sqrt{3}\pi^{13/3}} (g_{\text{eff}} \mu)^{2/3}\quad (3.5.3)$$

we can write the final result to the entropy correction as

$$\begin{aligned}\frac{S - S_0}{N_g} &= \frac{g_{\text{eff}}^2 \mu^2 T}{36\pi^2} \left(\ln \frac{4g_{\text{eff}} \mu}{\pi^2 T} - 2 + \gamma_E - \frac{6}{\pi^2} \zeta'(2) \right) \\ &\quad + c_{5/3} T^{5/3} + c_{7/3} T^{7/3} + O(T^3)\end{aligned}\quad (3.5.4)$$

and for the specific heat as

$$\begin{aligned}\frac{C_V - C_V^0}{N_g} &= \frac{g_{\text{eff}}^2 \mu^2 T}{36\pi^2} \left(\ln \frac{4g_{\text{eff}} \mu}{\pi^2 T} - 3 + \gamma_E - \frac{6}{\pi^2} \zeta'(2) \right) \\ &\quad + \frac{5}{3} c_{5/3} T^{5/3} + \frac{7}{3} c_{7/3} T^{7/3} + O(T^3)\end{aligned}\quad (3.5.5)$$

with the ideal-gas contribution of the specific heat as calculated in appendix C

$$C_V^0 = NN_f \left(\frac{\mu^2 T}{3} + \frac{7\pi^2 T^3}{15} - \frac{4\mu^2 T^3}{9 \left(\frac{T^2}{3} + \frac{\mu^2}{\pi^2} \right)} \right) + N_g \frac{4\pi^2 T^3}{15}. \quad (3.5.6)$$

3.5.1 Extension to full QED and QCD

Having calculated the large N_f result of entropy and specific heat, the natural question is how these results translate back to the full theory of QED or QCD. It turns out that for entropy and specific heat of QED and QCD all we calculated so far in the first few orders of $T \ll \mu$ is actually all there is.

In fact, our NLO expression for the pressure at large N_f (2.2.13) can be seen as the starting point for an expansion of small g but finite, smaller N_f in the regime $T/\mu \ll g$ with an error of order g^4 . This is because bosonic loop insertions that we could omit in the large N_f limit are also negligible in this regime to the order of interest. The pressure would then be given by

$$\begin{aligned} P = & NN_f \left(\frac{\mu^4}{12\pi^2} + \frac{\mu^2 T^2}{6} + \frac{7\pi^2 T^4}{180} \right) \\ & - N_g \int \frac{d^3 q}{(2\pi)^3} \int_0^\infty \frac{dq_0}{\pi} \\ & \times \left[2 \left(\left[n_b + \frac{1}{2} \right] \text{Im} \ln D_T^{-1} - \frac{1}{2} \text{Im} \ln D_{\text{vac}}^{-1} \right) \right. \\ & \left. + \left(\left[n_b + \frac{1}{2} \right] \text{Im} \ln \frac{D_L^{-1}}{q^2 - q_0^2} - \frac{1}{2} \text{Im} \ln \frac{D_{\text{vac}}^{-1}}{q^2 - q_0^2} \right) \right] \\ & + O(g^4 \mu^4), \quad (T/\mu \ll g) \end{aligned} \quad (3.5.7)$$

where $N = 3$, $N_g = 8$ for QCD, and both equal to one for QED. The temperature T is assumed to be the smallest mass scale in the problem. D_T and D_L are the spatially transverse and longitudinal gauge boson propagators at finite temperature T and (electron or quark) chemical potential μ obtained by Dyson-resumming one-loop fermion loops, and D_{vac} is the corresponding quantity at zero temperature and chemical potential, just as in equation (2.2.13). This expression is sufficient to obtain results up to (but not including) order T^4 in the pressure or to order T^3 in the entropy for the regime $T/\mu \ll g$. Since the fractional powers $T^{5/3}$ and $T^{7/3}$ are included in these bounds they indeed give the anomalous behavior also to full QED and QCD.

In order to obtain the anomalous terms through order $T^{7/3}$ one actually only needs the following terms of the real transverse part of the propagator

(3.3.17) where we only keep the lowest orders in q_0/q and q_0/μ

$$\begin{aligned} \text{Re } D_T^{-1} &= q^2 (1 + O(g_{\text{eff}}^2)) \\ &+ \left(\frac{g_{\text{eff}}^2 \mu^2}{\pi^2 q^2} - 1 + O(g_{\text{eff}}^2 q^0) + O(g_{\text{eff}}^2 q^2 / \mu^2) \right) q_0^2 \\ &+ O(g_{\text{eff}}^2 q_0^4). \end{aligned} \quad (3.5.8)$$

These are the necessary terms to give the same “low order front” as presented in equation (3.3.22).

For $T/\mu \ll g$ the anomalous contributions we calculated for the *pressure* are actually negligible compared to zero-temperature contributions $\sim g^4 \mu^4$ which we omitted in our starting formula (3.5.7) and which can be found for QED and QCD to order g^4 in references [72, 73]. However, when calculating the *entropy density* $\mathcal{S} = (\partial P / \partial T)_{V, \mu}$ or the *specific heat*, these terms drop out and we obtain the correct low temperature series expansions for QED and QCD by the results calculated above in equations (3.5.4) and (3.5.5).

A useful way of understanding the organization of the series expansion is to make explicit that T/μ is the smallest scale by writing $T/\mu \sim g_{\text{eff}}^{1+\delta}$ with $\delta > 0$. The terms in the expansion (3.5.4) then correspond to the orders $g_{\text{eff}}^{3+\delta} \ln(c/g_{\text{eff}})$, $g_{\text{eff}}^{3+(5/3)\delta}$, and $g_{\text{eff}}^{3+(7/3)\delta}$, respectively, with a truncation error of the order $g_{\text{eff}}^{3+3\delta}$. The expansion parameter in this low-temperature series is $T/(g_{\text{eff}} \mu)$, which is also the scaleless parameter appearing in the argument of the leading logarithm of (3.5.4) and (3.5.5), but interestingly only after the transverse and the longitudinal contributions have been added together. The combination $g_{\text{eff}} \mu$ is the scale of the Debye mass at high chemical potential, whose leading-order value is $m_D = g_{\text{eff}} \mu / \pi$. In fact, the calculation of the coefficients in (3.5.4) required keeping the leading-order “hard-dense-loop” (HDL) part of the gauge boson propagator [116, 117], in particular the dynamic screening in (3.3.18), but also a HDL correction to the real part of the transverse self energy in (3.5.8). The above calculation is therefore in a certain sense another application of HDL resummation [117], which thus turns out to be necessary also for a perturbative treatment of the low-temperature regime $T/\mu \ll g$.

Summarizing, we have found that for the entropy and the specific heat (but not for the pressure) the expressions given in (3.5.4) and (3.5.5) already give the leading order contribution for full QED and QCD in a regime of $T/\mu \ll g$ with $g_{\text{eff}}^2 = g^2 N_f$ for QED and $g_{\text{eff}}^2 = g^2 N_f / 2$ for QCD.

3.6 Discussion

3.6.1 Specific heat

The specific heat $C_V \equiv C_V / V$ is an important quantity for potential phenomenological applications in astrophysical systems. Figure 3.5 shows the

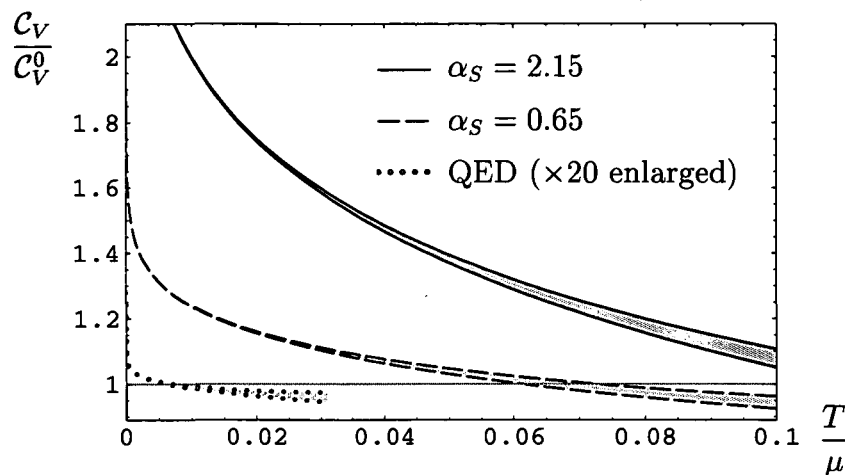


Figure 3.5: The perturbative result for the specific heat, normalized to the ideal-gas value, to order $T^{5/3}$ and $T^{7/3}$ (lower and upper curves, respectively) for two particular values of α_s in two-flavor QCD (chosen for comparability to reference [118]) and $g_{\text{eff}} \approx 0.303$ for QED. The deviation of the QED result from the ideal-gas value is enlarged by a factor of 20, and the plot terminates where the expansion parameter $(\pi^2 T)/(g_{\text{eff}} \mu) \approx 1$.

ratio of C_V as given by (3.5.5) to the ideal-gas value C_V^0 for QCD with two massless quark flavors. We compute the ratio for two values for α_s which have been used also in reference [118] and which correspond to one-loop running couplings with renormalization point 0.5 GeV (full line) and 1 GeV (dashed line). The upper limit of the shaded bands give the result to order $T^{5/3}$ and the lower band to order $T^{7/3}$. Alternatively we can think of the two QCD bands as roughly corresponding to QCD with a quark chemical potential of 0.5 GeV and the total variation corresponding to different renormalization schemes with minimal subtraction scale varied between μ and 2μ . The critical temperature for the color superconducting phase transition may be anywhere between 6 and 60 MeV [15], so the range $T/\mu \geq 0.012$ in figure 3.5 might correspond to normal quark matter. We will explore this region in more detail in the next section, looking at the anomalous correction at the critical temperature of color superconductivity. While it is certainly questionable to apply perturbative results for $\alpha_s \gtrsim 0.65$, figure 3.5 suggests that the anomalous feature of an excess of the specific heat over its ideal-gas value may possibly come into play in astrophysical situations, in particular in the cooling of (proto-)neutron stars [16, 119, 120]. The anomalous correction $C_V/C_V^0 > 1$ should be compared to the ordinary perturbative estimate for C_V/C_V^0 based on the well-known [20] exchange term $\propto g^2$ (which requires $T/\mu \gg g$). The latter would predict $C_V/C_V^0 \lesssim 0.6$ for $\alpha_s \gtrsim 0.65$.

In figure 3.5 we also show the effect on QED, where $g_{\text{eff}} = \sqrt{4\pi\alpha} \approx$

$\sqrt{4\pi/137} \approx 0.303$. Here the range of temperature, where the specific heat exceeds the ideal-gas value, and the deviations from the latter, are much smaller (the deviations from the ideal-gas value have been enlarged by a factor of 20 in figure 3.5 to make them more visible). As mentioned, the effect of the anomalous contribution to the specific heat remains small in QED, but it might play a noticeable role in the thermodynamics of a normal quark matter component of neutron or proto-neutron stars.

3.6.2 Effect near the CSC critical temperature

It has been argued recently that color superconductivity (CSC) will dominate dense quark matter long before non-Fermi liquid behavior becomes effective [109, 110]. The argument is based on simple dimensional analysis of the energy scale, which for the 2SC color superconducting gap is given by [109, 121, 122, 123, 124, 125, 126]

$$E = bb'_0 \mu g^{-5} \exp(-c/g), \quad (3.6.1)$$

$$b = 512\pi^4 \left(\frac{2}{N_f}\right)^{5/2}, \quad b'_0 = \exp\left(-\frac{4+\pi^2}{8}\right), \quad c = \sqrt{\frac{6N_c}{N_c+1}}\pi^2 \quad (3.6.2)$$

and for non-Fermi liquid effects is given by

$$\bar{E} = \bar{b}\mu g \exp(-x\bar{c}/g^2), \quad (3.6.3)$$

$$\bar{b} = \frac{4}{\pi^2} \sqrt{\frac{N_f}{2}} \exp\left(-3 + \gamma_E - \frac{6}{\pi^2} \zeta'(2)\right), \quad \bar{c} = \frac{24\pi^2 N_c}{N_g}. \quad (3.6.4)$$

This NFL result is obtained from equating x times the coefficient of the leading order T contribution to the $T \ln T^{-1}$ coefficient from the NFL entropy correction (3.5.4) (for the specific heat (3.5.5), \bar{b} gets another factor e). The parameter x gives the kind of NFL correction: for $x < 1$, \bar{E} gives the energy scale for corrections of the order x ; for $x \sim 1$ we get into non-perturbative NFL correction regime. Note that the pre-exponential factor b'_0 in the color superconducting energy gap (3.6.1) stems from non-Fermi liquid behavior through the quark-selfenergy [127, 124, 128].

In references [109, 110], the energy scale for color superconductivity is related to the energy scale where NFL effects get nonperturbative. For a 2SC system, the energy scale of the critical temperature of the color superconductor T_c is related to the gap energy (3.6.1) by $T_c = Ee^{\gamma_E}/\pi$ [126]. It is clear that for arbitrarily small couplings g the critical energy $T_c \propto E$ will be larger than the NFL energy \bar{E} . Thus, nonperturbative NFL effects will not play a role because color superconductivity will set in already at higher temperatures.

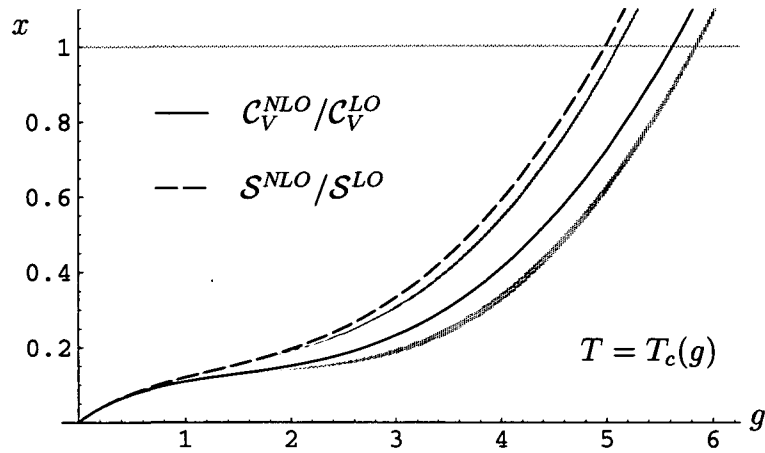


Figure 3.6: Non-Fermi liquid correction at the critical temperature T_c of the color superconductor as a function of the coupling g for entropy and specific heat. The factor x is the rate of the next-to-leading order contribution $\propto T \ln T^{-1}$ to the leading order (Stefan-Boltzmann) contribution $\propto T$. The shaded bands give the result including $T^{5/3}$ (lower limit of band) and $T^{7/3}$ (upper limit of band) contributions in the NLO expression. For $g \lesssim 5$, non-Fermi liquid corrections are perturbative ($x < 1$) and the size of correction is given by x for the specific heat and the entropy. For $g \gtrsim 5$ nonperturbative NFL contributions cannot be neglected. For asymptotically small $g \rightarrow 0$ the correction is linear $x = g/(3\sqrt{2})$.

On the other hand, if we are interested in when *perturbative* corrections cannot be neglected, it boils down to a choice of the size of corrections we wish to regard, entering via the parameter x : Indeed, if we want to study NFL corrections of the order of g by setting $x = g$ in (3.6.3), we find the same parametrical energy dependence $\propto \exp(-\bar{c}/g)$ for T_c and \bar{E} . Here of course the magnitudes of c , \bar{c} , and the large exponential prefactor b start to play a role and one has to be more careful. Solving for the correction in $T_c = \bar{E}$ gives

$$x = g \frac{c}{\bar{c}} + \frac{g^2}{\bar{c}} \ln \frac{\bar{b}g^6}{bb_0 e^{\gamma_E/\pi}}. \quad (3.6.5)$$

From another point of view, this is just the correction $x = C_V^{\text{NLO}}(T_c)/C_V^{\text{LO}}(T_c)$ evaluated at the critical temperature $T_c(g) = T_c(E(g))$ for each coupling g for the NLO contribution $\propto T \ln T^{-1}$. Figure 3.6 shows the dependence of the size of the correction x on the coupling g for the specific heat and the entropy. According to this plot, below $g \lesssim 5$ we are in the perturbative NFL regime where our formulae (3.5.4) and (3.5.5) are well applicable, as can be seen from the shaded bands in the plots which show the result including $T^{5/3}$ and $T^{7/3}$ contributions. These are the biggest corrections that we expect to see from perturbative non-Fermi liquids because for higher temperatures $T > T_c$ the NLO corrections get smaller, and for smaller temperatures $T < T_c$ we are in the color superconducting phase. Since the color superconductor gap equation (3.6.1) might not be valid in this coupling range anymore, this plot should be treated with care. The only purpose of this plot is to show that from the gap energy given above, one can not readily derive that perturbative NFL effects could be neglected. Indeed, the energy gap formula might break down for g as low as $g \gtrsim 0.8$ [129].

For small g the correction decreases linearly as $x = g/(3\sqrt{2})$. This is larger than naively expected from the perturbative NLO NFL term $\propto g^2 \ln g$ and an effect of the exponential decrease of the critical temperature T_c with $\exp(-c/g)$.

Chapter 4

Summary and Outlook

In this thesis we calculated pressure, entropy, and specific heat of the high-temperature and high-density quark-gluon plasma in the limit of a large number of quark flavors. The theoretical understanding of the quark-gluon plasma is of current interest, as existing heavy-ion colliders start to reach energy densities that allow for observation of this new state of matter. In the low-temperature but high-density region, the quark-gluon plasma features non-Fermi-liquid behavior with anomalous contributions to thermodynamic quantities. In this thesis we derived for the first time in a detailed calculation the low-temperature series beyond leading-log accuracy and including anomalous fractional powers.

We have focused on large N_f as the theoretical limit in which we let the number of flavors go to $N_f \rightarrow \infty$ and the coupling $g \rightarrow 0$ such that the effective coupling $g_{\text{eff}} \propto g^2 N_f$ stays of order $O(1)$. We argued that this theory is of particular interest because it is exactly solvable up to next-to-leading order (NLO) in the $1/N_f$ expansion and thus provides an ideal test for resummation schemes that try to overcome the poor convergence properties of strict perturbative expansions of thermodynamic quantities like the pressure. The NLO large N_f limit technically corresponds to resumming a boson loop with any number of fermion insertions which can be resummed by the Schwinger-Dyson method. Although we cannot give a closed form of the NLO pressure, we can numerically evaluate the result with a small error introduced by a cutoff due to a Landau singularity in the coupling. Given that the renormalization scale dependence is exact to the order of interest, we have an exact result for all couplings and renormalization scales. We calculated the pressure for the whole range of temperature and chemical potentials where the error introduced by the cutoff is negligible numerically. For small values of the coupling, our numerics turned out to be sufficiently accurate to allow comparison to perturbation theory and to extract coefficients in the perturbative expansion of the pressure that had not been calculated analytically before. This table shows a summary of our predictions:

Coefficient	Predicted value	Equation	Confirmed
$P: C_6$	+20(2)	(2.5.16)	not yet
$\chi: C_6$	-4.55(9)	(2.5.19)	not yet
$\partial^2 \chi / \partial \mu^2: C_4$	-7.02(3)	(2.5.20)	-6.9986997..[65]
$P_{T=0}: C_{6,\ln}$	+3.18(5)	(2.5.24)	not yet
$P_{T=0}: C_6$	-3.4(3)	(2.5.24)	not yet

Since the original publication of the predicted values in [68] so far only one has been confirmed by an analytic calculation. The other four constants still need to be confirmed by means of an analytic calculation.

For larger values of the coupling, we studied the convergence properties of perturbative series including renormalization scale dependence and the FAC (fastest apparent convergence) scale applied to m_E^2 (FAC-m) and to g_E^2 (FAC-g) at zero chemical potential. The latter choice leads to quite accurate results up to $g_{\text{eff}}^2 \sim 9$. We further studied the scaling from pressure at small chemical potentials to higher chemical potentials and noticed an unexpected breakdown at about $\mu \approx \pi T$. This might indicate a generic obstruction for extrapolating lattice data from $\mu \ll T$ to $\mu \gg T$.

In the second part of the thesis we examined the region of small T and large μ more closely and found non-Fermi-liquid behavior in an anomalous series expansion of the entropy and specific heat for small temperatures involving a leading $T \ln T^{-1}$ term and fractional powers $T^{(2n+3)/3}$. We gave a brief overview of the theoretical picture from the ideal gas to the non-Fermi liquid. While the classical ideal gas shows no temperature dependence in the specific heat, the ideal Fermi gas and the Landau-Fermi liquid show a linear dependence on temperature in the specific heat. Only the introduction of long-range interactions changes this behavior qualitatively: The leading $T \ln T^{-1}$ contribution in the entropy or the specific heat cannot be explained by classical Landau-Fermi liquid theory anymore and the system is therefore called a non-Fermi liquid. In our case long-range interactions are introduced by transverse gauge boson interactions which are only weakly screened at low frequencies q_0 and not screened at all in the static limit of $q_0 \rightarrow 0$. We showed that the anomalous leading logarithmic contribution leads to a range where the entropy exceeds the ideal gas value of the entropy for small temperatures. We calculated the leading log coefficient in a straightforward way, confirming a result by reference [103]. We further completed the argument of the leading logarithm and went beyond the leading order to find anomalous contributions to order $T^{5/3}$ and $T^{7/3}$ in the entropy and the specific heat. These contributions indeed come from transverse “non- n_b ” parts (i.e. contributions in the original expression of the pressure that do not contain a factor of the bosonic distribution function n_b) and we calculated them by spotting a “low order front” in the denominator of the pressure integral which we can factor into a sixth order and a fourth order polynomial, hiding higher order terms in the frequency q_0 in a correction term. The final result for the

entropy and the specific heat turns out to be readily applicable to full QED and full QCD in a range where $T/\mu \ll g_{\text{eff}}$. For the entropy we found the result

$$S = N_c N_f \frac{\mu^2}{3} T + \frac{g_{\text{eff}}^2 N_g \mu^2 T}{36\pi^2} \left(\ln \frac{4g_{\text{eff}}\mu}{\pi^2 T} - 2 + \gamma_E - \frac{6}{\pi^2} \zeta'(2) \right) + N_g c_{5/3} T^{5/3} + N_g c_{7/3} T^{7/3} + O(T^3) \quad (4.0.1)$$

from which the specific heat can be derived as

$$C_V = N_c N_f \frac{\mu^2 T}{3} + \frac{g_{\text{eff}}^2 N_g \mu^2 T}{36\pi^2} \left(\ln \frac{4g_{\text{eff}}\mu}{\pi^2 T} - 3 + \gamma_E - \frac{6}{\pi^2} \zeta'(2) \right) + N_g \frac{5}{3} c_{5/3} T^{5/3} + N_g \frac{7}{3} c_{7/3} T^{7/3} + O(T^3) \quad (4.0.2)$$

with

$$c_{5/3} = -\frac{8 \cdot 2^{2/3} \Gamma(\frac{8}{3}) \zeta(\frac{8}{3})}{9\sqrt{3}\pi^{11/3}} (g_{\text{eff}}\mu)^{4/3}, \quad (4.0.3)$$

$$c_{7/3} = \frac{80 \cdot 2^{1/3} \Gamma(\frac{10}{3}) \zeta(\frac{10}{3})}{27\sqrt{3}\pi^{13/3}} (g_{\text{eff}}\mu)^{2/3}. \quad (4.0.4)$$

We pointed out a possible implication in astrophysical situations, namely the cooling rate of proto-neutron stars, and calculated the effect of the non-Fermi-liquid contributions near the critical temperature of color-superconductivity. We found that while *non-perturbative* non-Fermi-liquid behavior might play a role for $g \gtrsim 5$, there are non-negligible *perturbative* non-Fermi-liquid effects for $g \sim O(1)$ of the order of 10% – 20% compared to the leading order contribution, and that perturbative non-Fermi-liquid effects are of the order of $g/(3\sqrt{2})$ for small g .

In the appendix we calculated the Feynman rules trying to match different conventions in the literature, gave a derivation of the specific heat at next-to-leading order and presented the zero-temperature limits of the boson self-energy with one fermion insertion. Finally, we provided a *Mathematica* extension that is necessary in order to correctly calculate the fractional power series. This calculation involves a series expansion that depends crucially on assumptions about the variables involved that standard symbolic manipulation programs implicitly ignore.

Possible extensions to the work presented here first of all include improvement of the non-Fermi-liquid series expansion. Within the large N_f limit, the T^3 contribution might be of special interest. With the tools presented here it seems straightforward to calculate it, but one has to take into account that disproportionately more contributions have to be considered at this order. Apart from higher orders in T , the series expansion could also be pushed towards higher orders in the coupling g_{eff} .

The analytic treatment of non-Fermi-liquid behavior presented in this work paves the way for various possible applications: One could try and repeat the calculation of neutron star cooling rates with the improved series expansion presented here; one could study the interplay of the effects of the non-Fermi-liquid contributions with color superconductivity; finally, one could extend the analysis to the nonrelativistic case (i.e. include fermion masses) which may be of interest in view of the recent experimental findings [17] in condensed matter physics.

Appendix A

Abbreviations

2PI	2 Particle Irreducible
2SC	2-Flavor Color Superconductor
CFL	Color-Flavor Locked
CSC	Color Superconductivity
DR	Dimensional Reduction
FAC	Fastest Apparent Convergence
HDL	Hard Dense Loop
HTL	Hard Thermal Loop
ITF	Imaginary Time Formalism
Large N_f	Large number of Quark Flavors
LHC	Large Hadron Collider
LO	Leading Order
NLO	Next-to-Leading Order
PMS	Principle of Minimal Sensitivity
QCD	Quantum Chromodynamics
QED	Quantum Electrodynamics
QGP	Quark Gluon Plasma
RHIC	Relativistic Heavy Ion Collider
RTF	Real Time Formalism
SPS	Super Proton Synchrotron

Appendix B

QCD Feynman rules

B.1 Motivation for a unifying approach

The theoretical description of the quark-gluon plasma is based on quantum field theory (QFT). Its application to a 'Many-Body Problem' using tools from statistical mechanics started in the late 1950s. In the mean-time the theoretical tools improved dramatically, for example by reorganized perturbation theory in the 1990's, and it is no wonder that a plethora of conventions and notations have been invented so far. The drawback of this kind of scientific independence is that it renders comparison between different authors often a tedious task. In this chapter we will try to find a formal "common denominator" for modern literature on thermal field theory, whilst providing a brief introduction to Feynman rules and some basic diagrams we will be using later on.

We will use the Imaginary Time Formalism (ITF) for the statistical description of the quantum field. This formalism is based on the observation that the statistical density matrix for a system $\rho(\beta) = \exp(-\beta H)$ with inverse temperature $\beta = 1/T$ looks similar to a quantum mechanical time evolution operator $\exp(iHt)$ if one uses formally imaginary time $t \rightarrow i\beta$. It is therefore tempting to simply rotate QFT formulae from zero temperature, as taught in modern textbooks like Peskin and Schroeder [130], in the complex time plane to finite temperature in ITF. Unfortunately, naive comparisons quickly result in missing factors of -1 or i , so that it seems worth to invest some effort in locating the sources of discrepancies. In the end we will see that only two factors determine the sign discrepancies for Feynman rules between various conventions, namely the sign in the generating functional, which we will call \tilde{s} , and a factor in the covariant derivative \tilde{g} .

Let us start by looking at the gluon propagator, which basically resembles the photon propagator up to group factors. It can be found in various

definitions in the literature:

$$\tilde{D}_F^{\mu\nu}(k) = \frac{-i}{k^2 + i\epsilon} \left(g^{\mu\nu} - (1 - \xi) \frac{k^\mu k^\nu}{k^2} \right), \quad (\text{B.1.1})$$

$$\begin{aligned} G_{\mu\nu}^0(k) &= -g_{\mu\nu} \Delta(k) + (\lambda - 1) k_\mu k_\nu \Delta^2(k) \\ &= -g_{\mu\nu} \frac{-1}{k^2} + (\lambda - 1) k_\mu k_\nu \frac{+1}{k^4}, \end{aligned} \quad (\text{B.1.2})$$

$$D_{\mu\nu}^F = \frac{1}{Q^2} \left(\delta_{\mu\nu} - (1 - \xi) \frac{Q_\mu Q_\nu}{Q^2} \right). \quad (\text{B.1.3})$$

Equation (B.1.1) for $T = 0$ can be found in Peskin and Schroeder [130], p. 297, equation (B.1.2) applies to the ITF and is the definition of Blaizot and Iancu [131], p. 176, while equation (B.1.3) is the ITF definition according to Le Bellac [132], p. 107. The first two equations make use of the Minkowski metric $g_{\mu\nu} = \text{diag}(1, -1, -1, -1)$ while the third equation does not. We can unify the first two equations, using the following “generic” equation:

$$\tilde{G}^{\mu\nu}(k) = -\tilde{\chi} \left(g^{\mu\nu} \frac{1}{k^2} - (1 - \xi) \frac{k^\mu k^\nu}{k^4} \right) \quad (\text{B.1.4})$$

where we introduced a “generic constant” $\tilde{\chi}$ whose value resembles different definitions. Here we can identify $\tilde{\chi} = i$ for the $T = 0$ case in equation (B.1.1) and $\tilde{\chi} = -1$ for the ITF in equation (B.1.2). We cannot easily identify equation (B.1.3) with this method, though, because it uses Euclidean metric. We will see later how we can convert results obtained in this work from Minkowski metric to Euclidean metric.

Another example of using different definitions is the covariant derivative. In [130], p. 490, it is defined as $D_\mu = \partial_\mu - igA_\mu^a t^a$, while [131], p. 171, defines the covariant derivative with a positive sign $\tilde{D}_\mu = \partial_\mu + igA_\mu^a t^a$. Again these two definitions can be easily unified, using the generic equation:

$$D_\mu \equiv \partial_\mu + \tilde{g} g A_\mu^a t^a \quad (\text{B.1.5})$$

with $\tilde{g} = -i$ in the first case and $\tilde{g} = +i$ in the second. Itzykson and Zuber [133], p. 584, use yet another convention $\tilde{g} = -1$.

Yet another striking difference concerns the definition of the generating functional. While [130], p. 290, defines the generating functional for $T = 0$ as

$$Z[J] = \int \mathcal{D}\phi \exp \left[i \int d^4x [\mathcal{L} + J(x)\phi(x)] \right] \quad (\text{B.1.6})$$

we can find the following definition for ITF in [131], p. 28,

$$Z[j] = \mathcal{N} \int_{\phi(0)=\phi(\beta)} \mathcal{D}(\phi) \exp \left\{ - \int_0^\beta d\tau \int d^3x (\mathcal{L}_E(x) - j(x)\phi(x)) \right\} \quad (\text{B.1.7})$$

where the Euclidean Lagrangian \mathcal{L}_E basically equals the negative Minkowski Lagrangian $-\mathcal{L}$ in the common Minkowski metric. Defining a “generic” position-integral as

$$\int d^4\tilde{x} \equiv \begin{cases} \int d^4x & \text{for } T = 0 \\ \int_0^\beta d\tau \int d^3\vec{x} & \text{for ITF} \end{cases} \quad (\text{B.1.8})$$

we can again combine the two equations to form the generic equation

$$Z[j] \equiv \mathcal{N} \int \mathcal{D}\phi \exp \left[\tilde{s} \int d^4\tilde{x} \left(\mathcal{L} + \tilde{j}j(x)\phi(x) \right) \right] \quad (\text{B.1.9})$$

with $\tilde{s} = i$, $\tilde{j} = 1$ for $T = 0$, and $\tilde{s} = 1$, $\tilde{j} = 1$ for ITF.

What we shall find in the following is that the Feynman rules can be derived basically from these three generic definitions presented here, namely the definition of the propagator (B.1.4), the definition of the covariant derivative (B.1.5) and the definition of the generating functional (B.1.9). From these definitions we can derive the QCD Feynman rules. In the end the Feynman rules will in a simple way depend on the constants $\tilde{\chi}$, \tilde{g} , and \tilde{s} .

B.2 Derivation of Feynman rules

In the following we will present the key equations that define constants like $\tilde{\chi}$, \tilde{g} , or \tilde{s} . The aim is to unify the Feynman rules for $T = 0$ and the Imaginary Time Formalism (ITF). We use natural units $\hbar = c = 1$.

Metric

Equations in both formalisms can be formulated using the Minkowski metric

$$g_{\mu\nu} = g^{\mu\nu} = \text{diag}(1, -1, -1, -1). \quad (\text{B.2.1})$$

In the case of the imaginary-time formalism we adopt the definition of Blaizot and Iancu [131] and write $x^\mu = (x_0, \mathbf{x}) = (t_0 - i\tau, \mathbf{x})$ with $0 \leq \tau \leq \beta$, with the inverse temperature $\beta = T^{-1}$, and $k^\mu = (k_0, \mathbf{k}) = (i\omega_n, \mathbf{k})$ with $\omega_n = 2n\pi T$ for bosonic fields or $\omega_n = (2n + 1)\pi T$ for fermionic fields. This definition has the advantage that the scalar product of position and momentum vector still has the form of the Minkowski metric:

$$k_\mu x^\mu = k_0 x_0 - \mathbf{k}\mathbf{x} = \omega_n \tau - \mathbf{k}\mathbf{x}. \quad (\text{B.2.2})$$

We define the generic position integral to be

$$\int d^4\tilde{x} \equiv \begin{cases} \int d^4x & \text{for } T = 0 \\ \int_0^\beta d\tau \int d^3\vec{x} & \text{for ITF.} \end{cases} \quad (\text{B.2.3})$$

Analogous “generic” definitions can be given for the position integral and the Dirac δ -function.

Lagrangian

In all textbooks compared in this paper, the Lagrangian takes the following form:

$$\mathcal{L} = -\frac{1}{4}F_{\mu\nu}^a F^{\mu\nu a} + \bar{\psi}_i (i\mathcal{D} - m)_{ij} \psi_j. \quad (\text{B.2.4})$$

The covariant derivative $\mathcal{D} = \gamma^\mu D_\mu$ is defined as

$$D_\mu \equiv \partial_\mu + \tilde{g}g A_\mu^a t^a \quad (\text{B.2.5})$$

with $\tilde{g} = i, -1$, or $-i$. We use the commutation relation of the generators t_a of the Lie algebra of the gauge group in the fundamental representation

$$[t^a, t^b] = i f^{abc} t^c \quad (\text{B.2.6})$$

where f^{abc} are the structure constants of the group. The commutator of the covariant derivative

$$[D_\mu, D_\nu] = \tilde{g}g \left(\partial_\mu A_\nu^a - \partial_\nu A_\mu^a + i\tilde{g}g f^{abc} A_\mu^b A_\nu^c \right) t^a \equiv \tilde{g}g F_{\mu\nu}^a t^a \quad (\text{B.2.7})$$

defines the field strength tensor $F_{\mu\nu}^a$. The adjoint representation is given by $(t_G^b)_{ac} = i f^{abc}$. In this representation the covariant derivative is given by

$$(D_\mu)_{ac} = \partial_\mu \delta_{ac} + i\tilde{g}g A_\mu^b f^{abc}. \quad (\text{B.2.8})$$

The generating functional for gluons can be written as

$$Z[j] \equiv \mathcal{N} \int [\mathcal{D}A^\mu] \exp \left[\tilde{s} \int d^4\tilde{x} \left(\mathcal{L} + \tilde{j} j^{\nu a}(x) A_\nu^a(x) \right) \right] \quad (\text{B.2.9})$$

with $\tilde{s} = i$ for $T = 0$ and $\tilde{s} = -1$ for imaginary time formalism. We usually find $\tilde{j} = 1$ in both cases. For the quarks which are fermions we have to consider two anticommuting fields and the generating functional takes the form

$$Z[\tilde{\eta}, \eta] \equiv \mathcal{N} \int \mathcal{D}\bar{\psi} \mathcal{D}\psi \exp \left[\tilde{s} \int d^4\tilde{x} \left(\mathcal{L} + \tilde{\eta} \tilde{\eta}_i(x) \psi_i(x) + \tilde{\eta} \bar{\psi}_i(x) \eta_i(x) \right) \right] \quad (\text{B.2.10})$$

with $\tilde{\eta} = 1$. For ghost fields there is a similar generating functional.

Propagators

Starting from the generating functional (B.2.9) we can write the two-point correlation function as

$$\begin{aligned} \langle 0 | T A_\mu^a(x_1) A_\nu^b(x_2) | 0 \rangle &\equiv \frac{\mathcal{N}}{Z[0]} \int [\mathcal{D}A^\alpha] A_\mu^a(x_1) A_\nu^b(x_2) \exp \left[\tilde{s} \int d^4\tilde{x} \mathcal{L} \right] \\ &= \frac{1}{Z[0]} \frac{\delta^2 Z[j]}{(\tilde{s} \tilde{j} \delta j^{\mu a}(x_1)) (\tilde{s} \tilde{j} \delta j^{\nu b}(x_2))} \Bigg|_{j=0} \end{aligned} \quad (\text{B.2.11})$$

It is interesting to see that the last line is actually independent of $\tilde{\chi}$ and thus independent of our choice of defining the propagator $G_{\mu\nu}^{ab}(x)$. It merely depends on the definition of the generating functional (B.2.9).

For fermions we can derive the propagator in a similar way starting from the generating functional equation (B.2.10). Again, we can shift the fermion field by introducing the fermionic Green's function $S_F^{ij}(x-y)$ which satisfies

$$(i\not{p} - m) S_F^{ij}(x-y) \equiv \tilde{\sigma}\delta^{(4)}(x-y)\delta^{ij}\mathbb{1}_{4\times 4} \quad (\text{B.2.18})$$

with $\mathbb{1}_{4\times 4}$ being the unit matrix in the space of the anticommuting γ -matrices and $\tilde{\sigma}$ a generic constant. Similarly as above, we can write the two-point correlation function of two fermionic fields as

$$\langle 0|T\psi^i(x_1)\bar{\psi}^j(x_2)|0\rangle = \frac{-1}{\tilde{\sigma}} S_F^{ij}(x-y) \quad (\text{B.2.19})$$

and we find for the propagator used in the Feynman rules

$$\begin{aligned} \begin{array}{c} i \xrightarrow{\hspace{2cm}} j \\ \xrightarrow[p]{\hspace{1cm}} \end{array} &= \frac{-1}{\tilde{\sigma}} \tilde{S}_F^{ij}(p) \\ &= \frac{-1}{\tilde{\sigma}} \frac{1}{\not{p} - m} \delta^{ij} = \frac{-1}{\tilde{\sigma}} \frac{\not{p} + m}{p^2 - m^2 + i\epsilon} \delta^{ij}. \end{aligned} \quad (\text{B.2.20})$$

Finally we have similar results for the ghost field. The ghost Green's function satisfies

$$(-\partial^2\delta^{ab}) G_{gh}^{bc}(x-y) \equiv \tilde{c}\delta^{ac}\delta^{(4)}(x-y) \quad (\text{B.2.21})$$

with the generic constant \tilde{c} . This Green's function gives the two-point correlation function

$$\langle 0|Tc^a(x_1)\bar{c}^b(x_2)|0\rangle = \frac{-1}{\tilde{c}} G_{gh}^{ab}(x_1-x_2) \quad (\text{B.2.22})$$

and the ghost propagator for the Feynman rules

$$\begin{array}{c} a \xrightarrow{\hspace{2cm}} b \\ \xrightarrow[k]{\hspace{1cm}} \end{array} = \frac{-1}{\tilde{c}} \tilde{G}_{gh}^{ab}(k) = \frac{-1}{\tilde{c}} \frac{\delta^{ab}}{k^2}. \quad (\text{B.2.23})$$

Vertices

We use the field strength tensor from equation (B.2.7)

$$F_{\mu\nu}^a = \partial_\mu A_\nu^a - \partial_\nu A_\mu^a + i\tilde{g}gf^{abc}A_\mu^b A_\nu^c \quad (\text{B.2.24})$$

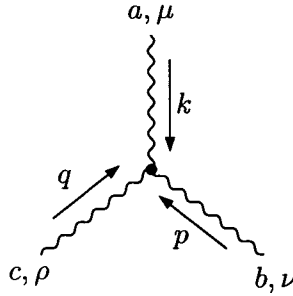
to calculate the expression we need for the Lagrangian (B.2.4)

$$\begin{aligned} \mathcal{L}_{gluon} = -\frac{1}{4}F_{\mu\nu}^a F^{\mu\nu a} &= -\frac{1}{2}(\partial_\mu A_\nu^a \partial^\mu A^{\nu a} - \partial_\mu A_\nu^a \partial^\nu A^{\mu a}) \quad (\text{B.2.25}) \\ &\quad -i\partial_\mu A_\nu^a \tilde{g} g f^{abc} A^{\mu b} A^{\nu c} \\ &\quad +\frac{1}{4}\tilde{g}^2 g^2 f^{abc} f^{ade} A_\mu^b A_\nu^c A^{\mu d} A^{\nu e}. \end{aligned}$$

The first line in equation (B.2.25) gave the gluon propagator (B.2.12). The following two lines can be treated as small perturbations with the order parameter g and contribute to the Feynman rules as 3-boson vertex (second line) and 4-boson vertex (third line). We can calculate the 3-boson vertex for example by calculating the 3-point function

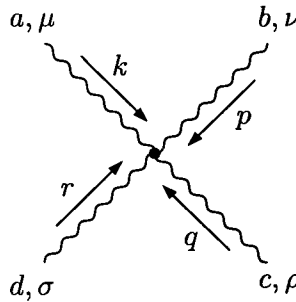
$$\begin{aligned} \langle \Omega | T A_\mu^a(x) A_\nu^b(y) A_\rho^c(z) | \Omega \rangle &= \langle 0 | AAA \exp(\tilde{s} \int d^4\tilde{x} (\partial A \tilde{g} g f AA)) | 0 \rangle \quad (\text{B.2.26}) \\ &= \langle 0 | AAA | 0 \rangle + \tilde{s} \tilde{g} g f \langle 0 | AAA \int (\partial A) AA | 0 \rangle + \dots \end{aligned}$$

and applying the Wick theorem. After some careful calculation we get for the 3-boson vertex



$$= (\tilde{s} \tilde{g}) g f^{abc} (g^{\mu\nu} (k-p)^\rho + g^{\nu\rho} (p-q)^\mu + g^{\rho\mu} (q-k)^\nu) \quad (\text{B.2.27})$$

where we use the short notation $(k-p)^\rho \equiv k^\rho - p^\rho$. For the 4-boson vertex we can start similarly from a 4-point correlation function and obtain

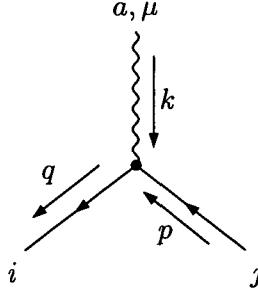


$$= (\tilde{s} \tilde{g}^2) g^2 (f^{abe} f^{cde} (g^{\mu\rho} g^{\nu\sigma} - g^{\mu\sigma} g^{\nu\rho}) + f^{ace} f^{bde} (g^{\mu\nu} g^{\rho\sigma} - g^{\mu\sigma} g^{\nu\rho}) + f^{ade} f^{bce} (g^{\mu\nu} g^{\rho\sigma} - g^{\mu\rho} g^{\nu\sigma})). \quad (\text{B.2.28})$$

The part of the Lagrangian (B.2.4) that describes the fermions is given by

$$\mathcal{L}_{quark} = \bar{\psi}_i (i \not{D} - m)_{ij} \psi_j = \bar{\psi}_i (i \not{\partial} - m) \delta_{ij} \psi_j + i \tilde{g} g \bar{\psi}_i \gamma^\mu A_\mu^a t_{ij}^a \psi_j \quad (\text{B.2.29})$$

where we used the covariant derivative $i\mathcal{D} = i\gamma^\mu\partial_\mu + i\tilde{g}g\gamma^\mu A_\mu^a t^a$ from equation (B.2.5). The first part of equation (B.2.29) gave the fermion propagator (B.2.20) while the second part gives the quark-gluon vertex

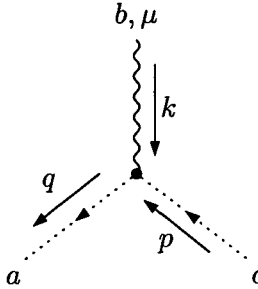


$$= (i\tilde{s}g)g\gamma^\mu t_{ij}^a. \quad (\text{B.2.30})$$

Similarly we can write down the Lagrangian part for the ghost fields

$$\mathcal{L}_{ghost} = \bar{c}^a (-\partial^\mu D_\mu^{ac}) c^c = \bar{c}^a (-\partial^\mu \partial_\mu \delta^{ac}) c^c + \bar{c}^a (-i\tilde{g}g f^{abc} \partial^\mu A_\mu^b) c^c \quad (\text{B.2.31})$$

where we used the adjoint representation of the covariant derivative (B.2.8). Note that the derivative in the second part acts on both the gauge field A_μ^b and the ghost field c^c . The first part determined the ghost propagator (B.2.23) while the second part gives the following Feynman rule:



$$= (-\tilde{s}g)gq^\mu f^{abc}. \quad (\text{B.2.32})$$

In this Feynman rule q^μ denotes the momentum of the outgoing ghost.

Euclidean metric

We can now transform our results into Euclidean metric. In deriving the Feynman rules we did not make use of the metric $g_{\mu\nu}$ other than contracting momentum vectors like $k^\mu k_\mu$ or momentum and position vectors as in the Fourier transform $k^\mu x_\mu$. The latter is taken care of by our generic definitions of the integrals (B.2.3) and delta functions. The former just needs “undoing” the contractions. Since we started with lower indices at the beginning

(B.2.26), resulting in propagators with lower indices and vertices with upper indices, we now have to "pull down" all indices. That is

$$\begin{aligned} k^\mu &\rightarrow g^{\mu\mu'} k_{\mu'}, \\ k^2 = k^\mu k_\mu &\rightarrow g^{\mu\mu'} k_{\mu'} k_\mu \end{aligned} \quad (\text{B.2.33})$$

such that in our formula there are only vectors $k_\mu, p_\mu, q_\mu, \dots$ with lower indices.

We could have done the complete calculation by using the Euclidean metric this way, so we can simply replace

$$g_{\mu\nu} = g^{\mu\nu} \rightarrow -\delta_{\mu\nu} \quad (\text{B.2.34})$$

and write $k^2 = g^{\mu\nu} k_\mu k_\nu \rightarrow -\delta_{\mu\nu} K_\mu K_\nu = -K^2$, where we use capital letters to denote vectors $K^2 = K_\mu K_\mu = K_4^2 + K_1^2 + K_2^2 + K_3^2$ in the Euclidean metric.

For example the gluon propagator (B.2.15) becomes

$$\begin{aligned} \tilde{G}_{\mu\nu}^{ab}(k) &= -\tilde{\chi} \left(g_{\mu\nu} \frac{1}{g^{\alpha\beta} k_\alpha k_\beta} + (\xi - 1) \frac{k_\mu k_\nu}{g^{\alpha\beta} g^{\gamma\delta} k_\alpha k_\beta k_\gamma k_\delta} \right) \delta^{ab} \quad (\text{B.2.35}) \\ &\rightarrow -\tilde{\chi} \left(-\delta_{\mu\nu} \frac{1}{-K^2} + (\xi - 1) \frac{K_\mu K_\nu}{+K^4} \right) \delta^{ab}. \end{aligned}$$

For vertices we have to pull down all indices, so for example the 3-boson vertex (B.2.27) changes to

$$\begin{aligned} (\tilde{s}\tilde{g})gf^{abc} &\left(g^{\mu\nu} g^{\rho\rho'} (k-p)_{\rho'} + g^{\nu\rho} g^{\mu\mu'} (p-q)_{\mu'} + g^{\rho\mu} g^{\nu\nu'} (q-k)_{\nu'} \right) \\ &\rightarrow (\tilde{s}\tilde{g})gf^{abc} (+\delta_{\mu\nu}(K-P)_\rho + \delta_{\nu\rho}(P-Q)_\rho + \delta_{\rho\mu}(Q-K)_\nu). \quad (\text{B.2.36}) \end{aligned}$$

In the case of slashed quantities \not{p} we apply the same transformation and write

$$\not{p} = \gamma^\mu p_\mu = g^{\mu\mu'} \gamma_\mu p_{\mu'} \rightarrow -\delta_{\mu\mu'} \gamma_\mu p_{\mu'} = -\not{P}. \quad (\text{B.2.37})$$

The fermion Green's function (B.2.20) then becomes

$$\tilde{S}_F^{ij}(p) = \tilde{\sigma} \frac{1}{\not{p} - m} \delta^{ab} \rightarrow -\tilde{\sigma} \frac{1}{\not{P} + m} \delta^{ab}. \quad (\text{B.2.38})$$

B.3 Comparison with literature

Values for constants

We want to compare our "generic" results to various results of Feynman rules in the literature. The results are summarized in table B.1. The first constant \tilde{s} describes the sign in the Lagrangian of the generating functional

Reference	M/E	T	\tilde{s}	\tilde{g}	$\tilde{\chi}$	$\tilde{\sigma}$	\tilde{c}
Peskin & Schroeder [130]	M	T_0	i	$-i$	i	i	
Itzykson & Zuber [133]	M	T_0	i	-1	i		
Le Bellac, QSFT [134]	M	T_0	i	$+i$	i	i	
Huang [135]	M	T_0	i	$+i$	i		
Le Bellac, TFT-M [132]	M	RTF	i	$+i$	i	i	
Blaizot & Iancu [131]	M	ITF	$+1$	$+i$	-1	-1	-1
Kapusta [136]	M	ITF	$+1$	$+i$	-1	$+1$	$+1$
Le Bellac, TFT-E [132]	E	ITF	$+1$	$+i$	-1	-1	

Table B.1: Comparison of definitions given in literature. “M/E” means the metric (Minkowski or Euclidean), T stands for temperature $T = 0$ (T_0), Imaginary Time Formalism (ITF) or Real Time Formalism (RTF). Le Bellac [132] gives two sets of Feynman rules which are compared independently. Only \tilde{s} and \tilde{g} are relevant for the sign changes in the Feynman rules.

$Z = \exp(\tilde{s} \int \mathcal{L})$ and can be obtained by comparing equations in the literature to equation (B.1.9). Another way is to compare the propagators of the Feynman rules as in equations (B.2.17), (B.2.20), and (B.2.23). These are independent of the sign of the Green’s function ($\tilde{\chi}$, $\tilde{\sigma}$, \tilde{c}) and are usually given in a table of Feynman rules. A first consistency check can be applied here to see whether the definitions of the three kinds of propagators (gluon, quark, and ghost) are consistent with each other.

The next constant \tilde{g} appears in the definition of the covariant derivative $D_\mu \equiv \partial_\mu + \tilde{g}g A_\mu^a t^a$ (B.2.5). The next three constants $\tilde{\chi}$, $\tilde{\sigma}$, \tilde{c} for the gluon, quark, and ghost Green’s functions respectively are not used in all books. They are not essential for the Feynman rules, though, as they do not enter the equations of the Feynman vertices and Feynman propagators.

Vertices

Table B.2 shows the prefactors of the Feynman rule vertices of the 3-gluon (B.2.27), 4-gluon (B.2.28), quark-gluon (B.2.30), and ghost-gluon (B.2.32) interactions. Before results from literature can be compared to our generic results, some obvious transformations have to be made: These include relabelling indices, using the antisymmetry property of the structure constants f^{abc} , or flipping signs because of different orientation of momentum vectors.

Our results agree with most of the authors. At $T = 0$ in the Minkowski metric our results perfectly agree with Peskin and Schroeder [130], Itzykson & Zuber [133] and Le Bellac [134]. In the imaginary time formalism in Euclidean metric our results agree with Le Bellac [132]. We calculated the prefactors for Euclidean metric in table B.2 by applying the transformation

Reference	3-Gluon	4-Gluon	Quark	Ghost
Generic - Minkowski	\widetilde{sg}	\widetilde{sg}^2	$i\widetilde{sg}$	$-\widetilde{sg}$
Peskin & Schroeder [130]	1	$-i$	i (†)	-1 (*)
Itzykson & Zuber [133]	$-i$	i	1	$+i$
Le Bellac, QSFT [134]	-1	$-i$	$-i$	1
Huang [135]	$-1 \neq -i \blacktriangleleft$	$-i \neq i \blacktriangleleft$	$-i$ (†)	$1 \neq ? \blacktriangleleft$
Le Bellac, TFT-M [132]	-1	$-i$	$-i$	1
Blaizot & Iancu [131]	i (†)	-1 (†)	-1 (†)	$-i$ (†)
Kapusta [136]	$i \neq -i \blacktriangleleft$	-1	$-1 \neq +1 \blacktriangleleft$	$-i$
Generic - Euclidean	\widetilde{sg}	\widetilde{sg}^2	$-i\widetilde{sg}$	$+\widetilde{sg}$
Le Bellac, TFT-E [132]	i	-1	1	$+i$

Table B.2: Prefactors of Feynman rule vertices. The vertex equations are given in (B.2.27), (B.2.28), (B.2.30), and (B.2.32) for the 3-gluon, 4-gluon, quark-gluon, and ghost-gluon vertices respectively. If results differ from literature (marked by \blacktriangleleft) then the l.h.s. of \neq denotes the generic value and the r.h.s. denotes the value from literature. The ghost vertex of Peskin and Schroeder (*) is wrong in the book (+1), but corrected in the online list of errata [137]. Blaizot and Iancu (†) do not give the Feynman rules explicitly, so the values in the table are the generic ones. Peskin and Schroeder and Huang (†) do not give the quark indices in the graphs, resulting in a possible ± 1 factor from the antisymmetric structure constants.

rules from Minkowski to Euclidean metric of section 9.

The results of Itzykson & Zuber [133] use structure constants $C_{abc} = if^{abc}$ and momentum vectors pointing outwards instead of inwards. Taking care of these obvious changes, their results are in accordance with our generic Feynman rules.

Our results do not agree entirely with Kapusta [136] in imaginary time formalism with Minkowski metric. There are relative sign errors -1 in the 3-gluon vertex and in the quark-gluon vertex. His group generators are labelled $G_{ij}^a = t_{ij}^a$.

In the case of Huang [135] Feynman rules disagree in a weird way for the 3-gluon vertex, the 4-gluon vertex and the ghost vertex. In the case of the ghost vertex, the momentum of the boson enters the Feynman rule instead of the momentum of the anti-ghost as in the rest of the literature cited.

Peskin and Schroeder [130] do not provide quark indices i, j in their Feynman graphs. A swapping of the quark indices results in a relative minus sign -1 stemming from the antisymmetric nature of the representation matrices $(t^a)_{ij} = if^{iaj} = -(t^a)_{ji}$. It is assumed that incoming quarks correspond to the second matrix index and outgoing quarks correspond to the first matrix index, matching the indices in the fermion interaction Lagrangian (B.2.29).

Conclusion

Only two generic constants determine the prefactors of all Feynman rules: \tilde{s} and \tilde{g} . The factor \tilde{s} is determined by the generating functional (B.1.9). It is i in the case of $T = 0$ or the Real Time Formalism (RTF). In the case of Imaginary Time Formalism (ITF) it takes the value -1 , corresponding to the change of sign in the time-component from $x_0 \rightarrow -i\tau$ and $dx_0 \rightarrow -id\tau_0$ in the exponent of the generating functional.

The second essential generic constant is \tilde{g} . Its choice is less motivated physically, but merely a matter of taste.

Together, these two constants ($\tilde{s} = i$ or -1 , $\tilde{g} = -i$, -1 , or $+i$) explain the prefactors of propagators and vertices used in Feynman rules.

B.4 Summary of rules

The constants \tilde{s} and \tilde{g} can be determined by comparison with the following formulae. In standard literature \tilde{g} assumes the values $-i$ [130], -1 [133], or $+i$ [138, 132, 134]. The constant \tilde{s} takes the value i for zero temperature field theory or real time formalism and -1 for imaginary time formalism. An overview of these constants can be found in the tables B.1 and B.2 of section B.3.

Lagrangian

$$\begin{aligned}
\mathcal{L} &= -\frac{1}{4}F_{\mu\nu}^a F^{\mu\nu a} + \bar{\psi}_i (i\not{D} - m)_{ij} \psi_j - \frac{1}{2\xi} (\partial^\mu A_\mu^a)^2 + \bar{c}^a (-\partial^\mu D_\mu^{ac}) c^c \\
&= -\frac{1}{2} (\partial_\mu A_\nu^a \partial^\mu A^{\nu a} - \partial_\mu A_\nu^a \partial^\nu A^{\mu a}) - \frac{1}{2\xi} (\partial^\mu A_\mu^a)^2 \\
&\quad - i\partial_\mu A_\nu^a \tilde{g} g f^{abc} A^{\mu b} A^{\nu c} + \frac{1}{4} \tilde{g}^2 g^2 f^{abc} f^{ade} A_\mu^b A_\nu^c A^{\mu d} A^{\nu e} \\
&\quad + \bar{\psi}_i (i\not{\partial} - m) \delta_{ij} \psi_j + i\tilde{g} g \bar{\psi}_i \gamma^\mu A_\mu^a t_{ij}^a \psi_j \\
&\quad + \bar{c}^a (-\partial^\mu \partial_\mu \delta^{ac}) c^c - i\tilde{g} g f^{abc} \bar{c}^a \partial^\mu (A_\mu^b c^c)
\end{aligned} \tag{B.4.1}$$

Generic integral and Generating functional

$$\int d^4\tilde{x} \equiv \begin{cases} \int d^4x & \text{for } T=0 \\ \int_0^\beta d\tau \int d^3\vec{x} & \text{for ITF} \end{cases} \longleftrightarrow Z \equiv \int D.. \exp \left(\tilde{s} \int d^4\tilde{x} \mathcal{L} \right) \tag{B.4.2}$$

Covariant derivative and Field strength tensor

$$D_\mu \equiv \partial_\mu + \tilde{g} g A_\mu^a t^a \longleftrightarrow F_{\mu\nu}^a = \partial_\mu A_\nu^a - \partial_\nu A_\mu^a + i\tilde{g} g f^{abc} A_\mu^b A_\nu^c \tag{B.4.3}$$

Feynman propagators

In the following, the arrow means conversion from Minkowski space result to Euclidean space result (Minkowski \rightarrow Euclidean).

$$\begin{aligned}
\begin{array}{c} a, \mu \\ \text{~~~~~} \\ \xrightarrow{k} \\ \text{~~~~~} \\ b, \nu \end{array} &= \frac{-1}{\tilde{s}\chi} \tilde{G}_{\mu\nu}^{ab}(k) \\
&= \frac{1}{\tilde{s}} \left(g_{\mu\nu} \frac{1}{k^2} + (\xi - 1) \frac{k_\mu k_\nu}{k^4} \right) \delta^{ab} \\
&\rightarrow \frac{1}{\tilde{s}} \left(g_{\mu\nu} \frac{1}{K^2} + (\xi - 1) \frac{K_\mu K_\nu}{K^4} \right) \delta^{ab}
\end{aligned} \tag{B.4.4}$$

$$\begin{aligned}
 \begin{array}{c} i \text{ --- } j \\ \xrightarrow{p} \end{array} &= \frac{-1}{\tilde{s}\sigma} \tilde{S}_F^{ij}(p) & (B.4.5) \\
 &= \frac{-1}{\tilde{s}} \frac{1}{\not{p} - m} \delta^{ij} = \frac{-1}{\tilde{s}} \frac{\not{p} + m}{p^2 - m^2 + i\epsilon} \delta^{ij} \\
 &\rightarrow \frac{1}{\tilde{s}} \frac{1}{\not{P} + m} \delta^{ij} = \frac{1}{\tilde{s}} \frac{\not{P} - m}{P^2 + m^2} \delta^{ij}
 \end{aligned}$$

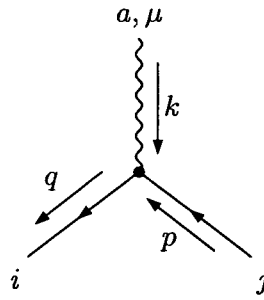
$$\begin{array}{c} a \text{ --- } b \\ \xrightarrow{k} \end{array} = \frac{-1}{\tilde{s}\tilde{c}} \tilde{G}_{gh}^{ab}(k) = \frac{-1}{\tilde{s}} \frac{\delta^{ab}}{k^2} \rightarrow \frac{1}{\tilde{s}} \frac{\delta^{ab}}{K^2} \quad (B.4.6)$$

Vertices

(Minkowski \rightarrow Euclidean)

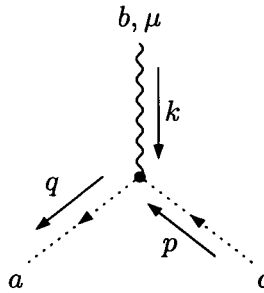
$$\begin{array}{c} a, \mu \\ \downarrow k \\ \begin{array}{c} q \nearrow \\ \text{---} \\ p \searrow \\ c, \rho \quad b, \nu \end{array} \end{array} = (\tilde{s}g) g f^{abc} \begin{aligned} &(g^{\mu\nu}(k-p)^\rho \\ &+ g^{\nu\rho}(p-q)^\mu \\ &+ g^{\rho\mu}(q-k)^\nu) \end{aligned} \quad (B.4.7) \\
 \rightarrow (\tilde{s}g) g f^{abc} \begin{aligned} &(\delta_{\mu\nu}(K-P)_\rho \\ &+ \delta_{\nu\rho}(P-Q)_\mu \\ &+ \delta_{\rho\mu}(Q-K)_\nu)
 \end{aligned}$$

$$\begin{array}{c} a, \mu \quad b, \nu \\ \begin{array}{c} \downarrow k \quad \nearrow p \\ \text{---} \\ \nearrow r \quad \downarrow q \\ d, \sigma \quad c, \rho \end{array} \end{array} = (\tilde{s}g^2) g^2 \begin{aligned} &(f^{abe} f^{cde} (g^{\mu\rho} g^{\nu\sigma} - g^{\mu\sigma} g^{\nu\rho}) \\ &+ f^{ace} f^{bde} (g^{\mu\nu} g^{\rho\sigma} - g^{\mu\sigma} g^{\nu\rho}) \\ &+ f^{ade} f^{bce} (g^{\mu\nu} g^{\rho\sigma} - g^{\mu\rho} g^{\nu\sigma})) \end{aligned} \quad (B.4.8) \\
 \rightarrow (\tilde{s}g^2) g^2 \begin{aligned} &(f^{abe} f^{cde} (\delta_{\mu\rho} \delta_{\nu\sigma} - \delta_{\mu\sigma} \delta_{\nu\rho}) \\ &+ f^{ace} f^{bde} (\delta_{\mu\nu} \delta_{\rho\sigma} - \delta_{\mu\sigma} \delta_{\nu\rho}) \\ &+ f^{ade} f^{bce} (\delta_{\mu\nu} \delta_{\rho\sigma} - \delta_{\mu\rho} \delta_{\nu\sigma}))
 \end{aligned}$$



$$= (i\tilde{s}g)g\gamma^\mu t_{ij}^a \quad (\text{B.4.9})$$

$$\rightarrow (-i\tilde{s}g)g\gamma_\mu t_{ij}^a$$



$$= (-\tilde{s}g)gq^\mu f^{abc} \quad (\text{B.4.10})$$

$$\rightarrow (\tilde{s}g)gQ_\mu f^{abc}$$

Green's functions

$$\left(\partial^2 g_{\mu\nu} - \left(1 - \frac{1}{\xi}\right) \partial_\mu \partial_\nu\right) G^{\nu\rho ab}(x-y) \equiv \tilde{\chi} \delta_\mu^\rho \delta^{ab} \delta^{(4)}(x-y) \quad (\text{B.4.11})$$

$$\tilde{G}_{\mu\nu}^{ab}(k) = -\tilde{\chi} \left(g_{\mu\nu} \frac{1}{k^2} + (\xi-1) \frac{k_\mu k_\nu}{k^4} \right) \delta^{ab} \rightarrow -\tilde{\chi} \left(g_{\mu\nu} \frac{1}{K^2} + (\xi-1) \frac{K_\mu K_\nu}{K^4} \right) \delta^{ab} \quad (\text{B.4.12})$$

$$(i\not{\partial} - m) S_F^{ij}(x-y) \equiv \tilde{\sigma} \delta^{(4)}(x-y) \delta^{ij} \mathbb{1}_{4 \times 4} \quad (\text{B.4.13})$$

$$\tilde{S}_F^{ij}(p) = \tilde{\sigma} \frac{1}{\not{p} - m} \delta^{ij} = \tilde{\sigma} \frac{\not{p} + m}{p^2 - m^2 + i\epsilon} \delta^{ij} \rightarrow -\tilde{\sigma} \frac{1}{\not{P} + m} \delta^{ij} \quad (\text{B.4.14})$$

$$\left(-\partial^2 \delta^{ab}\right) G_{gh}^{bc}(x-y) \equiv \tilde{c} \delta^{ac} \delta^{(4)}(x-y) \quad (\text{B.4.15})$$

$$\tilde{G}_{gh}^{ab}(k) = \tilde{c} \frac{\delta^{ab}}{k^2} \rightarrow \frac{1}{\tilde{s}} - \tilde{c} \frac{\delta^{ab}}{K^2} \quad (\text{B.4.16})$$

Appendix C

Thermodynamic relations

C.1 Specific heat at NLO

The specific heat can be calculated from the entropy by a transformation of thermodynamic quantities which can be found in [115]

$$c_V \equiv C_V/V = T \left\{ \left(\frac{\partial S}{\partial T} \right)_\mu - \frac{\left(\frac{\partial N}{\partial T} \right)_\mu^2}{\left(\frac{\partial N}{\partial \mu} \right)_T} \right\} \quad (\text{C.1.1})$$

where S is the entropy density

$$S \equiv S/V = \left(\frac{\partial P}{\partial T} \right)_{\mu, V}$$

and \mathcal{N} is the particle number density

$$\mathcal{N} \equiv N/V = \left(\frac{\partial P}{\partial \mu} \right)_{T, V} \quad (\text{C.1.2})$$

In order to calculate the next-to-leading order (NLO) specific heat in large- N_f we have to expand this equation around the leading order contribution (2.5.1). The denominator takes the form

$$\left(\frac{\partial \mathcal{N}}{\partial \mu} \right)_T = \left(\frac{\partial^2 P_0}{\partial \mu^2} \right)_T = NN_f \left(\frac{T^2}{3} + \frac{\mu^2}{\pi^2} \right) \quad (\text{C.1.3})$$

and the specific heat can then be written as

$$c_V = c_V^{\text{LO}} + c_V^{\text{NLO}}$$

with the leading order (LO) contribution

$$c_V^{\text{LO}} = NN_f \left(\frac{7\pi^2 T^3}{15} + \frac{\mu^2 T}{3} - \frac{4\mu^2 T^3}{9 \left(\frac{T^2}{3} + \frac{\mu^2}{\pi^2} \right)} \right) \quad (\text{C.1.4})$$

and the next-to-leading order (NLO) contribution

$$c_V^{\text{NLO}} = T \left\{ \left(\frac{\partial \mathcal{S}}{\partial T} \right)_\mu - \frac{4\frac{\mu T}{3} \left(\frac{\partial^2 P}{\partial \mu \partial T} \right)}{\frac{T^2}{3} + \frac{\mu^2}{\pi^2}} + \frac{\left(\frac{2\mu T}{3} \right)^2 \left(\frac{\partial^2 P}{\partial \mu^2} \right)_T}{\left(\frac{T^2}{3} + \frac{\mu^2}{\pi^2} \right)^2} \right\} + O\left(\frac{P_{\text{NLO}}^2}{P_0^2}\right) \quad (\text{C.1.5})$$

with NLO-contributions of \mathcal{S} and P . The ideal-gas limit of the specific heat contains, apart from the LO-contribution, a term proportional to N_f^0 and is given by

$$c_V^0 = NN_f \left(\frac{7\pi^2 T^3}{15} + \frac{\mu^2 T}{3} - \frac{4\mu^2 T^3}{9 \left(\frac{T^2}{3} + \frac{\mu^2}{\pi^2} \right)} \right) + N_g \frac{4\pi^2 T^3}{15}. \quad (\text{C.1.6})$$

C.2 Derivative relations

For the calculation of quark susceptibilities from the pressure in section 2.5.3, we evaluated the derivative with respect to a squared quantity. The derivation with respect to a squared quantity can be obtained as follows, using $\mu^2 = t$

$$\frac{\partial f(\mu)}{\partial \mu^2} = \frac{\partial f(\sqrt{t})}{\partial t} = f'(\sqrt{t}) \frac{1}{2\sqrt{t}} = f'(\mu) \frac{1}{2\mu}. \quad (\text{C.2.1})$$

The chain rule then works as follows

$$\frac{\partial g(f(\mu))}{\partial \mu^2} = \frac{\partial g(f(\sqrt{t}))}{\partial t} = g'(f(\sqrt{t})) \frac{\partial f(\sqrt{t})}{\partial t} = g'(f(\mu)) \frac{\partial f(\mu)}{\partial \mu^2}. \quad (\text{C.2.2})$$

Similarly for the second derivative we obtain

$$\frac{\partial^2}{(\partial \mu^2)^2} g(f(\mu)) = g''(f(\mu)) \left(\frac{\partial f(\mu)}{\partial \mu^2} \right)^2 + g'(f(\mu)) \frac{\partial^2 f(\mu)}{(\partial \mu^2)^2}. \quad (\text{C.2.3})$$

In the case of a quadratic lowest order term of the series expansion of $f(\mu)$ we can further write

$$\frac{\partial^2}{\partial \mu^2} f(\mu) \Big|_{\mu=0} = 2 \frac{\partial}{\partial \mu^2} f(\mu) \Big|_{\mu=0}. \quad (\text{C.2.4})$$

This is however only valid if $f(\mu) = O(\mu^2)$. If $f(\mu)$ contains a linear term, the l.h.s. vanishes, while the r.h.s. diverges. Similarly, for the fourth derivative we see that $\partial^4 \mu^4 / \partial \mu^4 = 24$ but $\partial^2 (\mu^2)^2 / (\partial \mu^2)^2 = \partial^2 t^2 / \partial t^2 = 2$ so that we can write the following relationship if $f(\mu)$ only contains positive even orders in μ up to $O(\mu^4)$, i.e. $f(\mu) = c\mu^2 + O(\mu^4)$:

$$\frac{\partial^4}{\partial \mu^4} f(\mu) \Big|_{\mu=0} = 12 \frac{\partial^2}{(\partial \mu^2)^2} f(\mu) \Big|_{\mu=0}. \quad (\text{C.2.5})$$

Appendix D

Gauge boson self-energy

D.1 Exact result at $T = 0$

In this section we will extend the calculation of the leading order gauge boson self-energy from section 2.3 to the limit of finite chemical potential μ and zero temperature $T = 0$. In this region, the fermionic distribution function from equation (2.2.14) is given by the step-function

$$n_f(k, T = 0, \mu) = \frac{1}{2} (\theta(\mu - k) + \theta(-\mu - k)) \quad (\text{D.1.1})$$

and we can explicitly calculate the real and imaginary parts of the bosonic self energy for Minkowski space.

Imaginary part

In the equations (2.3.25) we can calculate the functions F_i using the $T \rightarrow 0$ limit of the fermionic distribution function (D.1.1) which give

$$F_1(x) \equiv \int_x^\infty n_f(k) dk = \frac{\mu - x}{2} \theta(\mu - x), \quad (\text{D.1.2})$$

$$F_2(x) \equiv \int_x^\infty k n_f(k) dk = \frac{\mu^2 - x^2}{4} \theta(\mu - x), \quad (\text{D.1.3})$$

$$F_3(x) \equiv \int_x^\infty k^2 n_f(k) dk = \frac{\mu^3 - x^3}{6} \theta(\mu - x). \quad (\text{D.1.4})$$

The resulting functions can be further simplified. Using the following definitions

$$\begin{aligned} U(q_0, q) &= (2\mu - |q_0 + q|) \theta(2\mu - |q_0 + q|), \\ V(q_0, q) &= (2\mu - q - q_0)(2\mu + 2q - q_0), \\ W(q_0, q) &= \theta(q_0 + q)V(q_0, q) + \theta(-q_0 - q)V(-q_0, -q), \end{aligned} \quad (\text{D.1.5})$$

we get

$$\text{Im}G(q_0, q) = \frac{1}{16\pi q} (q^2 - q_0^2) \{U(|q_0|, q) - U(-|q_0|, q)\}, \quad (\text{D.1.6})$$

$$\text{Im}H(q_0, q) = -\frac{1}{96\pi q} \{W(|q_0|, q)U(|q_0|, q) - W(-|q_0|, q)U(-|q_0|, q)\}. \quad (\text{D.1.7})$$

From these we get the self-energies

$$\text{Im}\Pi_L(q_0, q) = \frac{-g_{\text{eff}}^2(q^2 - q_0^2)}{48\pi q^3} \{W(|q_0|, q)U(|q_0|, q) - W(-|q_0|, q)U(-|q_0|, q)\}, \quad (\text{D.1.8})$$

$$\text{Im}\Pi_T(q_0, q) = \frac{g_{\text{eff}}^2(q^2 - q_0^2)}{96\pi q^3} \{[W(|q_0|, q) + 6q^2]U(|q_0|, q) - [W(-|q_0|, q) + 6q^2]U(-|q_0|, q)\}. \quad (\text{D.1.9})$$

Real part

Also for the real part we can give the exact solution in the limit $T \rightarrow 0$. Starting from (2.3.21) and (2.3.22) the momentum integration can be analytically done since the distribution function reduces again to a step function for zero temperature. Rearranging the result, we can write

$$R(q_0, q) = (q_0 + q) \ln |q_0 + q| - (2\mu + q_0 + q) \ln |2\mu + q_0 + q|, \quad (\text{D.1.10})$$

$$S(q_0, q) = (-12\mu^2 q_0 + (2q - q_0)(q + q_0)^2) \ln |q_0 + q| + (2\mu - 2q + q_0)(2\mu + q + q_0)^2 \ln |2\mu + q + q_0|. \quad (\text{D.1.11})$$

We use the following abbreviation to keep a lot of terms in dense notation

$$R_{\pm}^{\pm}(q_0, q) \equiv R(q_0, q) - R(q_0, -q) + R(-q_0, q) - R(-q_0, -q) \quad (\text{D.1.12})$$

and similarly for S_{\pm}^{\pm} (just replace R by S). Then the real part of G and H can be written as

$$\text{Re}G(q_0, q) = \frac{1}{2\pi^2} \left(\mu^2 + \frac{q^2 - q_0^2}{8q} R_{\pm}^{\pm}(q_0, q) \right), \quad (\text{D.1.13})$$

$$\text{Re}H(q_0, q) = \frac{1}{96\pi^2} \left(32\mu^2 + \frac{1}{q} S_{\pm}^{\pm}(q_0, q) \right). \quad (\text{D.1.14})$$

Therefore the exact solution for the real part of the self-energies in Minkowski space is given by

$$\text{Re}\Pi_L(q_0, q) = \frac{g_{\text{eff}}^2(q^2 - q_0^2)}{48\pi^2 q^2} \left(32\mu^2 + \frac{1}{q} S_{\pm}^{\pm}(q_0, q) \right), \quad (\text{D.1.15})$$

$$\text{Re}\Pi_T(q_0, q) = \frac{g_{\text{eff}}^2}{96\pi^2 q^3} \{16\mu^2 q(q^2 + 2q_0^2) + (q^2 - q_0^2)(6q^2 R_{\pm}^{\pm}(q_0, q) - S_{\pm}^{\pm}(q_0, q))\}. \quad (\text{D.1.16})$$

D.2 Approximations to second order in frequency

We can calculate the following $T \rightarrow 0$ limits in Minkowski space by using our exact formulae for the imaginary part of the self-energies (D.1.8) and (D.1.9). In the following we will use these equations in a regime where $0 \leq q_0 \ll q, \mu$. This is a reasonable assumption, as the bosonic distribution function n_b will probe smaller and smaller q_0 if we let $T \rightarrow 0$. In this limit we can simplify our functions (D.1.5) to $U(q_0, q) \rightarrow (2\mu - q_0 - q)\theta(2\mu - q)$ and $W(q_0, q) \rightarrow V(q_0, q)$. (Actually in $U(q_0, q)$ we could have used $\theta(2\mu - q_0 - q)$ which would make the following expressions slightly more complicated, but it naturally reduces to $\theta(2\mu - q)$ as soon as we expand q_0 around 0.) The functions G and H from (D.1.6) and (D.1.7) then become

$$\text{Im}G(q_0, q) = \frac{q_0(q_0^2 - q^2)}{8\pi q} \theta(2\mu - q), \quad (\text{D.2.1})$$

$$\text{Im}H(q_0, q) = \frac{q_0(12\mu^2 + q_0^2 - 3q^2)}{48\pi q} \theta(2\mu - q), \quad (\text{D.2.2})$$

where the θ -functions come from the step-function shape of the fermionic distribution function at zero temperature. These are exact solutions in the limit of $T \rightarrow 0$ and $q_0 \rightarrow 0$. Furthermore, for the real parts of G and H we can provide the following expansions in small q_0 :

$$\begin{aligned} \text{Re}G(q_0, q) = & \frac{1}{8\pi^2} \{4\mu^2 + q [(2\mu - q) \ln |2\mu - q| + 2q \ln q \\ & - (2\mu + q) \ln |2\mu + q|]\} + O(q_0^2), \end{aligned} \quad (\text{D.2.3})$$

$$\begin{aligned} \text{Re}H(q_0, q) = & \frac{1}{24\pi^2 q} \{8\mu^2 q - (2\mu - q)^2 (\mu + q) \ln |2\mu - q| + 2q^3 \ln q \\ & + (\mu - q)(2\mu + q)^2 \ln |2\mu + q|\} + O(q_0^2), \end{aligned} \quad (\text{D.2.4})$$

with the chemical potential μ .

We can combine the functions G and H to form the self-energies Π_L and Π_T according to (D.1.8) and (D.1.9). Again, for the imaginary part we get nice analytic expressions in the limit of small T and q_0 :

$$\text{Im}\Pi_L(q_0, q) = -g_{\text{eff}}^2 \frac{q_0(-q_0^2 + q^2)(-12\mu^2 + 3q^2 - q_0^2)}{24\pi q^3} \theta(2\mu - q), \quad (\text{D.2.5})$$

$$\text{Im}\Pi_T(q_0, q) = -g_{\text{eff}}^2 \frac{q_0(-q_0^2 + q^2)(12\mu^2 + 3q^2 + q_0^2)}{48\pi q^3} \theta(2\mu - q). \quad (\text{D.2.6})$$

Since this is valid for small q_0 , it makes sense to expand these expressions for small q_0 . The first coefficient in the q_0 -expansion reads

$$\text{Im}\Pi_L(q_0, q) = -g_{\text{eff}}^2 \frac{(-4\mu^2 + q^2)}{8\pi q} q_0 \theta(2\mu - q) + O(q_0^2), \quad (\text{D.2.7})$$

$$\text{Im}\Pi_T(q_0, q) = -g_{\text{eff}}^2 \frac{(4\mu^2 + q^2)}{16\pi q} q_0 \theta(2\mu - q) + O(q_0^2), \quad (\text{D.2.8})$$

and for the real parts

$$\begin{aligned} \text{Re}\Pi_L(q_0, q) = & \frac{g_{\text{eff}}^2}{12\pi^2 q} \{ 8\mu^2 q - (2\mu - q)^2 (\mu + q) \ln |2\mu - q| + 2q^3 \ln q \\ & + (\mu - q)(2\mu + q)^2 \ln |2\mu + q| \} + O(q_0^2), \end{aligned} \quad (\text{D.2.9})$$

$$\begin{aligned} \text{Re}\Pi_T(q_0, q) = & \frac{g_{\text{eff}}^2}{24\pi^2 q} \{ 4\mu^2 q + (2\mu - q)(2\mu^2 + \mu q + 2q^2) \ln |2\mu - q| \\ & + 4q^3 \ln q - (2\mu + q)(2\mu^2 - \mu q + 2q^2) \ln |2\mu + q| \} + O(q_0^2). \end{aligned} \quad (\text{D.2.10})$$

For the temperature-independent vacuum contribution the imaginary part vanishes for small q_0 , $\text{Im}\Pi_{\text{vac}}(q_0, q) = O(q_0^2)$ while the real part takes the value

$$\text{Re}\Pi_{\text{vac}}(q_0, q) = -g_{\text{eff}}^2 \frac{q^2}{12\pi^2} \left(\ln \frac{q^2}{\bar{\mu}^2} - \frac{5}{3} \right) + O(q_0^2) \quad (\text{D.2.11})$$

with the renormalization scale $\bar{\mu}$.

Appendix E

Fractional power expansion

E.1 Introduction to Puiseux series

The first time fractional powers appear in (3.3.8). In this section we want to analyze where fractional powers come from and which terms determine their coefficients.

Series involving fractional powers are also known as Puiseux series [139]. They appear because one expands around a singular point that does not have a Taylor or Laurent series with integer powers at this point. A simple expansion where the singular point is inherent is

$$\exp(\sqrt{x}) \approx 1 + \sqrt{x} + \frac{x}{2} + \frac{x^{3/2}}{6} + O(x^2) \quad (\text{E.1.1})$$

which can be easily derived by variable substitution $x = y^2$. Another kind of example is

$$f(x) = (x + x^2)^{1/3} \approx x^{1/3} + \frac{x^{4/3}}{3} - \frac{x^{7/3}}{9} + O(x^{10/3}). \quad (\text{E.1.2})$$

In this case the famous Taylor series formula

$$f(x) \approx f(0) + f'(0)x + f''(0)\frac{x^2}{2} + \dots \quad (\text{E.1.3})$$

would give $0 + \infty x - \infty x^2/2 + \dots$ and clearly fails to work. One has to pull out the singular part of the function and perform the Taylor series on the rest:

$$(x + x^2)^{1/3} = x^{1/3} (1 + x)^{1/3} = x^{1/3} \left(1 + \frac{x}{3} - \frac{x^2}{9} + O(x^3) \right) \quad (\text{E.1.4})$$

which gives the result above. In this way, one can obtain fractional power series also from more complicated function compositions.

The simplest example of fractional powers of the kind we encountered appear in the following expression (for positive A , M , B , and C)

$$\begin{aligned} \int_{q_0}^{q_{\max}} \frac{Aq^5 q_0}{Mq^6 + Bq_0^2 + Cq^2 q_0^2} dq &= \frac{Aq_0}{6M} \ln \frac{Mq_{\max}^6}{Bq_0^2} \\ &- \frac{AC\pi}{9\sqrt{3}B^{2/3}M^{4/3}} q_0^{5/3} + \frac{AC^2\pi}{27\sqrt{3}B^{4/3}M^{5/3}} q_0^{7/3} \\ &- \frac{A(6B^3 + 9B^2Cq_{\max}^2 - C^3q_{\max}^6)}{36B^2M^2} q_0^3 \\ &+ \frac{5AC^4\pi q_0^{11/3}}{3^6\sqrt{3}B^{8/3}M^{7/3}} - \frac{7AC^5\pi q_0^{13/3}}{3^7\sqrt{3}B^{10/3}M^{8/3}} \\ &+ O(q_0^5) \end{aligned} \quad (\text{E.1.5})$$

Without the $q^2 q_0^2$ term in the denominator (that is $C = 0$) we would just get the leading logarithmic contribution and integer powers of q_0 (as one can also see from the series by setting $C = 0$). It is this additional term $Cq^2 q_0^2$ that determines additional fractional power terms. The integral can be calculated using the following formula [140] for square-free $g(x)$ and $\deg(f) < \deg(g)$:

$$\int \frac{f(x)}{g(x)} dx = \sum_{\alpha} \frac{f(\alpha)}{g'(\alpha)} \ln(x - \alpha) \quad (\text{E.1.6})$$

where α is the set of all roots of $g(\alpha) = 0$. In our case we get a sum over roots of a cubic equation which first have to be expanded for small q_0 . We can motivate the exponents by

$$x \ln(x + x^{1/3}) = \frac{x}{3} \ln x + x^{5/3} - \frac{x^{7/3}}{2} + \frac{x^3}{3} - \frac{x^{11/9}}{4} + O(x^4) \quad (\text{E.1.7})$$

but we cannot explain factors of $\pi/\sqrt{3}$ appearing in the coefficients of (E.1.5): They only appear together with pure fractional coefficients like $T^{5/3}$ and $T^{7/3}$, but not in the T^3 coefficient. We can give an idea of their appearance by this simple sum over roots

$$\sum_{\alpha \in (x|x^3+1=0)} (\alpha^2 + \alpha) \ln \alpha = -\frac{2\pi}{\sqrt{3}} \quad (\text{E.1.8})$$

but to fully calculate the complete coefficients of the series in (E.1.5) it seems unavoidable to plug in the roots of the denominator into (E.1.6).

In the course of the q_0 expansion, terms from the roots of the denominator of (E.1.5) contain expressions like $-9B\sqrt{M} + \sqrt{3}\sqrt{27B^2M + 4C^3q_0^2}$ which upon symbolic series expansion reduce to $-9B\sqrt{M} + 9\sqrt{B^2M}$. This expression is zero for positive B and non-zero for negative B which would result in two completely different series. It turns out that from the beginning

of the expansion, B and M have to be assumed to have a certain sign, in our case to be positive quantities, in order to get the correct series. Unfortunately, symbolic manipulation programs do not readily allow for this choice (in the course of an expansion, B is not considered equal to $\sqrt{B^2}$ which in our case means the implicit assumption that B is negative.) A possible way to accomplish the series expansion also for positive B in *Mathematica* is presented in the next section.

For the sake of completeness we also give the other integrals with the same denominator as (E.1.5) but different odd powers of q in the numerator:

$$\int_{q_0}^{q_{\max}} \frac{Aq q_0^3}{Mq^6 + Bq_0^2 + Cq^2 q_0^2} dq = \frac{A\pi}{3\sqrt{3}B^{2/3}M^{1/3}} q_0^{5/3} - \frac{AC\pi}{9\sqrt{3}B^{4/3}M^{2/3}} q_0^{7/3} - \frac{A(3B^3 + 6B^2Mq_{\max}^4 - C^2q_{\max}^4)}{12B^2Mq_{\max}^4} q_0^3 - \frac{5AC^3\pi q_0^{11/3}}{3^5\sqrt{3}B^{8/3}M^{4/3}} + \frac{7AC^5\pi q_0^{13/3}}{3^6\sqrt{3}B^{10/3}M^{5/3}} + O(q_0^5) \quad (\text{E.1.9})$$

$$\int_{q_0}^{q_{\max}} \frac{Aq^3 q_0^3}{Mq^6 + Bq_0^2 + Cq^2 q_0^2} dq = \frac{A\pi}{3\sqrt{3}B^{1/3}M^{2/3}} q_0^{7/3} - \frac{A(3B + C^2q_{\max}^2)}{6BMq_{\max}^2} q_0^3 + \frac{AC^2\pi q_0^{11/3}}{3^3\sqrt{3}B^{5/3}M^{4/3}} - \frac{4AC^3\pi q_0^{13/3}}{3^5\sqrt{3}B^{7/3}M^{5/3}} + O(q_0^5) \quad (\text{E.1.10})$$

Note that equation (E.1.9) contains the same fractional power coefficients as equation (E.1.5) up to a factor $-C/(3M)$. This is because the combination

$$\int \frac{6Mq^5 + 2Cq q_0^2}{Mq^6 + Bq_0^2 + Cq^2 q_0^2} dq = \ln(Mq^6 + Bq_0^2 + Cq^2 q_0^2) \quad (\text{E.1.11})$$

is a series in integer powers of q_0 .

E.2 Workaround for *Mathematica*

Assume positive

The calculation of fractional powers crucially depends on a series expansion which in the current version of *Mathematica* [141, 142] is not straightforward to calculate. As a simple example, let us calculate the series of

$$s = \frac{-A + \sqrt{A^2 + x}}{-A + \sqrt{A^2 + 2x}}. \quad (\text{E.2.1})$$

Expressions of the form of the denominator or numerator naturally appear when solving quadratic, cubic, or quartic equations. The series of s delicately depends on whether A is positive or negative. We get the following series expansion for $|x| < A^2/2$:

$$s \approx \begin{cases} \frac{1}{2} + \frac{x}{8A^2} - \frac{x^2}{8A^4} + \frac{19x^3}{128A^6} - \frac{25x^4}{128A^8} + O(x^5) & \text{for } A > 0, \\ 1 - \frac{x}{4A^2} + \frac{5x^2}{16A^4} - \frac{7x^3}{16A^6} + \frac{167x^4}{256A^8} + O(x^5) & \text{for } A < 0. \end{cases} \quad (\text{E.2.2})$$

Trying to calculate the series symbolically results in subexpressions of the form $-A + \sqrt{A^2}$ which is not automatically reduced to 0. Therefore *Mathematica* does not recognize that for positive A l'Hospital's rule has to be applied to calculate the series elements as $x \rightarrow 0$. Unfortunately, even in the most recent version of *Mathematica* (which by the time of writing is *Mathematica* 5.0 [142]) commands like `Assuming[{A>0}, ...]` or options like `Limit[s, x→0, Assumptions→{A>0}]` are applied only before or after a series calculation and not in the course of the calculation, and therefore only provides a solution which is valid for $-A + \sqrt{A^2} \neq 0$ which is satisfied by negative A . Trying to plug in positive A in the resulting series unfortunately gives the wrong result, as can be checked numerically or by plotting the functions. We get a complete nonsense result by the simple *Mathematica* command `s+O[x]^3//PowerExpand → 1+ComplexInfinity x+Indeterminate x^2+O[x]^3` since series expansion (implicitly) assumes $A < 0$ while `PowerExpand` assumes $A > 0$.

In order to get the correct result, we have to modify the standard behavior of the internal `Power[.]` function: Whenever we find an expression $(x^a)^b$ with positive x , we immediately expand it to x^{ab} . Our rules also include $(x^a y)^b \rightarrow x^{ab} y^b$ for $x > 0$ and its standard-case for $a = 1$. We use `Length[Cases[ListOfPositives,x]] > 0` to check whether x is part of varlist of positive variables. The attribute `HoldRest` is set first, so that expressions are only evaluated after the power rules have been modified. After calculation, the power rules are reset to their original state, and the new result is returned. The following routine also expands the `Log[.]` function accordingly.

```
SetAttributes[AssumePositive, HoldRest];
AssumePositive[varlist_, expression_] :=
  Block[{ListOfPositives = varlist},
    (*Andreas Ipp, Sept 12, 2003*)
    (*First we change Power Rules*)
    Unprotect[Power, Log];
    Power[Power[x_ /; (Length[Cases[ListOfPositives, x]]
      > 0), n_.]*y_, m_] := Power[x, n*m]*Power[y, m];
    Power[Power[x_ /; (Length[Cases[ListOfPositives, x]]
```

```

      > 0), n_], m_] := Power[x, n*m];
Log[Power[x_ /; (Length[Cases[ListOfPositives, x]] > 0),
  n_] * y_] := n Log[x] + Log[y];
Log[Power[x_ /; (Length[Cases[ListOfPositives, x]] > 0),
  n_]] := n*Log[x]; Protect[Power, Log];
(*There is a bug if we try to use FullSimplify[ ..],
  so we turn the Error Message off *)
Off[Pattern::"nodef"];
(*Then we evaluate expression*)
{expression,
  On[Pattern::"nodef"];
  (*and finally we change rules back to original state*)
  Unprotect[Power, Log];
  Power[Power[x_ /; (Length[Cases[ListOfPositives, x]]
    > 0), n_] * y_, m_] =.;
  Power[Power[x_ /; (Length[Cases[ListOfPositives, x]]
    > 0), n_], m_] =.;
  Log[Power[x_ /; (Length[Cases[ListOfPositives, x]]
    > 0), n_] * y_] =.;
  Log[Power[x_ /; (Length[Cases[ListOfPositives, x]]
    > 0), n_]] =.;
  Protect[Power, Log];
}[[1]] (*but we take the expression from before -
  in this way we don't have to introduce a new variable*)
]

```

Now it is straightforward to calculate the series above: Use `AssumePositive[{A}, s + O[x]^5]` for the upper series and `AssumePositive[{B}, s + O[x]^5 / . A → -B] / . B → -A` for the lower series in (E.2.2). `AssumePositive` can take any list of variables, e.g. `AssumePositive[{a, b}, $\sqrt{ab^2cd^2}$] → $\sqrt{a}b\sqrt{cd^2}$` . Possible extensions to this routine might include `Abs[x] → x` or `UnitStep[x] → 1 for x > 0`.

Bibliography

- [1] LHC, "The Large Hadron Collider."
<http://lhc-new-homepage.web.cern.ch/lhc-new-homepage/>.
- [2] RHIC, "Relativistic Heavy Ion Collider."
<http://www.bnl.gov/RHIC/>.
- [3] J. M. Jowett, "Ions in the LHC ring." Prepared for 12th Chamonix LHC Performance Workshop, Chamonix, France, 3-8 Mar 2003
http://ab-div.web.cern.ch/ab-div/Conferences/Chamonix/chamx2003/PAPERS/2_6_JJ.pdf.
- [4] J. Hoult, "Teachers notes on particle accelerators."
<http://teachers.web.cern.ch/teachers/materials/accelerators.htm>.
- [5] SPS, "Super Proton Synchrotron."
<http://ab-div-op-sps.web.cern.ch/ab-div-op-sps/>.
- [6] U. Heinz and M. Jacob, "Evidence for a new state of matter: An assessment of the results from the cern lead beam programme."
<http://cern.web.cern.ch/CERN/Announcements/2000/NewStateMatter/science.html>.
- [7] NA50 Collaboration, H. Santos *et al.*, *Recent results on anomalous J/ψ suppression in Pb-Pb collisions at 158 AGeV/c*, hep-ex/0306004.
- [8] C. L. Bennett *et al.*, *First year Wilkinson Microwave Anisotropy Probe (WMAP) observations: Preliminary maps and basic results*, *Astrophys. J. Suppl.* **148** (2003) 1 [astro-ph/0302207].
- [9] M. J. Fromerth and J. Rafelski, *Hadronization of the quark universe*, astro-ph/0211346.
- [10] K. Rajagopal and F. Wilczek, *The condensed matter physics of QCD*, hep-ph/0011333.
- [11] M. G. Alford, *Color superconducting quark matter*, *Ann. Rev. Nucl. Part. Sci.* **51** (2001) 131-160 [hep-ph/0102047].

- [12] D. Bailin and A. Love, *Superfluidity and superconductivity in relativistic fermion systems*, *Phys. Rept.* **107** (1984) 325–385.
- [13] B. C. Barrois, *Superconducting quark matter*, *Nucl. Phys.* **B129** (1977) 390.
- [14] M. G. Alford, J. A. Bowers, and K. Rajagopal, *Crystalline color superconductivity*, *Phys. Rev.* **D63** (2001) 074016 [hep-ph/0008208].
- [15] D. H. Rischke, *The quark-gluon plasma in equilibrium*, nucl-th/0305030.
- [16] N. Iwamoto, *Quark beta decay and the cooling of neutron stars*, *Phys. Rev. Lett.* **44** (1980) 1637–1640.
- [17] J. Custers, P. Gegenwart, H. Wilhelm, K. Neumaier, Y. Tokiwa, O. Trovarelli, C. Geibel, F. Steglich, C. Pépin, and P. Coleman, *The break-up of heavy electrons at a quantum critical point*, *Nature* **424** (2003) 524.
- [18] O. Trovarelli, C. Geibel, S. Mederle, C. Langhammer, F. M. Grosche, P. Gegenwart, M. Lang, G. Sparn, and F. Steglich, *YbRh₂Si₂: Pronounced non-Fermi-liquid effects above a low-lying magnetic phase transition*, *Phys. Rev. Lett.* **85** (1999) 626–629.
- [19] Particle Data Group Collaboration, K. Hagiwara *et. al.*, *Review of particle physics*, *Phys. Rev.* **D66** (2002) 010001.
- [20] J. I. Kapusta, *Finite-temperature field theory*. Cambridge University Press, Cambridge, UK, 1989.
- [21] A. D. Linde, *Infrared problem in thermodynamics of the Yang-Mills gas*, *Phys. Lett.* **B96** (1980) 289.
- [22] D. J. Gross, R. D. Pisarski, and L. G. Yaffe, *QCD and instantons at finite temperature*, *Rev. Mod. Phys.* **53** (1981) 43.
- [23] P. Arnold, G. D. Moore, and L. G. Yaffe, *Photon emission from ultrarelativistic plasmas*, *JHEP* **0111** (2001) 057 [hep-ph/0109064].
- [24] A. K. Rebhan, *The nonabelian Debye mass at next-to-leading order*, *Phys. Rev.* **D48** (1993) 3967–3970 [hep-ph/9308232].
- [25] P. Arnold and L. G. Yaffe, *The nonabelian Debye screening length beyond leading order*, *Phys. Rev.* **D52** (1995) 7208–7219 [hep-ph/9508280].
- [26] P. Arnold, D. Son, and L. G. Yaffe, *The hot baryon violation rate is $O(\alpha_w^5 T^4)$* , *Phys. Rev.* **D55** (1997) 6264–6273 [hep-ph/9609481].

- [27] D. Bödeker, *On the effective dynamics of soft non-abelian gauge fields at finite temperature*, *Phys. Lett.* **B426** (1998) 351–360 [hep-ph/9801430].
- [28] P. Arnold and C.-X. Zhai, *The three loop free energy for pure gauge QCD*, *Phys. Rev.* **D50** (1994) 7603–7623 [hep-ph/9408276].
- [29] P. Arnold and C.-X. Zhai, *The three-loop free energy for high temperature QED and QCD with fermions*, *Phys. Rev.* **D51** (1995) 1906–1918 [hep-ph/9410360].
- [30] C. Corianò and R. R. Parwani, *The three loop equation of state of QED at high temperature*, *Phys. Rev. Lett.* **73** (1994) 2398–2401 [hep-ph/9405343].
- [31] R. R. Parwani, *The free energy of hot QED at fifth order*, *Phys. Lett.* **B334** (1994) 420–426 [hep-ph/9406318].
- [32] R. R. Parwani and C. Corianò, *Higher order corrections to the equation of state of QED at high temperature*, *Nucl. Phys.* **B434** (1995) 56–84 [hep-ph/9409269].
- [33] R. Parwani and H. Singh, *The pressure of hot $g^2\phi^4$ theory at order g^5* , *Phys. Rev.* **D51** (1995) 4518–4524 [hep-th/9411065].
- [34] F. Karsch, A. Patkós, and P. Petreczky, *Screened perturbation theory*, *Phys. Lett.* **B401** (1997) 69–73 [hep-ph/9702376].
- [35] J. O. Andersen, E. Braaten, and M. Strickland, *Hard-thermal-loop resummation of the free energy of a hot quark-gluon plasma*, *Phys. Rev.* **D61** (2000) 074016 [hep-ph/9908323].
- [36] J. O. Andersen, E. Braaten, and M. Strickland, *Hard-thermal-loop resummation of the thermodynamics of a hot gluon plasma*, *Phys. Rev.* **D61** (2000) 014017 [hep-ph/9905337].
- [37] J. O. Andersen, E. Braaten, and M. Strickland, *Hard-thermal-loop resummation of the free energy of a hot gluon plasma*, *Phys. Rev. Lett.* **83** (1999) 2139–2142 [hep-ph/9902327].
- [38] J. O. Andersen, E. Braaten, E. Petitgirard, and M. Strickland, *HTL perturbation theory to two loops*, *Phys. Rev.* **D66** (2002) 085016 [hep-ph/0205085].
- [39] J. O. Andersen, *Hard thermal loops and QCD thermodynamics*, hep-ph/0210195.

- [40] R. Baier and K. Redlich, *Hard thermal-loop resummed pressure of a degenerate quark-gluon plasma*, *Phys. Rev. Lett.* **84** (2000) 2100 [hep-ph/9908372].
- [41] E. Braaten and R. D. Pisarski, *Simple effective lagrangian for hard thermal loops*, *Phys. Rev.* **D45** (1992) 1827–1830.
- [42] J. Frenkel and J. C. Taylor, *Hard thermal QCD, forward scattering and effective actions*, *Nucl. Phys.* **B374** (1992) 156–168.
- [43] G. Baym, *Self-consistent approximations in many-body systems*, *Phys. Rev.* **127** (1962) 1391.
- [44] B. Vanderheyden and G. Baym, *Self-consistent approximations in relativistic plasmas: Quasiparticle analysis of the thermodynamic properties*, *J. Stat. Phys.* **93** (1998) 843 [hep-ph/9803300].
- [45] J. P. Blaizot, E. Iancu, and A. Rebhan, *The entropy of the QCD plasma*, *Phys. Rev. Lett.* **83** (1999) 2906–2909 [hep-ph/9906340].
- [46] J. P. Blaizot, E. Iancu, and A. Rebhan, *Approximately self-consistent resummations for the thermodynamics of the quark-gluon plasma: Entropy and density*, *Phys. Rev.* **D63** (2001) 065003 [hep-ph/0005003].
- [47] J. P. Blaizot, E. Iancu, and A. Rebhan, *Quark number susceptibilities from HTL-resummed thermodynamics*, *Phys. Lett.* **B523** (2001) 143–150 [hep-ph/0110369].
- [48] J.-P. Blaizot, E. Iancu, and A. Rebhan, *Thermodynamics of the high-temperature quark gluon plasma*, hep-ph/0303185.
- [49] A. Peshier, *HTL resummation of the thermodynamic potential*, *Phys. Rev.* **D63** (2001) 105004 [hep-ph/0011250].
- [50] G. Boyd, J. Engels, F. Karsch, E. Laermann, C. Legeland, M. Lütgemeier, and B. Petersson, *Thermodynamics of SU(3) lattice gauge theory*, *Nucl. Phys.* **B469** (1996) 419–444 [hep-lat/9602007].
- [51] CP-PACS Collaboration, M. Okamoto *et. al.*, *Equation of state for pure SU(3) gauge theory with renormalization group improved action*, *Phys. Rev.* **D60** (1999) 094510 [hep-lat/9905005].
- [52] I. T. Drummond, R. R. Horgan, P. V. Landshoff, and A. Rebhan, *Foam diagram summation at finite temperature*, *Nucl. Phys.* **B524** (1998) 579–600 [hep-ph/9708426].

- [53] D. Bödeker, P. V. Landshoff, O. Nachtmann, and A. Rebhan, *Renormalisation of the nonperturbative thermal pressure*, *Nucl. Phys.* **B539** (1999) 233–263 [hep-ph/9806514].
- [54] E. V. Shuryak, *Theory of hadronic plasma*, *Sov. Phys. JETP* **47** (1978) 212–219.
- [55] S. A. Chin, *Transition to hot quark matter in relativistic heavy ion collision*, *Phys. Lett.* **B78** (1978) 552–555.
- [56] J. I. Kapusta, *Quantum chromodynamics at high temperature*, *Nucl. Phys.* **B148** (1979) 461.
- [57] T. Toimela, *The next term in the thermodynamic potential of QCD*, *Phys. Lett.* **B124** (1983) 407.
- [58] C.-x. Zhai and B. Kastening, *The free energy of hot gauge theories with fermions through g^5* , *Phys. Rev.* **D52** (1995) 7232–7246 [hep-ph/9507380].
- [59] P. Ginsparg, *First-order and second-order phase transitions in gauge theories at finite temperature*, *Nucl. Phys.* **B170** (1980) 388.
- [60] T. Appelquist and R. D. Pisarski, *Hot Yang-Mills theories and three-dimensional QCD*, *Phys. Rev.* **D23** (1981) 2305.
- [61] K. Kajantie, M. Laine, K. Rummukainen, and M. Shaposhnikov, *Generic rules for high temperature dimensional reduction and their application to the standard model*, *Nucl. Phys.* **B458** (1996) 90–136 [hep-ph/9508379].
- [62] E. Braaten and A. Nieto, *Free energy of QCD at high temperature*, *Phys. Rev.* **D53** (1996) 3421–3437 [hep-ph/9510408].
- [63] K. Kajantie, M. Laine, K. Rummukainen, and Y. Schröder, *The pressure of hot QCD up to $g^6 \ln(1/g)$* , *Phys. Rev.* **D67** (2003) 105008 [hep-ph/0211321].
- [64] K. Kajantie, M. Laine, K. Rummukainen, and Y. Schröder, *Four-loop vacuum energy density of the $SU(N_c)$ + adjoint Higgs theory*, *JHEP* **04** (2003) 036 [hep-ph/0304048].
- [65] A. Vuorinen, *The pressure of QCD at finite temperatures and chemical potentials*, *Phys. Rev.* **D68** (2003) 054017 [hep-ph/0305183].
- [66] G. D. Moore, *Pressure of hot QCD at large N_f* , *JHEP* **10** (2002) 055 [hep-ph/0209190].

- [67] A. Ipp, G. D. Moore, and A. Rebhan, *Comment on 'Pressure of hot QCD at large N_f ' with corrected exact result*, 2003.
- [68] A. Ipp and A. Rebhan, *Thermodynamics of large- N_f QCD at finite chemical potential*, 2003.
- [69] A. Hart, M. Laine, and O. Philipsen, *Static correlation lengths in QCD at high temperatures and finite densities*, *Nucl. Phys.* **B586** (2000) 443–474 [hep-ph/0004060].
- [70] E. Braaten, *Solution to the perturbative infrared catastrophe of hot gauge theories*, *Phys. Rev. Lett.* **74** (1995) 2164–2167 [hep-ph/9409434].
- [71] A. Vuorinen, *Quark number susceptibilities of hot QCD up to $g^6 \ln(g)$* , *Phys. Rev.* **D67** (2003) 074032 [hep-ph/0212283].
- [72] B. A. Freedman and L. D. McLerran, *Fermions and gauge vector mesons at finite temperature and density. 2. the ground state energy of a relativistic electron gas*, *Phys. Rev.* **D16** (1977) 1147.
- [73] V. Baluni, *Non-abelian gauge theories of Fermi systems: Quantum-chromodynamic theory of highly condensed matter*, *Phys. Rev.* **D17** (1978) 2092–2121.
- [74] Z. Fodor and S. D. Katz, *A new method to study lattice QCD at finite temperature and chemical potential*, *Phys. Lett.* **B534** (2002) 87–92 [hep-lat/0104001].
- [75] Z. Fodor, S. D. Katz, and K. K. Szabo, *The QCD equation of state at nonzero densities: Lattice result*, hep-lat/0208078.
- [76] P. de Forcrand and O. Philipsen, *The QCD phase diagram for small densities from imaginary chemical potential*, *Nucl. Phys.* **B642** (2002) 290–306 [hep-lat/0205016].
- [77] C. R. Allton *et. al.*, *The QCD thermal phase transition in the presence of a small chemical potential*, *Phys. Rev.* **D66** (2002) 074507 [hep-lat/0204010].
- [78] M. D'Elia and M.-P. Lombardo, *Finite density QCD via imaginary chemical potential*, *Phys. Rev.* **D67** (2003) 014505 [hep-lat/0209146].
- [79] R. V. Gavai and S. Gupta, *Pressure and non-linear susceptibilities in QCD at finite chemical potentials*, hep-lat/0303013.
- [80] A. Peshier, *Comment on 'Pressure of hot QCD at large N_f '*, hep-ph/0211088.

- [81] A. Peshier, B. Kämpfer, O. P. Pavlenko, and G. Soff, *A massive quasiparticle model of the $SU(3)$ gluon plasma*, *Phys. Rev.* **D54** (1996) 2399–2402.
- [82] P. Levai and U. Heinz, *Massive gluons and quarks and the equation of state obtained from $SU(3)$ lattice QCD*, *Phys. Rev.* **C57** (1998) 1879 [hep-ph/9710463].
- [83] A. Peshier, B. Kämpfer, and G. Soff, *The equation of state of deconfined matter at finite chemical potential in a quasiparticle description*, *Phys. Rev.* **C61** (2000) 045203 [hep-ph/9911474].
- [84] A. Rebhan, *HTL-resummed thermodynamics of hot and dense QCD: An update*, hep-ph/0301130.
- [85] T. van Ritbergen, J. A. M. Vermaseren, and S. A. Larin, *The four-loop beta function in quantum chromodynamics*, *Phys. Lett.* **B400** (1997) 379–384 [hep-ph/9701390].
- [86] H. A. Weldon, *Covariant calculations at finite temperature: The relativistic plasma*, *Phys. Rev.* **D26** (1982) 1394.
- [87] N. P. Landsman and C. G. van Weert, *Real and imaginary time field theory at finite temperature and density*, *Phys. Rept.* **145** (1987) 141.
- [88] J. P. Blaizot, E. Iancu, and A. Rebhan, *On the apparent convergence of perturbative QCD at high temperature*, hep-ph/0303045.
- [89] J. O. Andersen, E. Petitgirard, and M. Strickland, *Two-loop HTL thermodynamics with quarks*, hep-ph/0302069.
- [90] K. K. Szabo and A. I. Toth, *Quasiparticle description of the QCD plasma, comparison with lattice results at finite T and μ* , hep-ph/0302255.
- [91] A. Rebhan and P. Romatschke, *HTL quasiparticle models of deconfined QCD at finite chemical potential*, hep-ph/0304294.
- [92] E. S. Fraga, R. D. Pisarski, and J. Schaffner-Bielich, *Small, dense quark stars from perturbative QCD*, *Phys. Rev.* **D63** (2001) 121702 [hep-ph/0101143].
- [93] L. D. Landau and E. M. Lifshitz, *Statistical Physics (Part 1)*. Pergamon Press, London, 1985. Vol. 5.
- [94] F. Reif, *Fundamentals of Statistical and Thermal Physics*. McGraw-Hill, New York, 1965.

- [95] L. D. Landau *Zh. Eksp. Teor. Fiz.* **30** (1956) 1058. (Engl. Transl. Sov. Phys. JETP 3 (1956) 920).
- [96] E. M. Lifshitz and L. P. Pitaevskii, *Statistical Physics (Part 2)*. Pergamon Press, Oxford, 1980. (Landau and Lifshitz Vol. 9).
- [97] J. M. Luttinger, *Fermi surface and some simple equilibrium properties of a system of interacting fermions*, *Phys. Rev.* **119** (1960) 1153–1163.
- [98] G. M. Carneiro and C. J. Pethick, *Specific heat of a normal Fermi liquid. II: Microscopic approach*, *Phys. Rev.* **B11** (1975) 1106–1124.
- [99] G. Baym and S. A. Chin, *Landau theory of relativistic Fermi liquids*, *Nucl. Phys.* **A262** (1976) 527.
- [100] T. Holstein, R. E. Norton, and P. Pincus, *de Haas-van Alphen effect and the specific heat of an electron gas*, *Phys. Rev.* **B8** (1973) 2649–2656.
- [101] A. Ipp, A. Gerhold, and A. Rebhan, *Anomalous specific heat in high-density QED and QCD*, hep-ph/0309019.
- [102] N. W. Ashcroft and N. D. Mermin, *Solid State Physics*. Thomson Learning, 1985.
- [103] S. Chakravarty, R. E. Norton, and O. F. Syljuåsen, *Transverse gauge interactions and the vanquished Fermi liquid*, *Phys. Rev. Lett.* **74** (1995) 1423–1426.
- [104] J. Gan and E. Wong, *Non-Fermi-liquid behavior in quantum critical systems*, *Phys. Rev. Lett.* **71** (1993) 4226–4229.
- [105] D. Boyanovsky and H. J. de Vega, *The specific heat of normal, degenerate quark matter: Non-Fermi liquid corrections*, *Phys. Rev.* **D63** (2001) 114028 [hep-ph/0011354].
- [106] M. Y. Reizer, *Relativistic effects in the electron density of states, specific heat, and the electron spectrum of normal metals*, *Phys. Rev.* **B40** (1989) 11571–11575.
- [107] D. Coffey and C. J. Pethick, *Finite-temperature contributions to the specific heat of the electron-phonon system*, *Phys. Rev. B* **37** (1988) 442–447.
- [108] G. M. Eliashberg *Zh. Eksp. Teor. Fiz.* **43** (1962) 1005. Sov. Phys. JETP 16 (1963) 780.

- [109] D. T. Son, *Superconductivity by long-range color magnetic interaction in high-density quark matter*, *Phys. Rev.* **D59** (1999) 094019 [hep-ph/9812287].
- [110] T. Schäfer, *Loops and power counting in the high density effective field theory*, hep-ph/0310176.
- [111] P. Coleman, C. Pépin, Q. Si, and R. Ramazashvili, *How do Fermi liquids get heavy and die?*, *J. Phys.: Condens. Matter* **13** (2001) R723–R738.
- [112] Steglich, F. *et al.*, *Are heavy-fermion metals Fermi liquids?*, *Z. Phys. B* **103** (1997) 235 – 242.
- [113] Grosche, F.M. *et al.*, *Anomalous low temperature states in CeNi₂Ge₂*, cond-mat/9812133.
- [114] Gegenwart, P. *et al.*, *Breakup of heavy fermions on the brink of “Phase A” in CeCu₂Si₂*, *Phys. Rev. Lett.* **81** (1998) 1501–1504.
- [115] L. D. Landau and E. M. Lifshitz, *Statistical Physics*. Pergamon Press, London, 1985. Chap. 24, p. 71.
- [116] E. Braaten and R. D. Pisarski, *Soft amplitudes in hot gauge theories: A general analysis*, *Nucl. Phys.* **B337** (1990) 569.
- [117] T. Altherr and U. Kraemmer, *Gauge field theory methods for ultradegenerate and ultrarelativistic plasmas*, *Astropart. Phys.* **1** (1992) 133–158.
- [118] D. Boyanovsky and H. J. de Vega, *Non-fermi liquid aspects of cold and dense QED and QCD: Equilibrium and non-equilibrium*, *Phys. Rev.* **D63** (2001) 034016 [hep-ph/0009172].
- [119] G. W. Carter and S. Reddy, *Neutrino propagation in color superconducting quark matter*, *Phys. Rev.* **D62** (2000) 103002 [hep-ph/0005228].
- [120] K. W. Wong and M. C. Chu, *Signatures of QCD phase transition in a newborn compact star*, astro-ph/0304515.
- [121] T. Schäfer and F. Wilczek, *Superconductivity from perturbative one-gluon exchange in high density quark matter*, *Phys. Rev.* **D60** (1999) 114033 [hep-ph/9906512].
- [122] R. D. Pisarski and D. H. Rischke, *Gaps and critical temperature for color superconductivity*, *Phys. Rev.* **D61** (2000) 051501 [nucl-th/9907041].

- [123] D. K. Hong, V. A. Miransky, I. A. Shovkovy, and L. C. R. Wijewardhana, *Schwinger-Dyson approach to color superconductivity in dense QCD*, *Phys. Rev.* **D61** (2000) 056001 [hep-ph/9906478].
- [124] W. E. Brown, J. T. Liu, and H.-c. Ren, *Non-Fermi liquid behavior, the BRST identity in the dense quark-gluon plasma and color superconductivity*, *Phys. Rev.* **D62** (2000) 054013 [hep-ph/0003199].
- [125] T. Schäfer, *Hard loops, soft loops, and high density effective field theory*, hep-ph/0307074.
- [126] A. Schmitt, Q. Wang, and D. H. Rischke, *When the transition temperature in color superconductors is not like in BCS theory*, nucl-th/0209050.
- [127] W. E. Brown, J. T. Liu, and H.-c. Ren, *On the perturbative nature of color superconductivity*, *Phys. Rev.* **D61** (2000) 114012 [hep-ph/9908248].
- [128] Q. Wang and D. H. Rischke, *How the quark self-energy affects the color-superconducting gap*, *Phys. Rev.* **D65** (2002) 054005 [nucl-th/0110016].
- [129] K. Rajagopal and E. Shuster, *On the applicability of weak-coupling results in high density QCD*, *Phys. Rev.* **D62** (2000) 085007 [hep-ph/0004074].
- [130] M. E. Peskin and D. V. Schroeder, *An Introduction to quantum field theory*. Addison-Wesley, Reading, USA, 1995.
- [131] J.-P. Blaizot and E. Iancu, *The quark-gluon plasma: Collective dynamics and hard thermal loops*, *Phys. Rept.* **359** (2002) 355–528 [hep-ph/0101103].
- [132] M. Le Bellac, *Thermal Field Theory*. Cambridge University Press, Cambridge, UK, 1996.
- [133] C. Itzykson and J. B. Zuber, *Quantum field theory*. McGraw-Hill, New York, USA, 1980.
- [134] M. Le Bellac, *Quantum and statistical field theory*. Clarendon, Oxford, UK, 1991.
- [135] K. Huang, *Quarks, leptons and gauge fields*. World Scientific, Singapore, Singapore, 1982.
- [136] J. I. Kapusta, *Finite-temperature field theory*. Cambridge University Press, Cambridge, UK, 1989.

- [137] M. E. Peskin and D. V. Schroeder, "Corrections to an introduction to quantum field theory."
<http://www.slac.stanford.edu/~mpeskin/QFT.html>.
- [138] J. I. Kapusta and P. V. Landshoff, *Finite temperature field theory, J. Phys. G* **G15** (1989) 267.
- [139] J.-P. Allouche, *Transcendence of formal power series with rational coefficients, Theoret. Comput. Sci.* **218** (1999) 143–160.
- [140] M. Bronstein, *Symbolic integration I - transcendental functions. Algorithms and computations in mathematics I.* Springer, Berlin, 1997.
- [141] S. Wolfram, *The Mathematica Book, Fourth Edition.* Cambridge University Press, 1999. ISBN: 0521643147.
- [142] S. Wolfram, *The Mathematica Book, Fifth Edition.* Wolfram Media, Inc., 2003. ISBN: 1579550223.

Acknowledgements

I would like to thank my supervisor Anton Rebhan for excellently guiding me through my last two years as a doctoral candidate at the Technical University of Vienna. I am indebted to him for introducing Large N_f to me, a topic that during the last year turned out to be remarkably fruitful with new unexpected results, and let me rise to new challenges regarding my numerical computing skills.

Anton Rebhan's current team of doctoral candidates has been a wonderful environment for fruitful discussions: I want to thank Paul Romatschke for expertise on 2PI, Robert Wimmer for discussions regarding the foundations of quantum field theory, and Andreas Gerhold for insights regarding non-Fermi liquid and color superconductors.

During the last two years I profited a lot from lectures by Manfred Markytan who increased my interest in particle colliders, Dominik Schwarz who introduced me to hydrodynamics and kept me in touch with cosmology, and Albert Reiner who deepened my working knowledge on *Mathematica*.

From the Institute for Theoretical Physics I would like to single out the head of the institute Wolfgang Kummer for providing an open and lively working environment, and further Erwin Riegler, Herbert Balasin, Daniel Grumiller, and Maximilian Kreuzer for permanent helpfulness regarding computing and Linux support. Thanks also to Sebastian Guttenberg for his valuable experience with LyX which helped meeting the deadline. A big thank you also to the administration team of the institute Elfriede Mössmer, Roswitha Uden, and Franz Hochfellner who wonderfully help with all the important work "behind the scenes".

I also want to thank for the warm hospitality that I experienced during my stay at the SPhT, CEA-Saclay in France. Thanks to Jean-Paul Blaizot, Edmond Iancu, and especially Urko Reinosa for discussions on Large- N_f , 2PI, renormalization issues, and non-Fermi-liquids, amongst other topics.

On the technical side I would like to thank Dirk Rischke and Aleksi Vuorinen for correspondence.

I further would like to thank Daniel Hofmann and Christopher Summer for encouraging me during the tough initial part of my studies, and Mike Strickland for wonderful improvisational music sessions.

Last but not least I would like to thank my parents for their incessant

support, my grandmother, my brother and my sister for moral support, and of course Sun Ying for lovingly accompanying me through the final stages of my thesis.

This work has been supported by the Austrian Science Foundation FWF, project no. 14632-TPH.

Curriculum Vitae

Andreas Ipp

Address: Krottenbachgasse 27
A-2345 Brunn am Gebirge
AUSTRIA / EUROPE
Phone: +43-1-2236-378811
Email: ipp@hep.itp.tuwien.ac.at
Homepage: <http://hep.itp.tuwien.ac.at/~ipp/>

Personal information

Date and place of birth: July 12, 1975, Mödling, Austria.
Citizenship: Austria

Academic Career

since 2002	Ph.D. student, Institute for Theoretical Physics, TU Vienna
March 2000	Second Diploma Examination in physics (Master's degree) passed with distinction Diploma thesis: "Phase Transition of a Scalar Field Theory in the Early Universe" Advisor: Dr. Anton Rebhan, Dr. Laurence Yaffe
1998 - 1999	Exchange student, University of Washington Seattle, USA Advisor: Dr. Laurence Yaffe
June 1997	University of Music and Performing Arts Vienna First diploma examination in piano pedagogic
January 1996	Vienna University of Technology First diploma examination in physics passed with distinction
1985 - 1993	BG/BRG Mödling - Keimgasse Mödling (Secondary education) Final examination passed with distinction

International Experience

- 2000 - 2001 Alternative service / social service in Qiqihar, China
 1998 - 1999 Exchange student, University of Washington Seattle, USA
 Advisor: Dr. Laurence Yaffe

Talks given at Conferences and Workshops

- Oct 2003 FAKT 2003, Strobl am Wolfgangsee, Austria.
 "Thermodynamics of Large N_f QCD
 at Finite Chemical Potential"
 Sept 2003 Quantum fields in and out of equilibrium, Bielefeld, Germany.
 "Thermodynamics of Large N_f QCD
 at Finite μ and Non-Fermi-Liquid Behavior"
 June 2003 Common Trends in Cosmology and Particle Physics,
 Balatonfüred, Hungary.
 "Phase Transition of a Scalar Field Theory
 in the Early Universe"

Further Conferences and Workshops attended

- Feb 2003 41. Internationale Universitätswochen für Theoretische
 Physik, "Flavor Physics", Schladming, Austria.
 Oct 2002 Strong and Electroweak Matter 2002, Heidelberg, Germany.
 Sept 2002 WE-Heraeus-Doktorandenschule "Grundlagen und neue
 Methoden der theoretischen Physik", Wolfersdorf, Germany.
 Aug 1998 5th International Workshop on Thermal Field Theories
 and Their Applications, Regensburg, Germany.

International cooperation

- May 2003 Institute for Theoretical Physics, CEA Saclay, France,
 with Jean-Paul Blaizot, Edmond Iancu, and Urko Reinosa.

Professional Experience

- since 2002 TU Vienna, FWF research project no. 14632-PHY.
 2000 Part time computer support for In-Vision GmbH
 Oct 1999 - 2000 Part time computer support for Docter Optics
 July - Sept 1999 Docter Optics
 July-Aug 96, 97, 98 Siemens PSE / Competence Basis
 July 1995 Philips iR3 Video International GmbH
 July 1994 RZB Wien